Internalisation and Cytotoxicity of Alkyl-Capped Silicon Quantum Dots (SiQDs) in Various Mammalian Cell Lines

Wipaporn Phatvej, BSc, MSc

A thesis submitted in part requirement for the degree of Doctor of Philosophy (PhD)

School of Chemistry
Newcastle University

June 2015

Abstract

The increasing application of nanoparticles in medicine, particularly in imaging and therapy, is heavily reliant on fundamental understanding of their unique physicochemical properties. This thesis investigates the interactions that occur between nanoparticles and human cells, specifically their toxicity and the mechanism of their internalisation. Alkyl-capped silicon quantum dots (SiQDs) were chosen for this investigation because their physical properties have been well-characterised and they have very bright luminescence. These properties facilitate their detection inside cells by fluorescence microscopy and flow cytometry.

Toxicity and uptake mechanisms for SiQDs in human cells were investigated. The intestinal cell line CACO-2 was used as a model for ingestion of nanoparticles. Uptake and accumulation of SiQS in CACO-2 cells was demonstrated by epi-fluorescence microscopy and confocal fluorescence microscopy. Cytotoxicity in CACO-2 cells was studied by oxidative stress measurement using a intracellular dye method (H2DCFDA) (ROS assay), cell viability determination (MTT and ATP assays) and DNA damage measurement (Comet assay). Exposure of CACO-2 to SiQDs resulted in low cytotoxicity with regard to cell viability and effects on ATP production. SiQDs did not induce intracellular ROS production or DNA strand breaks. Over time periods up to 14 days, SiQDs showed no evidence of acute or chronic cytotoxicity.

Accumulation of SiQDs inside a selection of human cell lines (CACO-2, HeLa, HepG2, and Huh7) was studied in detail using flow cytometry. SiQDs were internalised by all four cell lines. The highest levels of accumulation were seen with HepG2 and HuH7 cells. Some evidence for a role for caveolin 2 in this process in HuH7 was obtained using inhibitors and by gene expression analysis. The reason why HepG2 cells showed the highest accumulation of SiQDs remains unclear as caveolin expression measured by quantitative reverse transcriptase-PCR in these cells is very low. Further work on a possible role for the protein clathrin in the endocytosis process in these cells is needed as the inhibitor used to investigate this was toxic to the cells and firm conclusions could not be obtained.

In summary, SiQDs are a highly promising alternative to heavy-metal based quantum dots and as a nanoparticle model to study mechanisms of uptake. SiQDs appear non-toxic in CACO-2 cells. However, the internalisation of SiQDs is cell-line dependent and further studies on their toxicity in cells such as HuH7 which show high levels of internalisation and cells relevant to immune responses such as macrophages are needed.

Dedication

To my cherished mom and dad as well as my two older brothers, my nephews and my nieces, who have all given me strength whilst they waited for my success.

Wi Phatvej

Acknowledgements

My deepest and most sincere gratitude goes to my supervisors Dr Benjamin Richard Horrocks and Dr Elaine Mutch. Their scientific skills, knowledge and vast experience have helped me and many native and international students. I thank them for encouraging and pushing me, their great support, advice, guidance and assistance throughout my PhD.

My sincere appreciation also goes to my supervisory team Prof. Ann Katherine Daly who I thank for her thoughtful guidance, advice and giving me the opportunity to finish the final part of my project as well as my thesis. I am also grateful to Dr Simon Charles Wilkinson for all his knowledge and help with dermatology, toxicology and biological statistics and would like to thank him for his guidance and assistance to help finish my project.

I also would like to thank Dr Eimer Tuite and Dr David Smith for training and assistance with absorption and fluorescent spectroscopy. I would like to thank Dr Passapan Sriwichai for cell laboratory training and my close friend Emma Louise Woodward for all her help inside and outside the laboratory. I would also like to thank Dr Noor Harun for her guidance in the synthetic laboratory. Likewise, I would like to thank Dr Scott Watson and Dr Jonathan Pate for Atomic Force training. I would like to thank Dr Trevor Booth for his help with confocal microscopy and Dr David McDonald for flow cytometry. I would like to thank to my close friend Yang Lin Liu for training in molecular techniques. In addition, I would like to thank all friends at Chemical Nanoscience and the Institute of Cellular Medicine (ICM) especially the pharmacogenetics group. I also would like to thank all staff from the School of Chemistry and ICM.

Finally I would like to thank the Royal Thai Government and Ministry of Science (MOST) for funding. Also, I would like to thank the Thailand Institute of Scientific and Technological Research (TISTR), Pharmaceutical and Natural Products Department (PNPD) and Newcastle University for giving me the opportunity to study for a PhD in the UK.

Table of Contents

List of Figures

Chapter 1. General Introduction

Chapter 3. Synthesis and Characterisation of Alkyl-Capped Silicon (SiQDs)

Chapter 4. Cellular Internalisation Studies: Imaging and Cellular Localisation of Alkyl-Capped Silicon Quantum Dots (SiQDs)

Chapter 5. Potential Cytotoxicity of Alkyl-Capped Silicon Quantum Dots (SiQDs)

List of Tables

List of Appendices

List of Abbreviations

Å	Angstrom
Ω	Ohms
λ	Lambda
$\Delta\psi_m$	Mitochondria membrane potential
AFM	Atomic force microscope
ATP	Adenosine triphosphate
BrdU	5-Bromo-2-deoxyuridine
^oC	Degree Celsius
CAV-1	Caveolin1
CAV-2	Caveolin2
cm	Centimetre
cm^2	Square centimetre
CPZ	Chlorpromazine
C_T	Threshold cycle
$^{64}Cu^{24}$	Copper-64
dATP	Deoxyadenosine triphosphate
DCFH	Dichlorofluorescin
DCFH-DA	Dichlorofluorescin diacetate
DCM	Dichloromethane
dCTP	Deoxycytidine triphosphate
dGTP	Deoxyguanosine triphosphate
DMSO	Dimethyl sulfoxide
DNA	Deoxyribonucleic acid
dNTP	Deoxyribonucleotide triphosphate
DNP	2,4-Dinitrophenol
DSBs	Double strand breaks

ECACC	European collection of cell cultures
EDTA	Ethylenediaminetetraacetic acid
e.g.	Exempli gratia (for example)
ENPs	Engineered nanoparticles
ER	Endoplasmic reticulum
et al	Et alia (and others)
eV	Electron volt
FBS	Foetal Bovine serum
FTIR	Fourier transform infrared spectroscopy
FWHM	Full width at half maximum
GAPDH	Glyceraldehyde-3-phosphatedehydrogenase
GC	Gas chromatography
GL	Grade level
GSH	Reduced Glutathione
H2DCFDA	Dichlorodihydrofluorescein
HO-1	Heme oxygenase
HOMO	Highest occupied molecular orbital
HPLC	High performance liquid chromatography
HRTEM	High resolution transmission electron microscopy
InAs	Indium arsenide
IL-6	Interleukin6
InP	Indium phosphide
IR	Infrared
KCl	Potassium chloride
LDH	Lactate dehydrogenase
Ltd	Limited company
LUMO	Lowest unoccupied molecular orbital
MβCD	Methyl-β-cyclodextrin

MTT	3-(4,5,-Dimethylthiazol-2yl)2,5- diphenyltetrazoliumbromide
NPs	Nanoparticles
$^1O_2$	Singlet oxygen
$O_2^{\bullet-}$	Superoxide anion
OECD	Organisation for economic co-operation development
$OH^{\bullet}$	Hydroxyl radical
OS	Oxidative stress
P	Pennicilin
PAAc	Poly-acrylic acid
PAH	Polycyclic aromatic hydrocarbon
PBS	Phosphate Buffered Saline
PCR	Polymerase chain reaction
PEG	Polyethelene glycol
PET	Positron emission tomograpy
PL	Photoluminescence
PPO	Poly (p-phenylene oxide)
PTFE	Polytetrafluoroethylene
QDs	Quantum dots
qPCR	Quantitative real time polymerase chain reaction
RNase	Ribonuclease
ROS	Reactive oxygen species
SD	Standard deviation
SI	International system of units
SiNP-COOH	Carboxylated silicon nanoparticle
SiQDs	Alkyl-capped silicon quantum dots
SSBs	Single strand beaks
TEM	Transmission electron microscopy
THF	Tetrahydrofuran

TNF-α	Tumour necrosis factor alpha
Tris-HCl	Tris hydrochloride
ufCB	Ultrafine carbon black
UFPs	Ultrafine particles

Chapter 1. General Introduction

1.1 Nanoparticles

Nanotechnology and nanoscience originate from the idea to make new devices and materials by exploiting the ability to change the structure of matter at very small (<100 nanometre (nm)) length scales (Leary, 2010, Doak et al., 2012). In particular, small particles of semiconductors show dramatic changes in the electronic structure compared to the bulk forms (O'Farrell et al., 2006). These changes are a result of the quantum confinement effect (O'Farrell et al., 2006, Roduner, 2006) and manifest themselves most notably in the optical spectra of the particles. Materials which do not emit luminescence in the bulk or emit only at wavelengths outside the visible range (400-700 nm) may become brightly fluorescent on the nanoscale, e.g., cadmium selenide (CdSe), silicon (Si) (O'Farrell et al., 2006). The rapid growth of knowledge of new material properties is paralleled by the exponential growth of applications. However, knowledge regarding the interaction of nanomaterials with the environment, animals, and humans generally lags behind (O'Farrell et al., 2006).

The nano prefix word has been used worldwide and ‘nano’ originated from the Greek meaning ‘dwarf’. In science it is a prefix whose meaning is one billionth. One billionth is equivalent within the international system of units (SI) of nanometre (nm) is equal to one-billionth of a metre, 10^{-9} m (The Royal Society, 2004, Buzea et al., 2007). Nanoscience is the part of science in which the properties of materials which have at least one small (<100 nm) dimension are studied and also include synthesis, characterisation and explanation of the novel properties that arise. Nanotechnologies are the technologies to take advantages of the unique properties of the small materials to generate novel tools or devices. Nanotechnology and nanoscience have great potential benefits and to increase the applications of materials in multidisciplinary fields including electronics, sensing and healthcare. Nanomaterials at the size range 1-100 nm reveal unique properties compared with the original materials (bulk): particularly surface area and quantum effects. These effects alter physicochemical properties and may lead to increased chemical reactivity as well as changed optical, magnetic and electrical properties. This particle size range of nanometres (nm) is also found in nature, for example as pollutants and viruses. Viruses have diameters or lengths in the range 10-150 nm and they are well-

known biological nanoparticles which also internalise into human cells by endocytosis mechanisms (The Royal Society, 2004, Eash et al., 2004). Nanoparticles have been found in nature; either as pollutants produced by deliberate manufacture or from natural processes. They have been produced by the photochemical activity of plants and algae, volcanic activity, combustion, and by human manufacturing, e.g., metal oxides (The Royal Society, 2004).

Nanomaterials or nanoparticles have been categorised into 3 categories: those with one ‘nano’ dimension such as thin films, layers, engineered surfaces; two ‘nano’ dimensions such as tubes and wires and three ‘nano’ dimensions such as particles, precipitates, colloids, and quantum dots (The Royal Society, 2004). The one and two dimensional nanomaterials are typically found in electronic device manufacture, chemistry, and engineering. The three dimensional nanomaterials are a huge group of nanoparticles and have been generated from various methods and sources. Nanoparticles can also be categorised into (at least) five groups: metal nanoparticles, metal-oxide nanoparticles, semiconductor nanoparticles, quantum dots (QDs) and fullerenes (Hardman, 2006, Singh et al., 2009).

In nanoparticles prepared from metals and semiconductors, the bond lengths and energies in the small particles are typically different from the bulk owing to the large fraction of the atoms that reside on the particle surface and play a crucial part in producing the alteration in the properties of nanomaterials compared to the bulk (Roduner, 2006). Another effect that occurs in small particles of semiconductor is the quantum confinement effect (Roduner, 2006). For QDs specifically, gaining knowledge of synthesis, physico-chemical properties, biological applications, biological interactions and mechanisms of interaction is important. QDs have an altered electronic structure. The energy levels are more widely separated and generate a larger band gap. The band gap in QDs determines the luminescence energy and colour (O'Farrell et al., 2006). From this perspective, the electronic structure of QDs is midway between that of bulk material (continuous energy bands with gaps) and molecules (discrete energy levels). The luminescence of QDs as of organic molecules has characteristics which are a consequence of their electronic structure (O'Farrell et al., 2006). Although both QDs and organic dyes generate

luminescence, QDs also have advantages over organic dyes with low sensitivity to high energy light and the ability to emit multiple colours with one excitation wavelength (Bruchez et al., 1998, O'Farrell et al., 2006). QDs are less susceptible to degradation under intense laser irradiation in a confocal microscope (O'Farrell et al., 2006).

1.2 Quantum Dots (QDs)

Semiconductor nanomaterials that are confined in all three dimensions are known as quantum dots (QDs). Often QDs are composed of a crystalline core and a layer of cap or shell which serves to protect and isolate the core from the environment (Hardman, 2006). Typical quantum dots consist of elements in groups II and VI (CdSe, CdTe, CdS, ZnS, and ZnSe), groups IV and VI (PbS and PbSe, or groups III and V (GaAs, GaN, InP, and InAs) (Erogbogbo et al., 2010). QDs in the size range smaller than the Bohr radius of the exciton reveal unique physicochemical properties and quantum confinement effects (Hardman, 2006). Quantum confinement results in an increase in the band gap, the threshold at which QDs absorb light is at an energy level higher than in bulk particles. In the limited space of a QD the electron-hole pair (exciton) formed by absorption of light is confined by the surface of the particle and this is responsible for the increase of the gap (Michalet et al., 2005). The size of the QDs is therefore a key factor to produce strong luminescence of controlled wavelength (Parak et al., 2005). **(Figure 1.1)** (O'Farrell et al., 2006). In general, smaller particles produce luminescence at higher energy, i.e., towards the blue end of the visible spectrum.

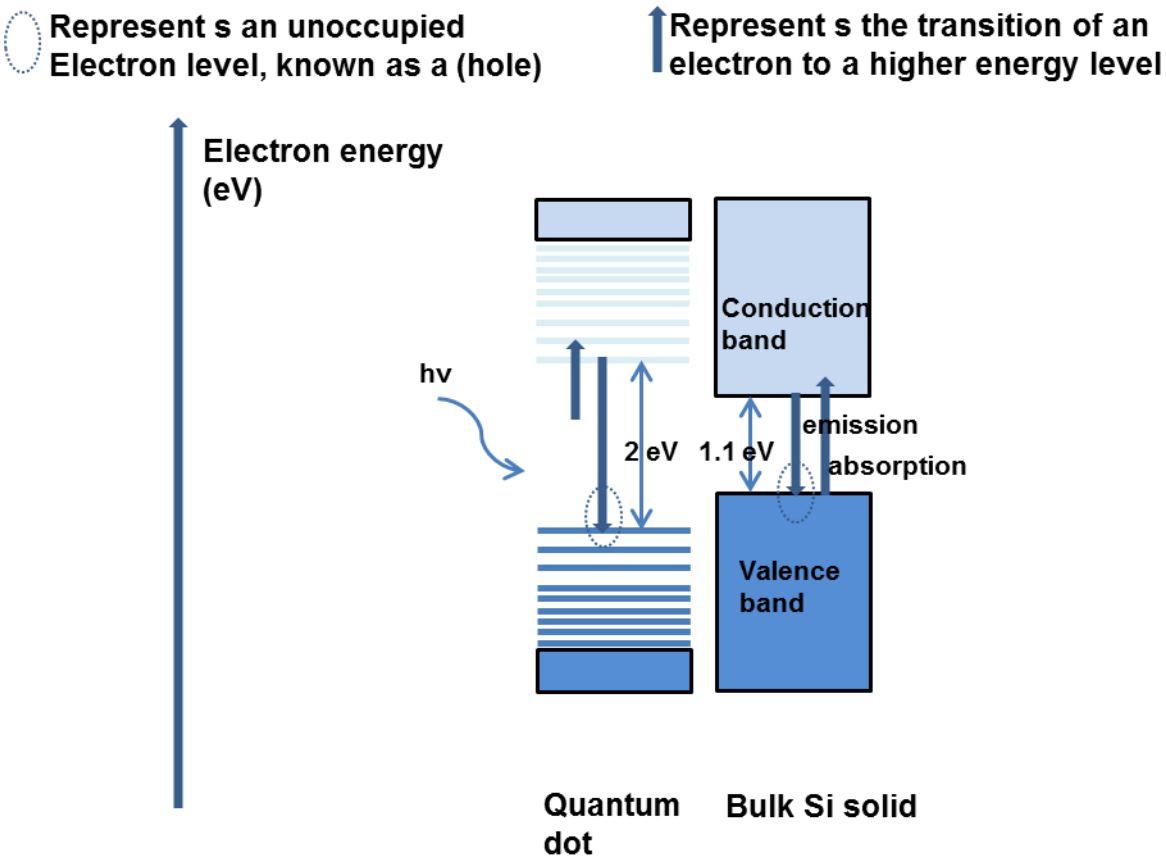

Figure1. 1 Schematic showing electron states of bulk and quantum dot. The bulk solid has continuous energy bands while the quantum dot has sequence of energy levels between two bands. The diagram was adapted from O'Farrell and colleagues, 2006 (O'Farrell et al., 2006).

Photo stable QDs with size-tuneable fluorescent emission are now widely employed in labelling techniques to investigate cells and cellular processes even to the level of tracking individual molecules (Fu et al., 2005, Parak et al., 2005). Initial investigations of QDs were focused on synthesis, characterisation and achieving a monodisperse distribution (narrow size). In the mid-1990s, there was a breakthrough in the development of synthetic routes to semiconductors comprising elements in groups II –VI; these syntheses provided highly crystalline material with good control over the particle size (Murray et al., 1993, Hines and Guyot-Sionnest, 1996). These syntheses employed organometallic reagents at high temperature in a high boiling point coordinating solvent (trioctylphosphine oxide). The QDs comprise a luminescent CdSe core and are generally capped with a shell of ZnS. ZnS has a larger energy gap than CdSe and therefore does not absorb the emitted light. It is crucial for the maintenance of the luminescence in biological media (Hines and Guyot-Sionnest, 1996, Dabbousi et al., 1997).

Zinc sulphide – capped cadmium selenide (CdSe) QDs have been studied further and researchers moved from development of synthetic methods and characterisation to in vitro biological investigation in human tumour-derived cell lines (e.g., HeLa) (Chan and Nie, 1998). In order to target specific molecules in the cell, QDs have been covalently bonded to antibodies (to target proteins, viruses) or oligonucleotides (to target nucleic acid sequences), Mercaptoacetic acid ligands or organic polymer coatings are used to make covalent bonds between the ZnS shell and the biological molecules; they also help to improve the water solubility of the QDs (Chan and Nie, 1998). Nowadays, such QDs are commercially available in defined sizes (colours) with a range of bioconjugates (antibodies, DNA probes) and are widely used as alternative fluorescent labels to organic dyes and/or radioactive tracers. They show high sensitivity and lower toxicity or adverse health effects than many of the alternatives.

New ways to prepare QDs with high biocompatibility have also drawn attention from many researchers. Hydrophilic QDs with phospholipid block-copolymer micelles help to increase applications of CdSe(ZnS) in *in vitro* and *in vivo* biological fluorescent labelling (Dubertret et al., 2002). Injection of QDs conjugated into micelles into Xenopus embryos revealed no adverse effects and

stable, long-term fluorescence was observed which allowed their use to trace the development of the embryo and determine cell lineage (Dubertret et al., 2002).

Fluorescent labelling is a powerful technique for exploring cell structure and cell function, but it is reliant on suitable fluorescent dyes. Organic dye molecules produce fluorescence following absorption of light to promote an electron from the highest occupied molecular orbital (HOMO) to the lowest unoccupied molecular orbital (LUMO). When the electron falls back into the HOMO, the energy difference is emitted as fluorescence. Although organic dyes have the capacity to aid microscopic examination of the cell and cell organelles, they are unable to maintain high intensity fluorescence for long periods of time because of photochemical side reactions that lead to degradation of the dye (O'Farrell et al., 2006).Therefore QDs, which are less sensitive to high energy irradiation and more stable during observation, are becoming popular as alternative choices for fluorescent labelling (Warner et al., 2005). The most studied of these new chromophores for biological labelling are CdSe quantum dots. CdSe with a ZnS shell emits light in the visible region and shows remarkable size-tuneable fluorescent emission (Medintz et al., 2005). Different sizes of CdSe with a ZnS shell QDs from left to right emitted different colours (blue to red) excitation with a single near –UV lamp **(Figure 1.2)**.

Another advantage of QDs over organic dyes lies in multicolour imaging. This has been achieved by embedding CdSe(ZnS) QDs of various sizes inside polymeric microbeads. One excitation wavelength in the near UV range (Mercury lamp) is sufficient to produce fluorescence from all the various-sized QDs in the microbeads and can even be used to encode the beads according to the particular combination of QDs embedded (Han et al., 2001). **Figure 1.1** illustrates in a schematic manner that absorption of a single high energy photon can occur over a wide range of energies because of the remnants of the bulk band structure; in molecules, only discrete energy levels are present and a separate excitation wavelength is often required to excite each dye.

QDs that are highly photo-stable with size tuneable fluorescent emission are being incorporated into new techniques along with powerful traditional

fluorescence labelling techniques to investigate cells and cellular process at the level of individual molecules (Fu et al., 2005, Parak et al., 2005). QDs are increasingly used as an alternative technique for biomedical applications over routine fluorophores in areas including multi cellular imaging, long term studies both *in vitro* and *in vivo*, high resolution tissue imaging and individual molecule trafficking (Fu et al., 2005).

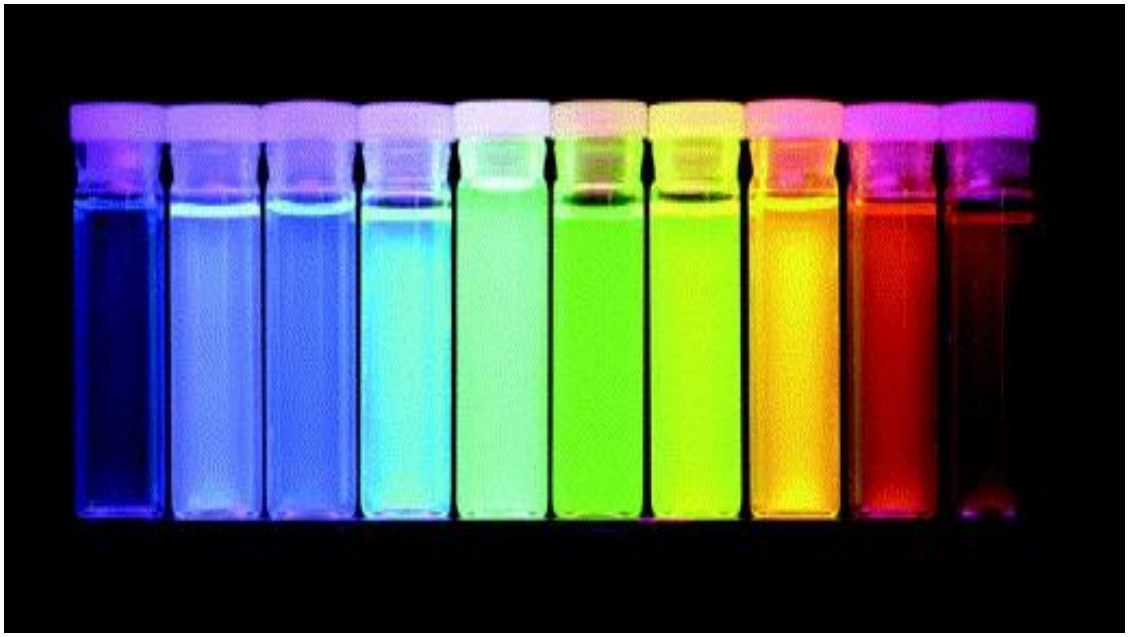

Figure 1. 2 The image shows ten luminescent colors of CdSe with ZnS shell QDs excited with a near-UV lamp. The colors show the range of particles sizes started from small to bigger size left to right (blue to red). The wavelengths correspond to fluorescent colors are 443, 473, 481, 500, 518, 543, 565, 587, 610, and 655 nm, respectively (Chan et al., 2002).

Despite the success of ZnS-capped CdSe QDs in biological applications, there is still some evidence of leaching of toxic heavy metal ions from the particles over long duration observation together with high intensity light which might be toxic to the cell. In addition the core-shell structure results in a large overall particle diameter of up to 20 nm which makes red-emitting QDs simply too large to be used for some intracellular imaging studies.

1.3 Alkyl- Capped Silicon Quantum Dots (SiQDs)

QDs present several useful points as advanced fluorophores but heavy metal issues are slowing down the process to apply QDs in biological and medical fields (Derfus et al., 2004, Hardman, 2006, Smith et al., 2008, Borsella et al., 2013). Some researchers have shown that the QD shell can restrict the amount of heavy metals in contact with living organisms and environment. However, there is still some difficulty because under biological environments or high intensity energy some studies reveal the release of metal ions from the core (Derfus et al., 2004). The adverse effects of QDs on living organisms result from release of metal ions (Derfus et al., 2004). However, small nanoparticles have a large surface to volume ratio and therefore are also often more reactive than the bulk materials from which they derive; they may therefore also induce toxic effects via other means such as redox reactions (Buzea et al., 2007).

Red photoluminescence from high porosity Si under excitation by a green or blue laser was observed by Leigh Canham in 1990 at room temperature (Canham, 1990); the luminescent image is shown in **Figure 1.3.** Moreover, Si technology is well developed and powerful. Si chips are already incorporated into everyday consumer products including some devices implanted within the body such as pacemakers (Canham, 2000).

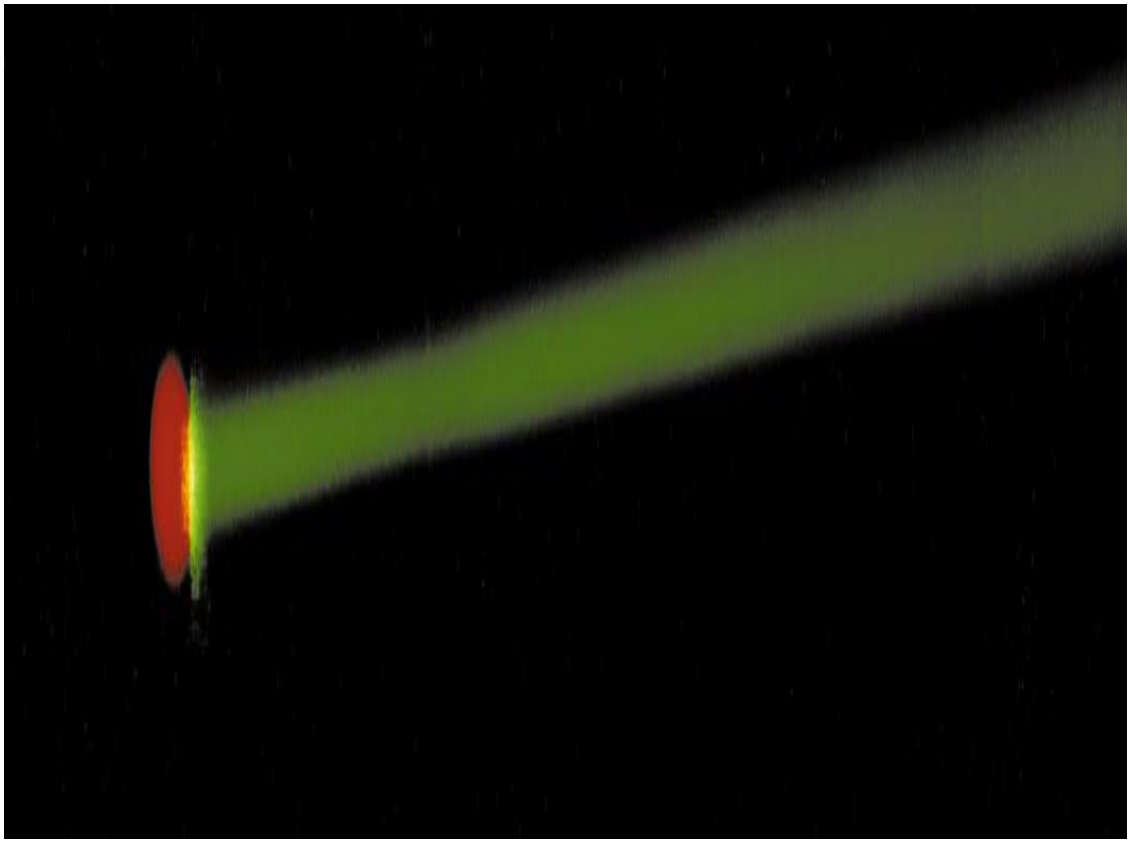

Figure 1. 3 The image shows the first observation of Si luminescence: the strong red luminescent of monocrystalline Si under irradiation by an argon ion laser beam (green light) (Canham, 1990, Canham, 2000).

Due to the unique fluorescence as well as protection from heavy metals resulting in no inherent toxicity, porous and nanocrystal QDs prepared from porous silicon have been increasingly investigated for various biological applications (Lie et al., 2002, Park et al., 2009). Many methods have been proposed to synthesise silicon QDs with visible photoluminescence: porous silicon as well as nanocrystalline silicon, including electrochemical etching and sonication (Sweryda-Krawiec et al., 1999, Lie et al., 2002), reactive sputtering (Furukawa and Miyasato, 1988), sol-gel techniques (Zhang et al., 1998), Si into SiO_2 implantation (Kovalev et al., 1998), self-assembly (Choi et al., 1998), synthesis in inverse micelles (Wilcoxon et al., 1999), laser ablation (Hata et al., 2001), thermal annealing (Schoenfeld et al., 1996), thermal vaporization (Dinh et al., 1996), decomposition of silanes (Littau et al., 1993), solution synthesis (Bley et al., 1996), hybrid techniques (Botti et al., 2001), and plasma processing (Mangolini et al., 2005). However, to achieve useful applications in many fields, the synthesis methodology must be capable of providing a narrow and controllable size distribution, chemical stability, and strong photoluminescence. Si nanoparticles have been widely incorporated in various applications in the electronics field; however current synthetic techniques either produce material that is not monodisperse or is only available in very small amounts. Consequently, Si nanoparticle synthesis is an ongoing field of research. Silicon QDs have high potential as an alternative to II-VI semiconductor QDs and organic dyes (O'Farrell et al., 2006).

1.3.1 Alkyl-Capped Silicon Quantum Dots (SiQDs) Characteristics

Silicon (Si) nanoparticles have been increasingly investigated in multidisciplinary fields: studying physicochemical properties, improving the synthesis process, increasing yield, making the particles stable in physiological conditions, and exploring fabrication methodologies suitable for biological and medical applications. For biological and medical applications high specifications are needed such as: strongly fluorescence, less sensitive to colour quenching, suitable for multicolour investigations, biodegradable, a small particle size suitable for studying at the molecular level as well as low toxicity (O'Farrell et al., 2006).

SiQDs are one type of semiconductor nanoparticles know as quantum dots. The particles sizes are less than 10 nm. SiQDs are composed of a silicon core and covered by a C_{11} alkyl monolayer (C_{11} = undecyl). The core diameter is about 2.5 nm and the diameter of the whole particle including the undecyl capping layer is about 5 nm (Alsharif et al., 2009). A schematic model of the whole particle is shown in **Figure 1.4.** Alkyl-capped silicon quantum dots (SiQDs) are synthesised from porous silicon under high current densities with hydrofluoric (HF) solution (1:1 (HF: ethyl alcohol)) and reacted with undecene by hydrosilation reaction (Lie et al., 2002). Similar to hydrosilanes, the highly active hydrogen-terminated silicon surface undergoes a hydrosilation reaction with the undecene to form an alkyl monolayer in a toluene solution and the layer makes the particles hydrophobic as well as highly stable in the ambient environment. The stability is a result of the strong, inert Si-C bond which anchors the undecyl chain to the Si core. SiQDs are easy to prepare as colloidal suspensions and dry silicon powders using the fabrication method described by Lie et al., 2002. In addition, SiQD preparation using an electrochemical technique, etching is convenient, cheap, and uses pure silicon (Si wafer) (Kang et al., 2011).

SiQDs can be conveniently dispersed in various organic solvents and may also be prepared as non turbid suspensions in physiological solutions with high stability (Dickinson et al., 2008). The photo properties of colloidal SiQDs in aqueous solutions show stability over the pH range of 5-9. SiQDs suspension solutions reveal no turbidity over 6 months (Dickinson et al., 2008). In addition, SiQDs with strong fluorescence, biocompatibility and high stability in physiological solutions have been studied in primary and tumour-derived human cells as fluorescent probes (Alsharif et al., 2009, Park et al., 2009). The SiQDs were found to show no acute toxicity, were successfully used to image tumours and then observed to degrade in mouse after 2 hours of exposure.

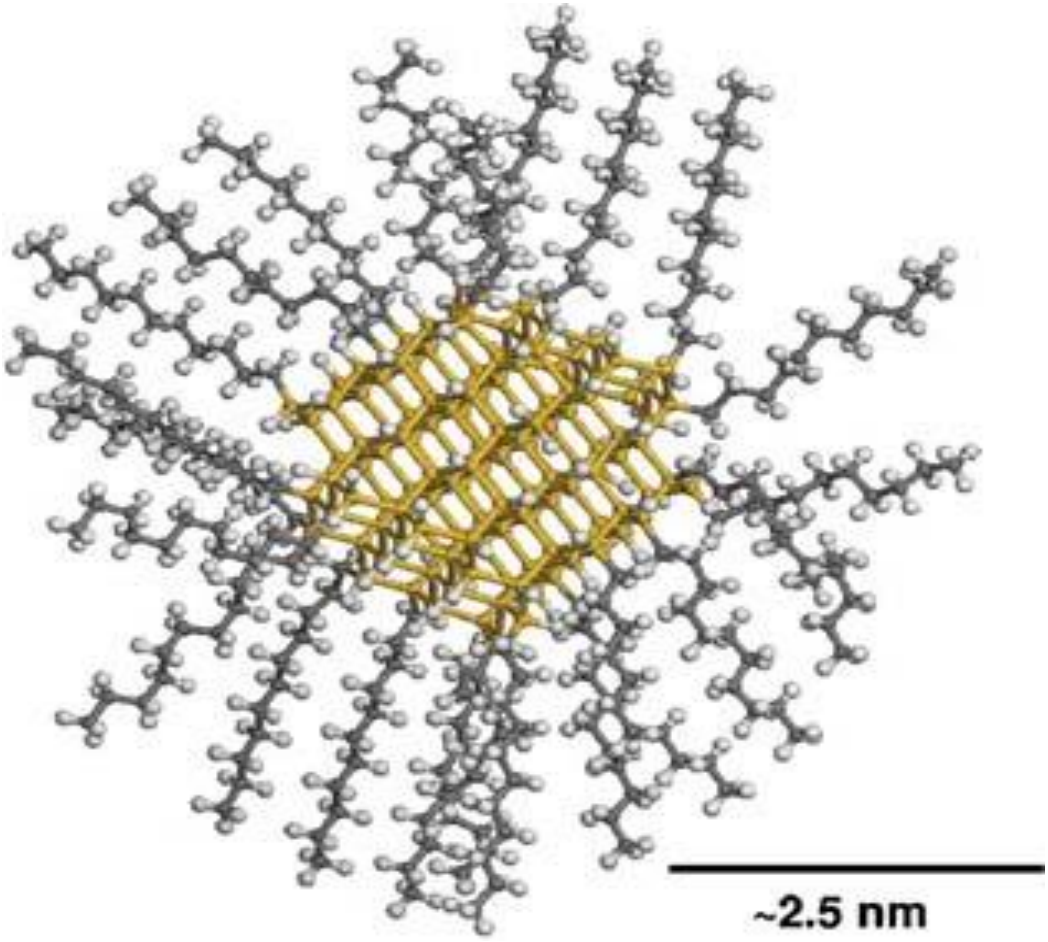

Figure 1. 4 Schematic model of the whole particle of SiQDs. The diameter of the whole particle including the crystalline silicon core and surrounding undecyl layer is about 5 nm. The core itself is width 2.5 nm (Alsharif et al., 2009).

The 11- carbons surrounding the particle core help to stabilise against flocculation and protect SiQDs from oxidation under ambient conditions as well as make the particle hydrophobic (Lie et al., 2002, Dickinson et al., 2008). The Si-C covalently bonding of SiQDs protects the particles from oxidation reactions and the particles are also resistant to strongly alkaline solutions (Lie et al., 2002). Though SiQDs are water insoluble, they may be dispersed in aqueous media after dissolving first in organic solvents in which they are readily soluble. Suitable solvents include tetrahydrofuran (THF), dimethyl sulfoxide (DMSO), diethyl ether (ether), and dichloromethane (DCM).

1.3.2 Alkyl-Capped Silicon Quantum Dots (SiQDs) Physicochemical Properties

The physicochemical changes in metals and semiconductor nanoparticles when the particle size gets smaller are known as quantum confinement effects - the size dependent changes of physicochemical properties. In theory, there are two main effects at nano size stage: the surface effects and the quantum effects (Roduner, 2006). The surface effects changes in reactivity because more atoms are on the particle surface and fewer in the bulk. The quantum effects changes in electronic structure due to confinement (already discussed). According to the quantum effects, the fluorescent characteristics of nanoparticles exhibit a discrete energy level spectrum (O'Farrell et al., 2006). Also the energy gap gets bigger and shows high efficacy of the inter-band radiative recombination because the electron and hole are confined in close proximity as shown in **Figure 1.5** (Canham, 1990).

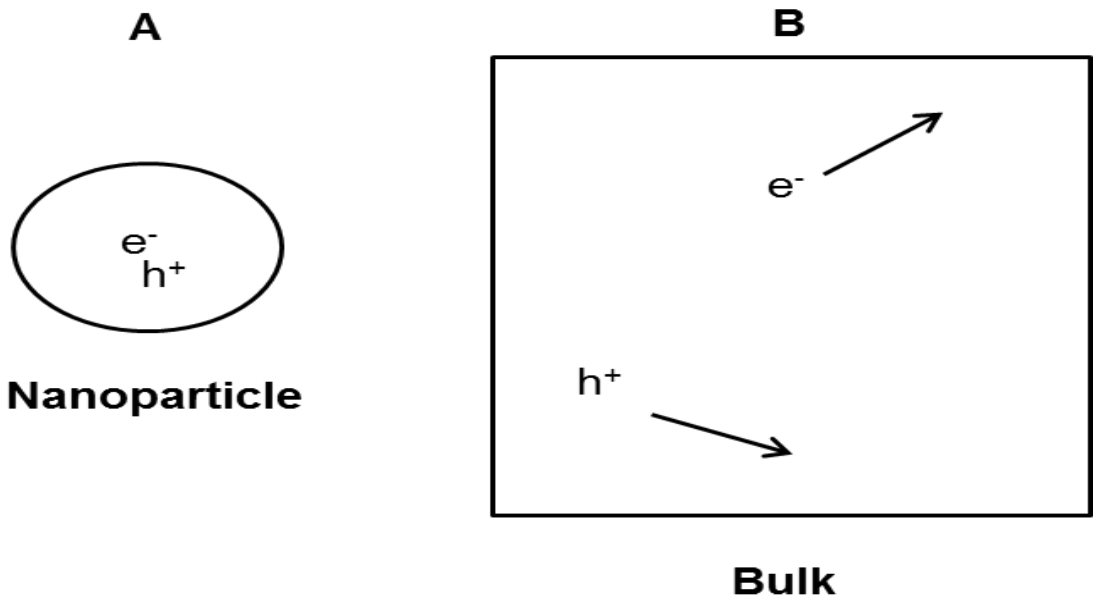

Figure 1. 5 Schematic diagram: **A** shows electron and hole confinement in close proximity in a nanoparticle and **B** shows electron and hole free to move throughout a large space in a bulk sample. In **A** the chance of electron-hole recombination is greater and this increases the quantum yield of fluorescence and the brightness.

Therefore, the two characteristics of nanoparticles surface area and electrical properties have a huge impact on the physicochemical properties, and in addition these properties are very sensitive to diameter change. There has been intense research into the properties and potential applications of Si nanomaterials with many studies synthesising particles and trying to find out the correlation between particle size and electrical characteristics. In 1988, Furukawa and Miyasato fabricated binary nanoparticles: small crystalline silicon particles with a hydrogen shell. Determination using reactive sputtering technique revealed an optical band gap of 2.4 eV inside the Si:H nanoparticles (particle size 20-30 Å). The optical band gap is increased about two-fold in Si:H nanoparticles (20-30 Å) when compared with the bulk Si optical band gap (1.1 eV width) (Shirahata, 2011). Moreover, the mesoporous Si layers produced from high porosity bulk Si wafer using electrochemical and chemical technique also showed photoluminescence (excited with green or blue laser) (Canham, 1990). This implied that the altered diameter, mesoporous Si had higher band gap energy than the bulk material.

The luminescent Si nanoparticle can also be prepared as a luminescent colloidal silicon suspension (Heinrich et al., 1992). To make the luminescent silicon suspension, an electrochemical technique was used to break down the porous Si of silicon wafer (n or p type) and disperse it into organic solvents such as methylene chloride, acetonitrile, methanol, and toluene (Heinrich et al., 1992). Transmission electron microscopy (TEM) revealed that the Si particles had high surface area with irregular shapes and strongly polydisperse size distribution including both micrometre and nanometre sizes (Heinrich et al., 1992).

Si is a well-known and important material in microelectronics and most Si comes from flat, crystalline silicon wafers (Buriak, 1999). Immediately when a Si wafer is exposed to the air the single crystal Si is coated with oxygen (O_2) and turned into Si oxide (Buriak, 1999). Si oxide has proved to be a very useful in passivating bulk Si and it is well used in electronic devices (Buriak, 1999). The crystalline Si and the Si oxide on the top of Si wafer have been broken down into porous Si using ultrasonic dispersion in organic solvents (Bley et al., 1996). The particle characterisation of porous Si using high-resolution transmission electron microscopy (HRTEM), Fourier transform infrared spectroscopy (FTIR), and fluorescence spectroscopy revealed heterogeneous particles sizes with the diameters in the range of 2 to 50 nm (Bley et al., 1996). The porous Si also containing the oxidised form showed a unique photoluminescence (PL) spectrum at 680 nm and between 415 to 446 nm using fluorescence spectroscopy. It was proposed that the red fluorescence at 680 nm was attributed to quantum confinement effects and the blue fluorescence between 145 to 446 was attributed to extremely small crystalline Si (Bley et al., 1996). The surface area and the electrical properties are the key factors in properties of nanoparticles.

1.3.3 Alkyl-Capped Silicon Quantum Dots (SiQDs) Preparation

Since Canham, (1990) accidently discovered photoluminescence of mesoporous Si this has also advanced nanotechnology. Consequently, because of its unique physicochemical properties, porous Si has been fabricated and incorporated into the optical and electronic elements of integrated circuits as

well as being used for studying fundamental photoluminescence characteristics (Buriak, 1999). Moreover, most porous Si is prepared directly from oxidised Si crystallites. Using stable form of porous Si, SiQDs have been prepared using electrochemical etching. In this procedure, the oxide surface of crystallite Si is replaced with the hydride terminated (Si-H) form. The hydrogen-terminated silicon exhibits similarities in behaviour to molecular hydrosilanes (Lie et al., 2002). To make stable SiQDs with less sensitivity to ambient conditions, the alkyl termination (Si-C) is inserted by a hydrosilation reaction at hydride terminated Si. The Si-C bonds can be formed by direct reaction with the undecene and no catalyst. The alkyl termination also allow passivation with other chemicals to increase SiQDs applications (Bateman et al., 1998).

1.4 Biomedical Applications of Alkyl-Capped Silicon Quantum Dots (SiQDs)

As they are composed of just a crystalline silicon (Si) core surrounded with alkyl monolayers, SiQDs have a very small size and are stable in an aqueous environment. Moreover, SiQDs emit strong fluorescence at the red end of the visible region which is low emission in cells as well as cell organelles (O'Farrell et al., 2006). In addition, SiQDs reveal outstanding characteristics such as the ability to be monitored, high surface areas, and biocompatibility. It has been suggested that the small size of SiQDs which is similar to some cell organelles increases the potential of SiQDs to internalise into cells. Their characteristics are promising for biomedical applications as fluorescent probes both *in vivo* and *in vitro*. Consequently, they can be classified as multifunctional nanoparticles based on their physicochemical characteristics which make them potentially suitable for both diagnosis and treatment of disease at the same time (Park et al., 2009).

SiQDs were used as fluorescent labels in in vitro studies by Alsharif and colleagues in 2009 in the first study of cytotoxicity. They found SiQDs accumulated inside cells and found no adverse effects in malignant and non-malignant cells. Moreover, the internalisation and accumulation of SiQDs were high in malignant cells. In addition, the internalisation process was completely blocked by well-known inhibitors of cholesterol-dependent endocytosis. They

proposed that in HeLa and SW1353 cells, the internalisation process was cholesterol dependent (Alsharif et al., 2009).

A number of cell imaging studies have used Si quantum dots as probes to study cell function and cell organelles. But not many studies have used simple SiQDs directly to study the cells. Almost the entire cell imaging studies used different bio-conjugated Si molecules for many purposes particularly for specific cell targets as well as to improve the solubility of the particles. Si has been conjugated with an oligonucleotide together with a photo inducer and used for DNA labelling (Wang et al., 2004). Proving stable and remaining fluorescent in aqueous solution as well as a valuable optical probe, Si was coated with phospholipid micelles (Erogbogbo et al., 2008). Fujioka and colleagues employed the active form of Si nanoparticles, Si oxide for studying oxygen radical production in harmful environments and compared this with the use of cadmium selenite (CdSe). They found ten times less toxicity of Si oxide than CdSe upon exposure to UV (Fujioka et al., 2008). Amino-terminated Si has also been studied in HepG2 cells. The cells accumulated Si quantum dots with strong fluorescence distributed throughout the cells without cytotoxicity effects based on confocal microscopy and assessment of cell viability within 48 hours by the MTT assay (Ahire et al., 2012). Si quantum dots with various biological conjugations (lysine, folate, antimesothelin, and transferrin) have also been studied using human pancreatic cancer cells (Panc-1) (Erogbogbo et al., 2011a). Si with different charges conjugated with amine, azide, and carboxylic acid have been used as a cell labelling probe to study cytotoxicity effects of surface charge and oxidative stress in a macrophage cell line NR8383 (Bhattacharjee et al., 2010). This study found that cytotoxic effects and ROS production were higher from positively and neutrally charged Si nanoparticles than from those with a negative charge. Positively charged particles are more toxic because they can penetrate cells and organelles more easily. In addition, they are capable of generating ROS more effectively than neutral or negatively charged particles (Bhattacharjee et al., 2010, Froehlich, 2012). To adjust the physicochemical properties of Si for biological applications, using biocompatible materials is important. Si has been conjugated with poly-acrylic acid (PAAc) to improve stability and increase fluorescence and this showed low cytotoxicity in

several mammalian cell lines (HHL5, HepG2, and 3T3-L1) within 24 and 48 hours (Wang et al., 2012).

The toxicity issues relating to traditional quantum dots (cadmium selenite, CdSe) remain an important concern for QD applications in biological and medical fields (O'Farrell et al., 2006). Many studies have applied functional techniques to cover and hide the heavy metals to decrease or get rid of the adverse effects. However, under ambient environment and at long exposure times (for 2 to 8 hours) with high intensity irradiation during confocal microscopy, the biocompatibility might be altered with the heavy metal or the core revealed (Derfus et al., 2004). Unlike traditional QDs, SiQDs do not contain any heavy metals. Likewise, SiQDs are stable under strong luminescence. The optical properties are also less sensitive to high intensity energy during prolonged investigation under a fluorescent microscope compared with conventional organic fluorophores (Alivisatos, 2005, Michalet et al., 2005, Ipe et al., 2005, O'Farrell et al., 2006) Consequently, SiQDs have been used as alternative safety choice of traditional QDs for cell imaging and biological probe as well as use as a template for studying the role of surface charge to generate cytotoxicity effects (Wang et al., 2005, Erogbogbo et al., 2008, Alsharif et al., 2009, Park et al., 2009, Bhattacharjee et al., 2010, Shen et al., 2011, Tu et al., 2011, Erogbogbo et al., 2012, Ohta et al., 2012). However, silicon dioxide (SiO_2) can be generated when silicon (Si) nanoparticles (NPs) are exposed to an aerobic atmosphere in biological and medical applications (Bhattacharjee et al., 2010). Moreover, Si NP surface groups may vary in their toxicity effects depending on the charge of the group (Lie et al., 2002, Ruizendaal et al., 2009). Many researchers are interested in making Si NPs stable and safe in a biological environment.

1.5 Toxicity studies on Nanoparticles

1.5.1 General Toxicity of Nanoparticles

Many studies using quantum dots (QDs) as fluorescent labels have shown that these QDs are strongly luminescent probes but there remain concerns about the use of heavy metals such as Cd. A significant concern is the toxic effects of

heavy metal contamination and release to biological materials (O'Farrell et al., 2006). Furthermore, the size of QDs, which are less than 100 nanometre (nm), may result in different pathways of uptake in tissues and cells. QDs have been widely used, leading to increase concern about their toxicity and potential impact on the environment (Hardman, 2006). The impact of QDs on living organisms and the environment do not just originate from their physicochemical properties, but also from the composition of the QD. The composition of most QDs is metallic or semiconducting and most QDs are hydrophobic and may accumulate in membranes. Many researchers are interested in developing novel technologies to make QDs even more powerful tools for biology and medicine. Furthermore, QDs which absorb energy and emit fluorescence, can also generate reactive oxygen species which may cause adverse effects to living organisms (Oberdorster et al., 2007). Li et al (2003) studied the effect of particle size and composition on cellular uptake and toxicity. They found that ultrafine (100 μm) particle (UFPs) with a polycyclic aromatic hydrocarbon (PAH) coating had the potential to cause mitochondrial damage in macrophages and epithelial cells via oxidative stress (Li et al., 2003). Kirchner et al. (2005) studied the cytotoxicity of QDs (CdSe and CdSe/ZnS) with various surface modifications, including QDs coated with mercaptopropionic acid, silane, and polymer. They studied cytotoxicity of these QDs in various cell lines such as fibroblasts and breast cancer cells (Kirchner et al., 2005). They found that many parameters were associated with toxicity, including the release of Cd^{2+} ions from the core, the coating material, the stability of the particles, and perturbation of ion channels (Kirchner et al., 2005). Localization studies of heavy metals, cadmium chloride and QDs containing, CdTe/ZnS/PEG500 found that QDs accumulated with time in immunologic cells while cadmium chloride ($CdCl_2$) did not accumulate (Yeh et al., 2011). The oxidative stress and cell signalling effects on macrophage cells by various surface coated quantum dots (CdTe/CdSe/ZnS) were characterized by Clift et al (2010). QDs showed effects on oxidative stress parameters on the basis of a decreased glutathione (GSH) concentration and impaired ability of the antioxidant Trolox to protect the cells from stress. Calcium (Ca^{2+}) and pro-inflammatory cytokine tumour necrosis factor-alpha (TNF-α) were measured to determine cell signalling effects. The researchers suggested that organic QDs caused oxidative stress and disturbed cellular signalling (Ca^{2+}) in macrophages (Clift et al., 2010). Hepatotoxicity effects of QDs

(Cd/Se/Te/ZnS/PGE-5000) have been studied in mice (Lin et al., 2011). The results showed that QDs 705 altered the balance of antioxidant systems, the uptake of essential elements and induced inflammation. However, liver morphology was unaffected.

1.5.2 Cytotoxicity

Cytotoxicity studies are a widely used technique for evaluating potential biological effects of nanoparticles in in vitro models. They have been used to investigate cellular interactions with nanoparticles. They are useful tools for investigation of the mechanism of nanoparticle adverse effects (Fotakis and Timbrell, 2006). The common cytotoxicity assays include 3-(4,5-dimethylthiazol-2yl)-2,5-diphenyltetrazolium bromide (MTT), lactate dehydrogenase leakage assay (LDH), neutral red, and protein assay (Fotakis and Timbrell, 2006). Specific cytotoxicity designs to investigate the unique cellular responses include measurement of adenosine triphosphate (ATP) production, reactive oxygen species production (ROS) and cellular inflammatory responses including tumour necrosis factor-alpha (TNF-α), interleukin6 (IL-6), and nitric oxide (NO) production. Various cell lines have been explored as models of specific target organs to find out the adverse effects of nanoparticles. Multi-safety evaluations are still needed for overall safety evaluation studies of nanoparticles.

Oxygen-passivated Si-QDs have been used for biological labelling in living cells. The cytotoxicity effects of these QDs on HeLa cells were investigated using LDH release assay, succinate dehydrogenase mitochondrial activity, and superoxide anion detection assay (Fujioka et al., 2008). Low toxicity of Si-QDs under UV exposure compared with cadmium selenite QDs (CdSe-QDs) which caused cytotoxicity by increasing radical production was shown. The safely of Si nanoparticles and microparticles in macrophages (RAW 264.7) was investigated by measuring MTT (mitochondrial dye reduction), Trypan blue assays, and the inflammatory biomarkers TNF-α, IL-6, and NO (Choi et al., 2009). This study found changes induced by both types of particle but low concentrations of nanoparticles did not affect cell viability or inflammatory markers. The cytotoxicity effects of Si nanoparticle (NPs) with a series of different surface charges (positive, neutral, and negative) have been studied in

CACO-2 cells using the MTT and 5-bromo-2-deoxyuridine (BrdU) assays to assess cell proliferation (Ruizendaal et al., 2009). This study found differences between the surface charges with negatively charged NPs less cytotoxic. The surface charge of Si QDsc to generate cytotoxicity effects on rat macrophages (NR8383) has been investigated using MTT and ROS determination assays (Bhattacharjee et al., 2010). This study concluded that surface charge was important in determining toxicity. In order to establish safe concentrations of nanotechnology materials that can be used without disturbing cellular activities and functions, colorimetric MTT and Trypan blue staining assays have been used to evaluate the safety of chemical poly-acrylic acid (PAAc) coated on silicon (Si) quantum dots (QDs) on human liver cells (HHL5, HepG2) and mouse embryonic fibroblasts (3T3-L1)(Wang et al., 2012). That study found that the coated QDs did not affect cell morphology, cell proliferation or viability, and did not cause DNA damage in the cell lines studied. The cytotoxicity effects of amine-terminated Si NPs on HepG2 cells have been investigated using the MTT assay but no significant toxicity was detected (Ahire et al., 2012). Recently, the mechanisms by which nanoparticles might cause cytotoxicity have been suggested to involve effects on parameters such as mitochondria membrane potential ($\Delta\psi_m$), cytoplasmic free Ca^{2+} content, and caspase-3 activity. The cytotoxicity effects of Si NPs with different charged groups together with germanium NPs on CACO-2 cells and rat alveolar macrophage cells (NR8383) have been examined using MTT, BrdU, ROS assays, mitochondrial membrane potential, ATP content, cytoplasmic free Ca^{2+} content, TNF-α, and caspase-3 activity (Bhattacharjee et al., 2013). The results obtained were complex but cationic NPs showed the most cytotoxicity with carboxylic acid-coated, dextran-coated and PEG-coated Si and Ge NPs displaying no toxicity. The cytotoxicity with positively charged NPs could be detected by the MTT assay but there were other effects including increased levels of ROS, decreased mitochondrial membrane potential and increased caspase-3 activity and it was suggested that mitochondria played a key role in toxicity.

Though there have been quite a few studies on possible toxicity of other Si NPs in mammalian cells as summarised above, information on SiQD interaction with mammalian cells is very limited. There is one study from Alsharif et al. (2009) which reported SiQD internalization by HeLa with no harmful effects.

1.5.3 Oxidative Stress

Oxidative stress is a result of the imbalance of cell activity, with a high production of reactive oxygen species (ROS) and decreasing levels of antioxidants (Singh et al., 2009). Nanoparticles, size (< 100 nm), large surface areas and containing transition metal ions have a strong potential to generate cellular oxidative stress. There are two main hypothesises by which QDs could generate free radicals: photogenerated and surface oxide generated (Green and Howman, 2005). The possible pathways by which NPs might generate reactive oxygen species (ROS) and the effects of this including possible DNA damage are summarised in **Figure 1.6.**

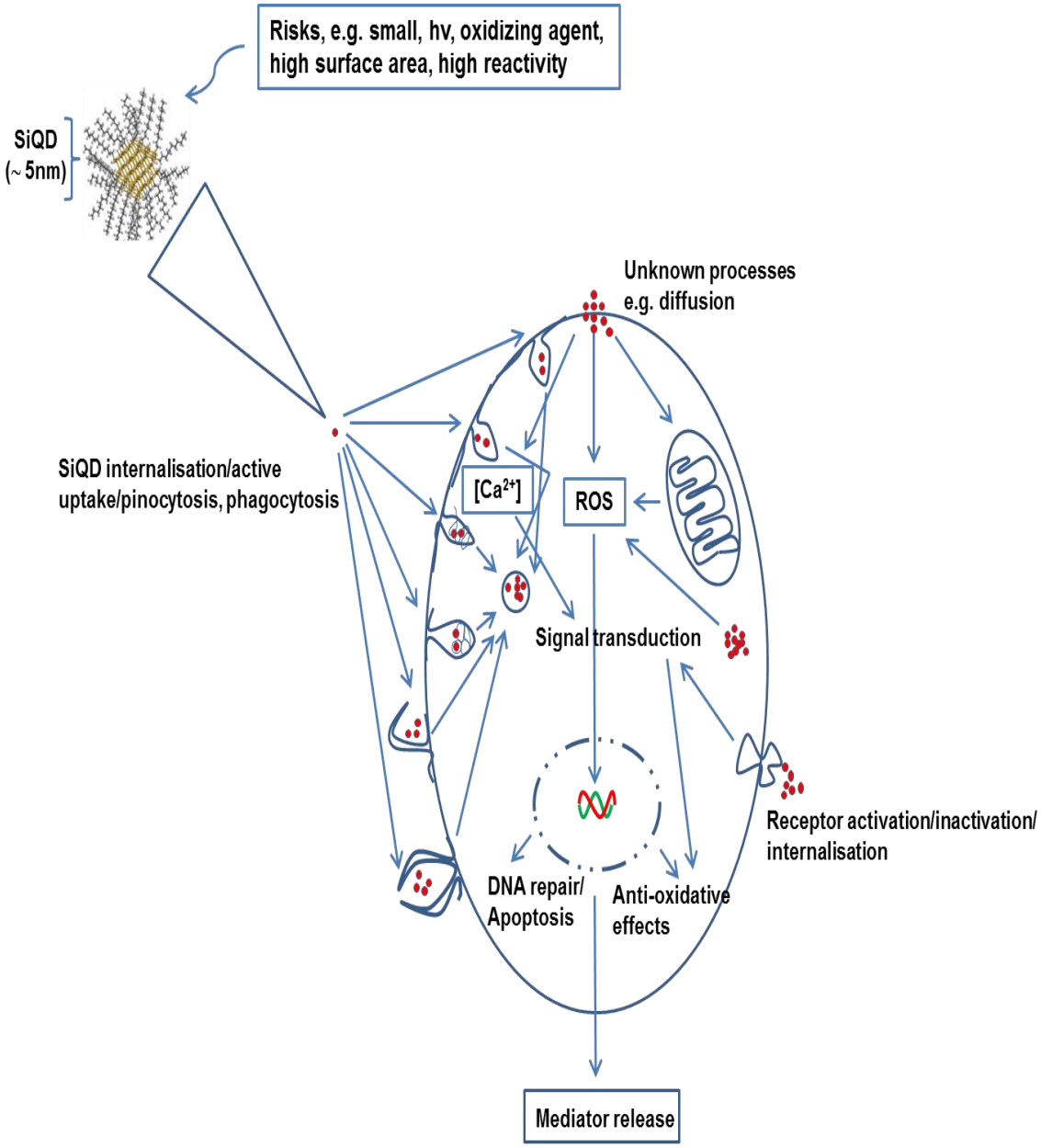

Figure 1. 6 Possible pathways of internalization and the mechanisms by which alkyl-capped silicon quantum dots (SiQDs) generate ROS and cytotoxicity (Simko and Mattsson, 2010).

Ultrafine (UFPs) (< 0.1 μm) and fine (<2.5 μm) have been localised inside treated murine macrophage (RAW 246.7) and human bronchial epithelial (BEAS-2B) cells using electron microscopy. When these cells were exposed to UFPs (containing organic carbon and polycyclic aromatic hydrocarbon (PAH)) they showed high expression of oxidative stress markers: increased haem oxygenase-1 (HO-1), decreased intracellular glutathione, and increased free radical production (ROS) (Li et al., 2003).

There have been few studies that considered oxidative stress-induced effects of Si NPs. However, Sood and colleagues reported that NP accumulation inside cells was a possible cause of indirect DNA damage via ROS production (Sood et al., 2011).

1.5.4 Genotoxicity

Genotoxicity is the potential of the test substance to induce DNA damage (Singh et al., 2009). Carcinogenesis and fertility abnormality are strongly correlated with DNA damage and genotoxicity. QDs might promote DNA damage via a free radical pathway or some other effects on DNA possibly by direct interaction. (Singh et al., 2009, Sood et al., 2011). There are three possible mechanisms involved in genotoxicity. Nanoparticles may generate reactive oxygen species (ROS) thereby altering the balance of redox homeostasis. Consequently, the highly production of reactive oxygen species interact to the cellular macromolecules (DNA). Secondly, oxidative stress produces free radicals and leads to an inflammatory response. The cells respond to tissue injury or infection by releasing a large variety of soluble factors including cytokines and ROS. Finally, when DNA damage occurs, they invoke various cellular responses such as cell apoptosis and p53 gene triggers apoptosis (extensive DNA damage).

There is no standard safety evaluation in general available to assess genotoxicity of nanomaterials at the moment. The alteration of genetic material can cause reactions such as carcinogenesis or have a reproductive impact (Doak et al., 2012). According to the Organization for Economic Co-operation

and Development (OECD) there are three standard guidelines for genetic material toxicity evaluation; bacterial reverse mutation test (OECD 471), in vitro micronucleus assay (MNvit OECD 487), and HPRT forward mutation assay (OECD 476). The bacterial reverse mutation test or Ames test explores the mutation point of Salmonella Typhimurium and Escherichia Coli by using essential amino acid requirements. Mnvit is using to evaluate genotoxicity by detecting micronuclei in the cytoplasm during the cell's interphase. The HPRT assay investigates the point mutation at the hypoxanthine-guanine phosphoribosyl transferase. However, the assays are originally intended to assess conventional chemicals and their use for nanoparticles may not be appropriate.

1.6 Endocytosis

Internalization of small and large molecules is one of most important functions of the cell. These molecules include essential small molecules such as amino acids, sugars and ions as well as macromolecules, albumins, hormones, and antigens but also NPs including SiQDs (Conner and Schmid, 2003, Alsharif et al., 2009). The internalization of macromolecules is known as endocytosis. Endocytosis functions to control cell survival and response to the environment (Conner and Schmid, 2003). The endocytosis process starts at the cell membrane (Zimmerberg and Gawrisch, 2006). Endocytosis pathways can be classified in several ways but can be divided into phagocytosis and pinocytosis (Conner and Schmid, 2003). Pinocytosis pathways include those involving clathrin-mediated endocytosis, caveolin-mediated endocytosis involving caveolae and macropinocytosis. The phagocytosis and endocytosis processes are showed in **Figure 1.7**.

Caveolae are located in the cell membrane and have an outstanding mini invagination structure compared with other vesicle portal of entry. A cholesterol-/sphingolipid-rich lipid bilayer occupies the main part of the vesicle with the shape conferred by a caveolin protein dimer (Conner and Schmid, 2003). Cholesterol and caveolin are the key factors in determining caveolae stability and function (Silvius, 2003, Tedrick et al., 2004, Alsharif et al., 2009). The cholesterol constituent is a target for many pharmacological/chemical inhibitors

of lipid raft/caveolae mediated endocytosis process such as statins, methyl-β-cyclodextrin (MβCD), filipin, nystatin, and cholesterol oxidase (Ivanov, 2008). The protein caveolin is also used as marker to distinguish caveolae from other membrane compartments (Cohen et al., 2004). Moreover, caveolin deficiency has been studied in mice and mice with this deficiency are subject to many diseases such as diabetes, cancer, cardiovascular, atherosclerosis, pulmonary fibrosis, and variety of degenerative muscular dystrophies (Cohen et al., 2004). Caveolae are flask-shaped vesicles and are coated with three different proteins: caveolin-1, caveolin-2, and caveolin-3 (Cohen et al., 2004). The proteins function as structural components and also have a capacity to recruit numerous signalling molecules. The vesicle also contains a unique lipid composition, so-called lipid rafts, which are enriched with cholesterol (Cohen et al., 2004).

Most molecules in the size range smaller than 120 nm are internalised by eukaryotic cells using clathrin-mediated endocytosis, caveolin-mediated endocytosis, and clathrin- and caveolin-independent endocytosis (Conner and Schmid, 2003). QDs including SiQDs have particle sizes smaller than 100 nm and are proposed to be internalised by cells using the same mechanisms as macromolecules (Canton and Battaglia, 2012). Though roles for clathrin-mediated endocytosis and clathrin and caveolin-independent endocytosis in nanoparticle entry into cells are also possible, several studies point to a more important role for caveolin-mediated endocytosis in nanoparticle entry. For example, Wang et al. (2009) showed that nanoparticle internalization was more efficient for particles smaller than the size of caveolae with the uptake of 20 nm and 40 nm nanoparticles 5-10 times greater than 100 nm particles. However, they found that caveolae were still able to take up 100 nm nanoparticles though with reduced efficiency (Wang et al., 2009). Further evidence that SiQD entry into cells involves caveolae comes from studies showing that filippin inhibits SiQD entry into HeLa cells (Alsharif et al., 2009). Information on the entry process for SiQDs in other cell types is still limited.

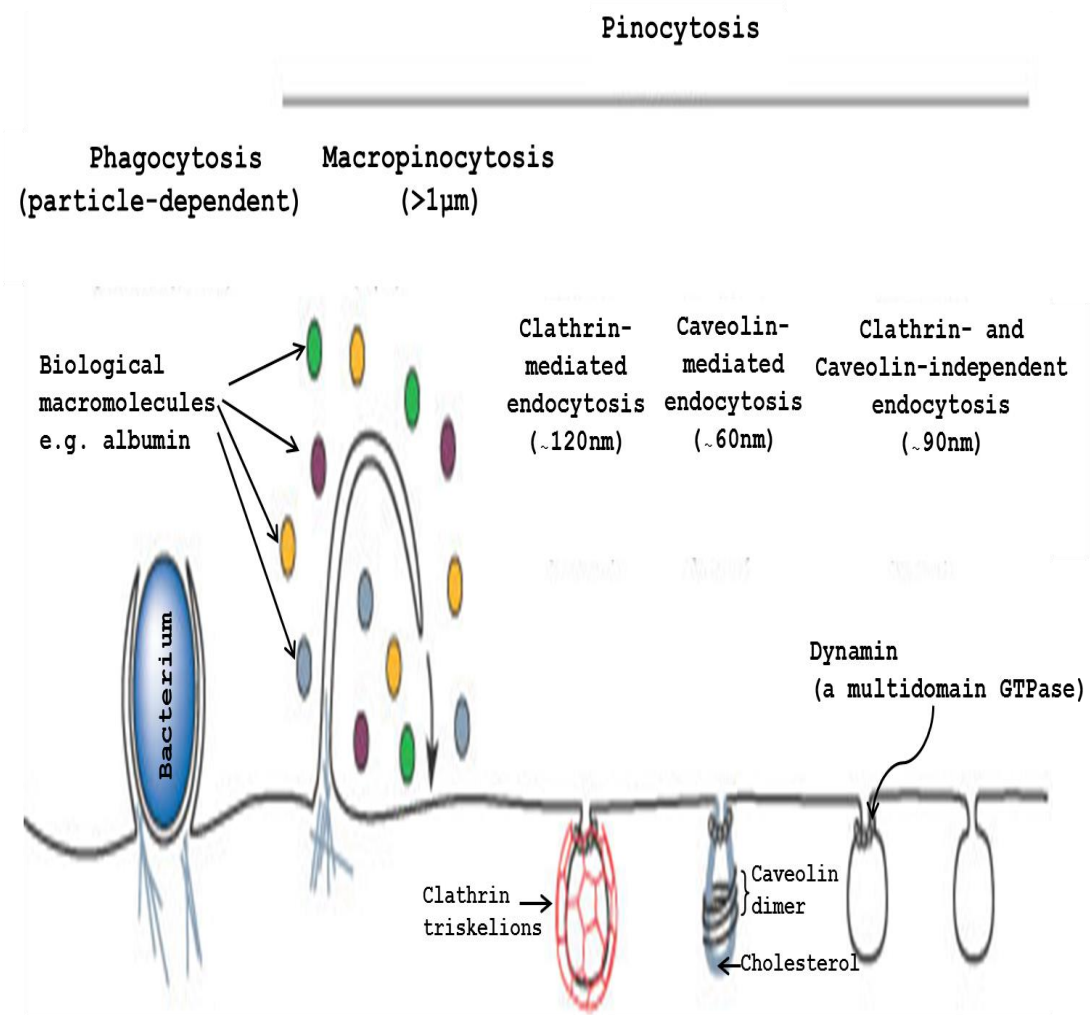

Figure 1. 7 Endocytosis processes, the dominant endocytosis pathways are micropinocytosis, clathrin-mediated endocytosis, caveolin-mediated endocytosis, and clathrin- and caveolin- independent endocytosis (Conner and Schmid, 2003).

1.7 Aims of the studies described in this thesis

The studies described in this thesis have the following aims:

(i) To prepare and characterise the physical and optical properties of alkyl-capped silicon quantum dots (SiQDs)

(ii) To characterise and quantify the optical properties of SiQDs in physiological solutions and human cells

(iii) To elucidate the interaction of SiQDs with gastrointestinal cells (CACO-2) in short and long term exposure studies

(iv) To explore systematically the uptake of fluorescent SiQDs in various human cell lines

Chapter 2. General Materials and Methods

2. General Materials and Methods

This chapter describes all the materials used in the thesis together with methods that are relevant to more than one Chapter. Other methods are described in Chapters 3 to 6.

2.1 Materials

Chemicals and reagents were purchased from Sigma-Aldrich, Fisher Scientific, Scientific Laboratory supplies, Vector Labs, Flowgen Bioscience, Culture Collection Public Health England, Compart Technology, UK, Life Technologies, New England Biolabs, and Qiagen. More details are given below in **Table 2.1.**

Table 2. 1 Materials and suppliers

Nanoparticles synthesis	
Materials	**Suppliers**
Silicon wafer, boron-doped p-Si<100> oriented wafer (10 Ω cm resistivity)	Compart Technology, Peterborough, UK
Dichloromethane 99.8%	Fisher Scientific
Ethanol 95% GL	Fisher Scientific
Hydrofluoric acid ≥40%	Sigma-Aldrich
Toluene anhydrous, 99.8%	Sigma-Aldrich
1-Undecene,97%	Sigma-Aldrich

Mammalian cell culture	
Materials	**Suppliers**
IGE Intestinal epithelial	Asmaa Alharbi (researcher), Saudi Arabia
CACO-2 Human epithelial colorectal adenocarcinoma cells	European Collection of Cell Cultures (ECACC) Public Health England, UK
HeLa Human cervical cancer cells	Institute of Cellular Medicine, Newcastle University
Huh7 Human liver cancer cells	Institute of Cellular Medicine, Newcastle University

Mammalian cell culture	
Materials	**Suppliers**
HepG2 Human hepatoblastoma	Institute of Cellular Medicine, Newcastle University
Trypan blue solution 0.4%	Sigma-Aldrich
Dulbecco's phosphate buffered saline modified, without calcium chloride and magnesium	Sigma-Aldrich
Fetal bovine serum-heat inactivated	Sigma-Aldrich
Dulbecco's Modified Eagle's Medium - high glucose With 4500 mg/L glucose and sodium bicarbonate, without L-glutamine, sodium pyruvate, and phenol red, liquid, sterile-filtered, suitable for cell culture	Sigma-Aldrich
L-Glutamine solution 200 mM, solution, sterile-filtered, BioXtra, suitable for cell culture	Sigma-Aldrich
Penicillin/Streptomycin: with 10,000 units penicillin and 10 mg streptomycin per mL in 0.9% NaCl, sterile-filtered, BioReagent, suitable for cell culture	Sigma-Aldrich
MEM Non-essential Amino Acid Solution (100×) without L-glutamine, liquid, sterile-filtered, BioReagent, suitable for cell culture	Sigma-Aldrich
Trypsin-EDTA Solution 10X 0.5% trypsin, 0.2% EDTA, trypsin gamma irradiated by SER-TAIN Process, without phenol red, in saline	Sigma-Aldrich

Mammalian cell culture	
Materials	**Suppliers**
Fetal bovine serum-heat inactivated	Sigma-Aldrich
Dulbecco's Modified Eagle's Medium - high glucose With 4500 mg L^{-1} glucose and sodium bicarbonate, without L-glutamine, sodium pyruvate, and phenol red, liquid, sterile-filtered, suitable for cell culture	Sigma-Aldrich
Sodium pyruvate solution 100 mM, sterile-filtered, BioReagent, suitable for cell culture	Sigma-Aldrich
Millex® syringe filter units, disposable, mixed esters pore size 0.22 µm, diam. 33 mm	Sigma-Aldrich
Greiner culture flasks (filter cap), tissue culture treated surface area 75 cm2, canted neck	Sigma-Aldrich
Centrifuge tube flat top cap sterile polypropylene non-pyrogenic 25 tubes per rack 28 x 115mm 6000 x g max 50mL x 5mL Fisherbrand	Fisher Scientific
Centrifuge tube flat top cap conical bottom sterile / non-pyrogenic polypropylene 15mL x 0.5mL 17 x 119mm 6000 x g max 10 racks of 50 tubes Fisherbrand	Fisher Scientific
Needle 38mm hypodermic syringe sterile disposable 21 gauge Terumo	Fisher Scientific
Syringe disposable eccentric sterile plastic for gases and liquids without needles 20mL x 1.0mL Terumo	Fisher Scientific

Mammalian cell culture	
Materials	**Suppliers**
Pipette serological sterile plastic with magnifier stripe individually wrapped 4 subpacks of 50 pipettes purple 25mL x 0.2mL Fisherbrand	Fisher Scientific
Pipette serological sterile plastic with magnifier stripe individually wrapped 4 subpacks of 50 pipettes orange 10mL x 0.1mL Fisherbrand	Fisher Scientific

Cellular internalization	
Materials	**Suppliers**
Microscope slide ground edges, twin frosted glass wrapped in cellophane 76 mm x 26 mm 0.8 mm to 1.0 mm thick	Fisher Scientific
Coverslips No 1 24 x24 mm	Scientific Laboratory Supplies
Mowiol 40-88poly(vinyl alcohol)	Sigma-Aldrich
Glycerol BioXtra, ≥99% (GC)	Sigma-Aldrich
VECTASHIELD mounting medium	Vector Labs

MTT assay	
Materials	**Suppliers**
Thiazolyl Blue Tetrazolium Bromide powder, BioReagent, suitable for cell culture, suitable for insect cell culture, ≥97.5% (HPLC)	Sigma-Aldrich
Microcentrifuge tube Safe-Lock write-on graduated with lid latch 2.0mL colourless Eppendorf	Fisher Scientific
Transfer pipette fine tip sterile polyethylene 50 subpacks of 20 pipettes 144mm length 3.5mL	Fisher Scientific

MTT assay	
Materials	**Suppliers**
Hydrogen peroxide solution 30% (w/w) in H2O, containing stabilizer	Sigma-Aldrich
Propan-2-ol 99.5+% (GLC) SpeciFied	Fisher Scientific
Tissue culture dish Nunclon flat bottom polystyrene radiation sterilised 128mm x 86mm 12 round well Thermo Scientific Nunc	Fisher Scientific
Tissue culture dish Nunclon 132mm x 88mm flat bottom 6 round well	Fisher Scientific
Nunclon® MicroWell plates for automation 96 well (with lid), flat bottom, clear	Sigma-Aldrich

ATP assay	
Materials	**Suppliers**
Adenosine 5′ – triphosphate (ATP) bioluminescent somatic cell assay kit	Sigma-Aldrich
Microcentrifuge tube Safe-Lock write-on graduated with lid latch 1.5mL amber (light protection) Eppendorf	Fisher Scientific

ROS assay	
Materials	**Suppliers**
2,′7′ – Dichlorofluorescin diacetate ≥ 97%	Sigma-Aldrich
Corning® 96 well plates, clear bottom 96 well plate, polystyrene, TC-treated, clear flat bottom wells, sterile, w/lid, black, 48/cs	Sigma-Aldrich

ROS assay	
Materials	**Suppliers**
BRAND™ UV cuvettes micro, center height 15 mm, chamber volume 70-550 µL, window W × H 2 mm × 3.5 mm	Sigma-Aldrich

Comet assay	
Materials	**Suppliers**
Greiner culture flasks, tissue culture treated T-25 flask, canted neck, surface area 25 cm2, capacity 50 mL, w/ filter cap (filter cap not pictured)	Sigma-Aldrich
Microscope slide superfrost plus adhesion glass grounded edges with white superfrost marking area 25 mm x 75 mm x 1 mm	Fisher Scientific
Dimethyl sulfoxide	Fisher Scientific
Macrosive agarose low melt seaplaque 25g	Flowgen Bioscience
SYBR® Gold nucleic acid gel stain (10,000 x concentrate in DMSO)	Life technologies
Ethylenediaminetetraacetic acid BioUltra, anhydrous ≥ 99% (titration)	Sigma-Aldrich
Trizma® base, primary standard and buffer ≥ 99.9% (titration), crystalline	Sigma-Aldrich
Sodium chloride, BioXtra ≥ 99.5% (AT)	Sigma-Aldrich
Phosphate buffer saline tablet	Sigma-Aldrich
Sodium hydroxide, BioXtra ≥ 98% (acidimetric) pellets (anhydrous)	Sigma-Aldrich
Hydrochloric acid ACS reagent, 37%	Sigma-Aldrich

Gene expression	
Materials	**Suppliers**
Moloney Murine Leukemia Virus (M-MuLV) Reverse Transcriptase	New England Biolabs
dNTP mix	New England Biolabs
RNase inhibitor	New England Biolabs
TaqMan® Universal Master Mix II, no UNG	Life Technologies
TaqMan® Gene Expression Assay, SM(CAV-1)	Life Technologies
TaqMan® Gene Expression Assay, SM VIC (GAPDH)	Life Technologies
TaqMan® Gene Expression Assay, SM(CAV-2)	Life Technologies
MicroAmp® Fast Optical 48-Well Reaction Plate 4375816	Life Technologies
MicroAmp® Optical Adhesive Film 4360954	Life Technologies

2.2. Confocal Luminescence and Confocal Laser Scanning Microscopy

These methods were used in the studies described in Chapters 3 and 4.

A CRM200 confocal Raman microscope (Witec GmbH, Ulm, Germany) and a confocal laser scanning microscope (The Leica TCS SP2 system, with Leica DM IRE2 microscope, Argon/Krypton Laser (spectral confocal and multiphoton microscope, Leica microsystems Ltd, Milton Keynes, U.K.)) were used to visualise luminescence of SiQDs inside the cells and quantify the localisation as well as luminescent spectra of SiQDs. An Argon Ion laser with high power intensity 35 mW at wavelength 488 nm is the power source of the confocal Raman microscope and was used as excitation source for SiQDs visualisation. The acquisition was performed with scan size 50x50 μm and 100x100 pixels. The confocal microscope detects structure of SiQDs by collecting light from a single focal plane and excludes the light that is out of focus. A fluorescent image

is generated by the laser moving rapidly across the SiQDs sample. The spectrum image of SiQDs was acquired by Raman spectroscopy.

An Argon/Krypton laser at wavelength 488 nm is the power source for the confocal laser scanning microscope. This microscope generates an image in three dimensions: plane, horizontal and vertical (X, Y, and Z) by moving the sample with movable objective stage (stage scanning) and fixed the position of the laser source. Samples were observed using a HCX PLAPOCS 40x1.25 oil immersion objective lens.

2.3 Culture of CACO-2 cells

CACO-2 cells were used in experiments described in Chapters 4, 5 and 6. These cells were cultured in 75cm^2 flasks containing sterile complete medium (syringe filter pore size 0.22 μm, diam. 33 mm) containing 15 mL of Dulbecco's modified Eagle's medium (D1145) supplemented with 20% (v/v) foetal Bovine serum (FBS) (F9665), 1% (v/v) penicillin/streptomycin (P0781), 1% (v/v) MEM non-essential amino acid solution (M7145), 1% (v/v) L-glutamine solution (G7531), and 1% (v/v) sodium pyruvate solution (S8636). The cells were grown at 37 ^{o}C, 5% CO_2.The cell culture medium was changed every 2-3 days by replacing with warmed Dulbecco's phosphate buffered saline (PBS) (D8537) and after washing twice, warmed complete medium was added using sterile 10 mL pipette. After reaching 70-80 % confluence, cells were sub-cultured using trypsin-EDTA solution (5X dilution) (59418C). The culture medium was replaced with warmed PBS and washed twice. Then 5 mL of trypsin was added to replace the PBS and left on the cells for approximately 5 minutes till the cells were rounded up. Ten mL warmed complete medium was added to the flask to inhibit the trypsin reaction. The cell suspension was transferred using 10 mL pipette and placed in a 50 mL centrifuge tube. The cell pellet was collected by centrifugation at 1000g for 5 minutes and used for new cultures or experiments or cell storage. For new cultures or experiments, the cell pellet was re-suspended in warmed complete medium and divided into portions. For new cultures, the cell solution was pipetted into a new flask and made up to 10 mL with new warmed medium.

To measure cell density, cells were counted using a haemocytometer. The same amount of cell solution and Trypan blue solution (T8154) (total volume 20 µL) was mixed. The mixed solution (10 µL) was dropped into half cone notch of haemocytometer or the edge of the counting area. Each counting area of haemocytometer is divided into nine equal portions of 1 mm by 1 mm. The cell counting was counted in 4 areas of the nine portions at the corner (top and bottom) using a hand held tally counter. After counting, the cells density was calculated as equation below.

Cell density (cells mL^{-1}) = Counting cells x 2 (dilution factor) x 10^4 (mL^{-1}) / 4 (areas)

From the known cell density (cells mL^{-1}), the required cell density was prepared by making serial dilutions using warmed complete medium.

Cell stocks were stored in liquid nitrogen for further studies. To freeze down cells, the cell pellet was re-suspended in PBS and centrifuged at 1000g for 5 minutes. The cell pellet was re-suspended in 10% (v/v) (dimethyl sulfoxide (DMSO) in FBS and aliquoted (1 mL) into cryo-tubes. The tubes were then frozen slowly in a 'Mr Frosty' to control the optimal rate of freezing and to preserve the cells (-1 ^oC $minute^{-1}$) which had been filled with isopropanol and put in -80 ^oC overnight. After 24 hours all the tubes were transferred into liquid nitrogen for longterm storage.

To grow the cells, frozen cells in a cryo-tube were thawed at room temperature. After thawing, the cell solution was transferred into a 15 mL centrifuge tube and mixed with 4 mL warmed complete medium. The cell pellet was collected by centrifugation at 1000g for 5 minutes and re-suspended in 10 mL warmed complete medium. The cell solution was placed in a 75cm^2 flask and incubated at 37 ^oC with 5% CO_2.

Chapter 3. Synthesis and Characterisation of Alkyl-Capped Silicon (SiQDs)

3.1 Introduction

The semiconductor from which quantum dots (QDs) have been prepared include binary compounds consisting of elements in groups II-VI and III-V of the periodic table as well as elemental semiconductors such as Si. A quantum dot is a particle of semiconductor whose size is less than the Bohr radius of the bulk material (O'Farrell et al., 2006). In this context, the Bohr radius is the radius of the 1s orbit of an electron and the hole in the valence band produced by absorption of light in the semiconductor; if the particle itself is smaller than this, then the energy of the exciton increases and the properties of the particle change from that of the bulk material. The size of QDs are generally small as 1-10 nm (Yu, 2008); QDs show unique optical properties (Alivisatos, 1996). In particular, the photon energy of the light emitted by QDs is greater than that of the bulk material of which they are formed (Alivisatos, 1996). The fluorescence characteristics of QDs are also strongly dependent on their size; as they become smaller, their electronic structure changes and the wavelength of the emitted light shifts towards the blue part of the spectrum. This allows the fluorescence of QDs to be tuned to emit at any wavelength simply by adjusting their size. QDs have drawn attention from researchers in many fields because of their unique photo-physical properties and their potential for diverse applications from the life sciences to optoelectronics. The commonly used QDs and dominant in biological fluorescence microscopy are comprised of CdSe and samples may be prepared which emit from the red to the blue region of the spectrum, with narrow line widths that allow multi-colour imaging (Yu, 2008).

The most technologically important semiconductor, silicon is the second most abundant element on earth behind oxygen (Martin, 2013). Silicon in elemental form is rarely found in nature and classified as group 4 in the periodic table and as a metalloid as well as an inorganic element. The most common form of silicon in nature is silicon dioxide, sand or quartz. Silicon in the form of silicon dioxide is widely used in many industries, particularly in biological/medical applications such as food and cosmetics as well as in the electronics industry. The biological applications have claimed benefits to human health from water soluble forms e.g., silicic acid. The dominant form of silicon found in human body is orthosilicic acid (Park et al., 2009, Martin, 2013).

The metalloid silicon is widely used in electronics in the form of bulk single crystal wafers. Silicon wafer plays an essential role as the substrate on which integrated circuits for consumer electronics are formed (Canham, 1990). Porous silicon was discovered by A. Uhlir of Bell laboratories in 1956 during the anodic etching process as part of standard semiconductor manufacturing techniques, but its true nature was not understood until the discovery of room temperature luminescence from porous silicon by Canham, 1990. Later on luminescent colloidal suspensions of silicon nanoparticles were prepared by electrochemical etching of n- or p-type silicon (Heinrich et al., 1992).

Porous silicon is comprised of pores and thin, nanometre scale pore walls of Si. It was originally generated by wet chemical techniques, i.e., anodic etching of silicon wafer (Canham, 1990, Buriak et al., 1999). Porous silicon has sufficiently fine structures that it displays quantum confinement effects (increase in band gap) as well as a substantial surface chemistry (Buriak, 1999). In bulk form, silicon has a low band gap energy (1.1 eV corresponding to emission in the infrared) and poor photoluminescence because the transition across the bandgap is indirect. An indirect gap is one in which the electron must undergo a large change in momentum as well as energy in order to cross the gap; light cannot supply the momentum and therefore this must be obtained from another source, typically the vibrations of the solid lattice and the transition probability is reduced (Mangolini et al., 2006, O'Farrell et al., 2006). Absorption of light in bulk silicon produces an electron in the conduction band which may either fall back into the hole, it left in the valence band with emission of light or it may lose its energy in a non-radiative manner by interacting with defects. Because the transition has a low probability, the nonradiative process dominates, and the energy of the electron is transferred to vibrations of the solid lattice (O'Farrell et al., 2006). However, the optical properties are improved in porous silicon (Mangolini et al., 2006). The emission intensity increases because the transition is no longer indirect and also the gap between energy levels widens to typical values of about 2 eV corresponding to red light (O'Farrell et al., 2006). Bulk silicon also has a direct energy gap, but this is at about 3.4 eV and therefore corresponds to absorption of blue/near UV light in porous silicon (Lie et al., 2002).

The luminescence properties of porous silicon are determined by the quantum confinement and the effects of surface chemical species. In particular silicon tends to oxidise and this is known to have a strong effect on the colour of luminescence (Wolkin et al., 1999) . Silicon quantum dots (QDs) have been synthesised by various methods (Furukawa and Miyasato, 1988, Littau et al., 1993, Bley et al., 1996, Dinh et al., 1996, Schoenfeld et al., 1996, Choi et al., 1998, Kovalev et al., 1998, Zhang et al., 1998, Wilcoxon et al., 1999, Botti et al., 2001, Mangolini et al., 2005, O'Farrell et al., 2006).

Alkyl-capped silicon quantum dots (SiQDs) are one of many types of quantum dots (QDs). Silicon quantum dots (SiQDs) have been synthesised at Newcastle University via the intermediate formation of porous silicon. This process starts with Si wafer <100> (p-type, B-doped) (**Figure 3.1**) (10 Ω cm resistivity, Compart Technology, Peterborough, UK) as a silicon source and follows a two-step procedure of etching and then hydrosilation under reflux (Lie et al., 2002, Dickinson et al., 2008, Alsharif et al., 2009).

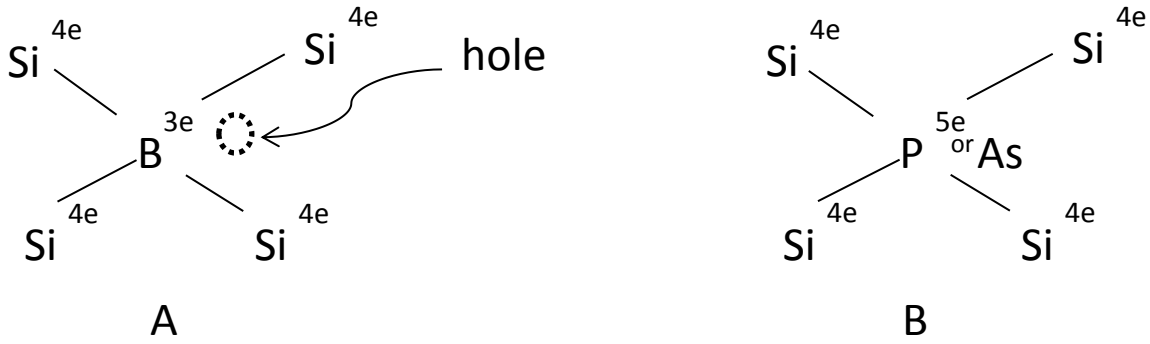

Figure 3. 1 The diagram shows **A** boron-doped (p-type); boron lacks one valence electron (compared to silicon) and **B** phosphorus or arsenic-doped (n-type); these atoms contain one extra valence electron compared to silicon.

These QDs do not have a heavy metal core and they might provide a solution to the problem of developing bright QD fluorescent labels with minimal effect on living organisms (Lie et al., 2002). The silicon quantum dots are composed of a crystalline silicon core and C11 alkyl monolayer shell (Alsharif et al., 2009). These SiQDs are very hydrophobic, but can nevertheless be dispersed in aqueous media where they were stable against oxidation and retained strong luminescence for several days (Chao et al., 2007, Dickinson et al., 2008). The

stability of alkyl-capped SiQDs is a result of the strong, nonpolarised Si-C bond at the surface; this covalent linkage also facilitates functionalization organic compounds (Shirahata, 2011).

SiQDs are a promising alternative to organic fluorescent dyes because they are stability under irradiation in various physiological media and do not contain heavy metals. SiQDs with strong fluorescence and simple structure have small overall particle size of about 5 nanometre (nm) which is an advantage for biological and medical applications (Alsharif et al., 2009). SiQDs have been used as a fluorescent probe to studies the particle internalisation by human cell lines as well as the potential cytotoxicity and the mechanism of internalisation by cells (Alsharif et al., 2009).

The characterisation of the photo-physical properties of SiQDs in physiological solutions is crucial before applying the SiQDs for biological studies as fluorescent probes. The best way to characterise the relevant properties of SiQDs for biological applications is to determine their absorption and emission spectra. The typically characteristics of the photo-physical properties include three parameters: the emission wavelength, the full width at half maximum (FWHM) of the emission spectrum peak, and the quantum yield (Yu, 2008). Overall the absorption and emission wavelengths depend on the size of the SiQDs via the confinement effect. The FWHM of the emission reflects the particles size distribution and the quantum yield depends on the quality of the particle surface (Yu, 2008); highly defective surfaces result in energy lose by non-radiative processes and produce a low fluorescence quantum yield.

Quantum yield of fluorescence = number of photons emitted as fluorescence / number of photons absorbed

Because the photo-physical properties of SiQDs are strongly dependent on the particles size, this should also be studied. Electron microscopy is not so as well-suited as it is for CdSe QDs because the atomic number of Si is smaller and it is a weaker scattered of electrons. However, atomic force microscopy (AFM) was found to be ideally suited to directly observe individual particles and to allow the measurement of the particle size distribution by collection of many images.

This chapter: synthesis and characterisation of SiQDs is part of a complete study of SiQDs. The study comprised four parts: synthesis and characterisation of SiQDs, cellular internalisation studies of SiQDs, potential cytotoxicity of SiQDs, and endocytosis mechanism. The SiQDs core was synthesised from bulk crystalline silicon also known as silicon wafer. The bulk silicon or silicon wafer was etched to form the structure known as porous silicon; this was then broken down into fragments (SiQDs) and simultaneously capped with an organic monolayer to increase the stability of the particles. The organic monolayer (shell or cap) comprised an 11-carbon alkyl chain anchored to the Si core via robust Si-C covalent bonds. In this form SiQDs are stable towards oxidation by air or water and had a very hydrophobic. The final SiQDs were characterised for their size and shape using Tapping Mode Atomic Force Microscopy (AFM). The SiQDs were characterised by absorption and emission spectroscopies. In particular, the emission (luminescence) intensity was found to be the simplest method to quantify the SiQDs. Furthermore the spectroscopic properties and luminescence of SiQDs in physiologically-relevant media were also determined. Finally, confocal microscopy/spectroscopy and luminescence microscopy were used to observe the distribution and aggregation of SiQDs in various media.

3.2 Methods

3.2.1 Alkyl-Capped Silicon Quantum Dots (SiQDs) Preparation

SiQDs were prepared according to the procedure developed by Lie et al. (2002) with minor modifications as in Dickinson et al. (2008) and Al-sharif et al. (2009). Silicon wafer is the silicon source. The wafer Si<100> (P100) (10Ω cm resistivity, Compart Technology, Peterborough, UK) was cut into 1.1 x 1.1 = 1.2 cm^2 chips. Each chip was used as a substrate for etching in a 1:1 v/v solution of 48% aqueous hydrogen fluoride (HF) and ethanol to produce porous silicon. The etching was carried out in a cylindrical PTFE electrochemical cell of internal diameter 1.5 cm) with a constant current at 400 mA for 5 minutes, supplied by a bench top power supply (Keithley 2601 system source meter). After 5 minutes the porous silicon, a roughly circular brown-yellow area, was formed on the top of the silicon chip **(Figure 3.2A)**. Fluorescence of the porous silicon was

confirmed by eye with a hand-held UV lamp (365 nm) and the orange luminescent indicated successful etches **(Figure 3.2B)**. Next, the porous silicon chips (x4) were placed in a Schlenk flask and refluxed under nitrogen (N_2) in an anhydrous toluene solution (~20 mL) containing 1 M of the alkene (1-undecene). During the refluxing process the hydrosilation reaction occurs at the Si surface and the stress of bubble formation helps to break-up the porous layer into individual SiQDs **(Figure 3.2)**.

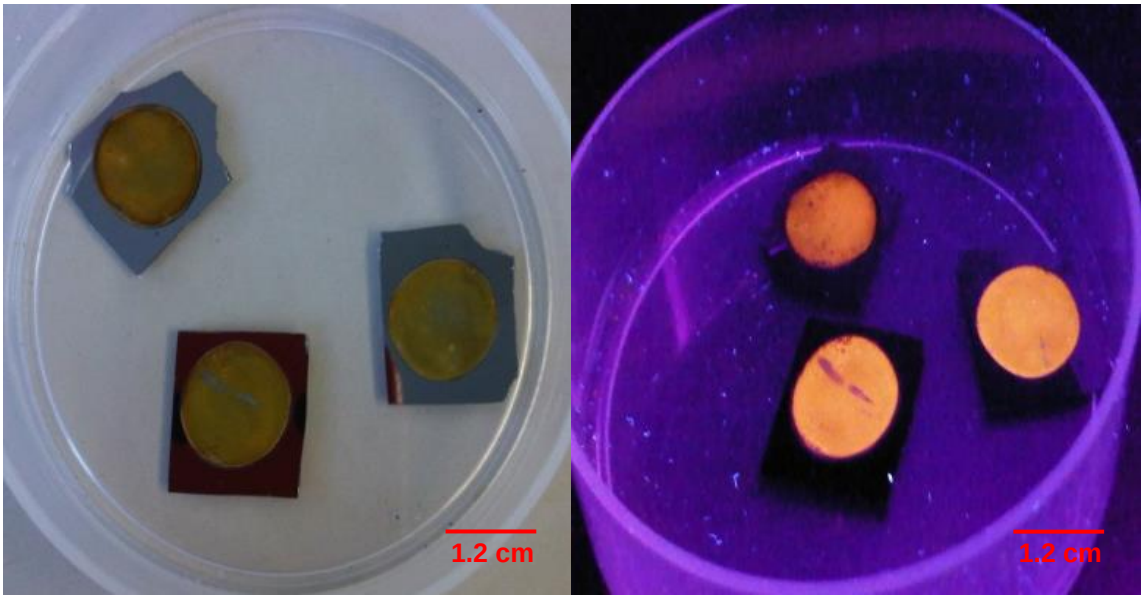

Figure 3. 2 The porous silicon, a roughly circular brown-yellow area formed on the top of the silicon chip (**A**) and fluorescent image of porous silicon under UV-lamp 365 nm (**B**).

The reflux was continued for at least 4 hours till the colourless solution changed to a pale yellow colour. The pale yellow solution was decanted into a new flask. Solvent from the solution was removed under vacuum on a glass vacuum line - the solvent was trapped in a liquid nitrogen-cooled flask till a waxy yellow solid remained. The waxy yellow solid was re-dissolved in 200 µL dichloromethane (DCM) and excited with a UV lamp (365 nm) to produce orange luminescence (**Figure 3.3**). The DCM solution was divided into small portion in little glass vials with 10 µL each and left to allow evaporation of the DCM at room temperature. The residual yellow wax of alkyl-capped silicon quantum dots was stored in the vial, under which conditions it is known to be stable, Dickinson et al. (2008) and used as required in other experiments.

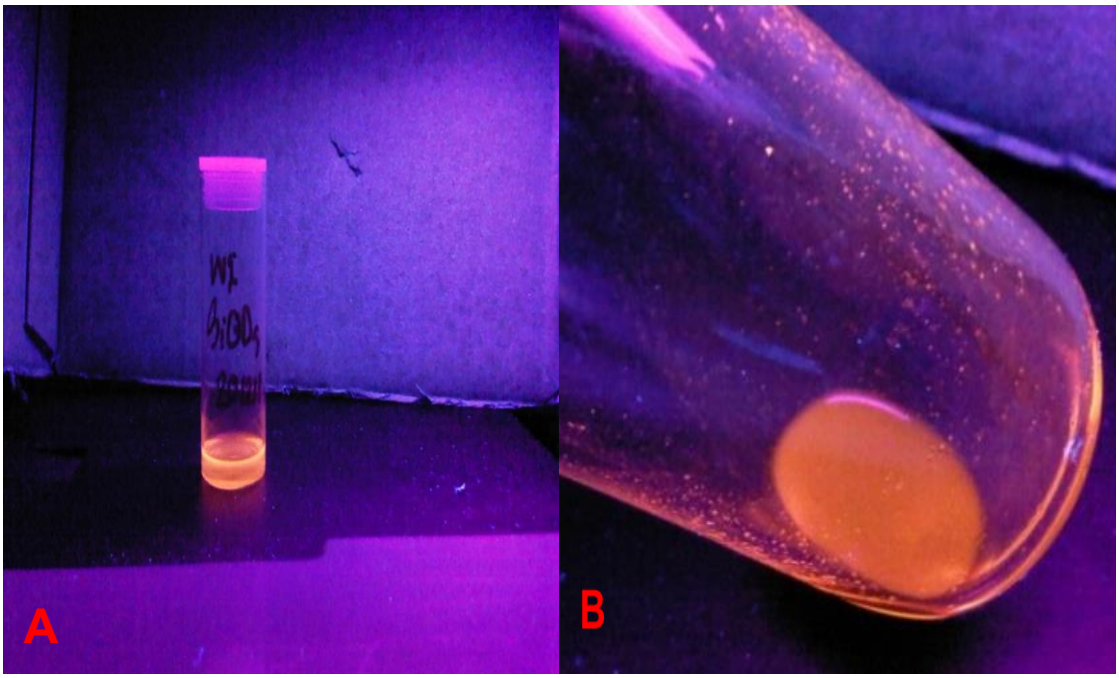

Figure 3. 3 Alkyl-capped silicon quantum dots (SiQDs) in DCM which were excited by a UV lamp box (365 nm) to produce orange luminescence (**A** and **B**).

3.2.2 SiQDs Particle Height and Shape Characterisations

Atomic Force Microscopy (AFM)

The particle size and shape (images) of alkyl-capped silicon quantum (SiQDs) dots were characterised using AFM in Tapping Mode™, a Multimode Nanoscope IIIA (Veeco Instruments Inc., Metrology Group, Santa Barbara) instrument. Tapping mode is preferred for these measurements over contact mode AFM because the SiQDs are weakly-adherent to the substrates and in tapping mode there is less tendency for the tip to push the particles around. The tip, which is attached to a flexible cantilever, moves across the surface of sample as well as executing a tapping motion normal to the surface. Meanwhile the laser beam which is focused on the back of the cantilever is deflected according to the displacement of the tip as it passes over topographical features. The deflected beam is focused on a four-quadrant split photodiode so that as the tip moves up/down or twists left/right the amount of light falling on each quadrant changes and can be converted electronically into a measurement of the tip deflection and therefore the feature height on the surface. Finally, the signal from the beam detector is converted into a grayscale or false colour image. In tapping mode, not only the height of surface features is measured, but the interaction of the tip with the surface changes the phase of the tapping motion. The tip deflection may lag the driving force and a phase image which provides information on mechanical properties of the surface is produced simultaneously with the height image.

Sample preparation: 5 µL of 10% v/v SiQDs in DCM solution was dropped onto the top of cleaved mica (using tape) and left overnight. Next day, the mica was mounted on the steel chuck. Then the laser beam and the tip were aligned on the area of dried SiQDs on the mica. The scanner head was then placed on the isolation table (TMC) to prevent noise and vibration. The manufacturer's instrument control software was used to set up the scan size at 10 µm then the integral gain and the proportional gain were set at 0.3 and 0.5. Finally, height and phase images were investigated.

3.2.3 Purification Studies of SiQDs

3.2.3.1 Absorption Spectroscopy

Optical property of alkyl-capped silicon quantum dots (SiQDs) to absorb energy was specified using absorption spectroscopy scanning from infrared (IR) to ultraviolet (UV), low to high energy (800-200 nm). The energy (of light) of which absorption occurs determines the excitation wavelength in the fluorescence spectra (below).

The optical spectroscopic properties of SiQDs were characterised by absorption spectra (Cary model 100 spectrometer). A quartz cuvette of 1 cm path length was used to measure the absorption spectra. The wavelength range was 800-200 nm and a baseline correction was set for each absorption measurement. The absorption spectra of SiQDs dispersed in an organic solvent, dichloromethane (DCM), were measured using UV-Vis absorption spectroscopy SiQDs at concentration 1 mg mL^{-1} in DCM was used as stock solution. The serial dilution of SiQDs was prepared by dilution 1 mg mL^{-1} SiQDs into 1.25 and 10 µg mL^{-1} in DCM. The absorption spectrum was scanned from lower energy 800 nm to high energy 200 nm excitation wavelengths. All experiments were repeated at least 3 times.

3.2.3.2 Emission Spectroscopy

To characterise the optical property of SiQDs to emit fluorescence, emission spectroscopy was employed.

The photoluminescence of SiQDs was characterised by fluorescence emission spectra (SpexFluoroMax/GRAMS 32). A quartz cuvette of 1 cm path length was used to measure the emission spectra. The excitation wavelength was set at 330 nm and the range scan 345-850 nm were set for emission measurement. The emission slits were set at 5 nm. SiQDs were dispersed in organic solvent, dichloromethane (DCM), and their fluorescence was characterised using emission spectroscopy (Spex FluoroMax/GRAMS 32). The same samples of SiQDs from 3.2.3.1, the concentration of 1.25 and 10 µg mL^{-1} of SiQDs in DCM were measured for fluorescent intensities using emission spectroscopy. All experiments were repeated at least 3 times.

3.2.4 Quantifying Photochemical Properties and Luminescent Intensity per Mass (mg) of SiQDs

3.2.4.1 Absorption Spectroscopy

The optical absorbance of SiQDs as a function of concentration was determined in a similar manner to the spectra of section 3.2.3.1 Absorption Spectroscopy. Serial dilution of SiQDs was carried out starting from 1 mg mL^{-1} SiQDs to produce concentrations of 0.27, 0.29, 0.31, 0.33, 0.36, 0.40, 0.44, 0.50, 0.57, 0.67, 0.80, and 1.00 mg mL^{-1} in DCM. The absorption spectrum of SiQDs in various concentrations were scanned from lower energy 800 nm to high energy 200 nm excitation wavelengths.

3.2.4.2 Emission Spectroscopy

To study the relationship between concentrations and the corresponding photoluminescence intensities of SiQDs, SiQDs dispersed in organic solvent, dichloromethane (DCM) and characterised using emission spectroscopy (Spex FluoroMax/GRAMS 32). The same samples of SiQDs as in section 3.2.4.1 were prepared at the concentration of 0.27, 0.29, 0.31, 0.33, 0.36, 0.40, 0.44, 0.50, 0.57, 0.67, 0.80, and 1.00 mg mL^{-1} in DCM.

3.2.5 Photochemical Properties Studies of SiQDs in Physiological Solutions

3.2.5.1 Absorption Spectroscopy

The stability of the optical properties of SiQDs in physiological solutions was investigated by absorption spectra in various types of physiological solutions. Stock solution 1 mg mL^{-1} of SiQDs in 0.7% (v/v) cremophor was dispersed in physiological solutions and the final concentration of SiQDs was 0.2 µg mL^{-1} each of phosphate- buffered saline (PBS), Krebs solution, complete RPMI medium with phenol red and 10% (v/v) foetal Bovine serum (FBS), and complete DMEM medium with phenol red and 20% (v/v) FBS.

3.2.5.2 Emission Spectroscopy

The stability of the luminescence properties of SiQDs in physiological solutions was investigated by emission spectra in various types of physiological solutions. Stock solution 1 mg mL^{-1} of SiQDs in 0.7% (v/v) cremophor was dispersed in physiological solutions and the final concentration of SiQDs was 0.2 µg mL^{-1}

each of phosphate- buffered saline (PBS), Krebs solution, complete RPMI medium with phenol red and 10% (v/v) foetal Bovine serum (FBS), and complete DMEM medium with phenol red and 20% (v/v) FBS.

3.2.6 Luminescent Morphology, Particles Distribution, and Aggregation Studies of SiQDs in Physiological Solutions

3.2.6.1 Scanning Confocal Microscope

Morphology and fluorescence of SiQDs in organic solvent, cremophor and dispersed in physiological solution were visualised using a confocal microscope (Leica TCS SP2,UK) with the 488 nm line of an Argon ion laser as the excitation light. SiQDs in 0.7% v/v cremophor solution (50 µL) were dried on the top of cleaned slide and fluorescent images were captured using a confocal microscope/spectrograph. All experiments were repeated at least 3 times.

3.2.6.2 Fluorescent Microscope

Morphology, particles distribution, and aggregation of SiQDs in organic solvent, diethyl ether (ether) and dispersed in physiological solution were visualised using epi-fluorescence microscope (Leica Laborlux) with excitation provided by a mercury arc lamp and a 300-400 nm bandpass filter which selects mainly the 365 nm line of the mercury lamp. SiQDs at concentration 1 mg mL^{-1} in 50 µL ether were dispersed in complete medium without phenol red and prepared the final concentration at 100 µg mL^{-1} and 1 mg mL^{-1} of SiQDs in medium. The SiQDs 50 µL from both concentrations were dropped on the top of cleaned slide and covered with cleaned coverslid. The slide was then visualised using epi-fluorescent microscope. All experiments were repeated at least 3 times.

3.2.6.3 Studies on cell uptake of SiQDs by Confocal-Raman microscopy

A cell line IGE which is derived from rat intestinal epithelium was used for preliminary SiQD uptake studies. We stopped using IGE cells because of uncertainty in the original background and stability. The cells were cultured as described for CACO2 cells in Section 2.3. Cell internalisation of SiQDs and photoluminescent stability of SiQDs inside the cells was examined by confocal microscopy. A stock solution at 1 mg mL^{-1} of SiQDs in 0.7% (v/v) cremophor was dispersed in physiological solution to prepare the final concentration of 0.2 µg mL^{-1} of SiQDs in complete medium without phenol red. The cells were

treated with the SiQDs suspension for 1 hour and the fluorescence of SiQDs internalised by the cells was imaged using a confocal microscope/spectrograph with an argon ion laser (488 nm) as excitation source (WiTec model CRM 200, Ulm, Germany). All experiments were repeated at least 3 times.

3.3 Results

3.3.1 SiQDs preparation

The preparation of SiQDs which comprise a silicon core and an organic capping layer of C_{11} alkyl chains used electrochemical etching in hydrofluoric-ethanol solution and refluxing in anhydrous toluene with 1-undecene. During the etching, the brown/grey Si wafer is coated with an orange/yellowish layer of porous silicon. This porous silicon is then broken-up and dispersed in the toluene during the reflux; simultaneously, the hydrogen-terminated surface of the porous silicon reacts with the undecene to produce the C_{11} capping layer. After evaporation of the solvent, a yellow wax of SiQDs remains. The SiQDs are an intense pale yellow colour at room temperature and revealed strong orange luminescence under a hand-held UV lamp at an excitation wavelength of 365 nm. The SiQDs were water insoluble but when they were dispersed in organic solvents, e.g., dichloromethane (DCM) or diethyl ether, colloidal SiQDs showed a transparent yellowish solution and revealed strong orange luminescent under the handheld UV lamp with excitation wavelength 365 nm. The homogenous SiQDs solution in organic solvents was therefore used to make dilutions and to measure the concentration via luminescence spectrophotometry for the rest of the project.

3.3.2 Particle Height and Shape Characterisation of SiQDs

Atomic Force Microscopy (AFM)

AFM is a microscope which employs a very sharp probe scanning on the top of the sample to record the sample topography. Probe deflection as it moves over protrusions in the sample is recorded by reflecting a small diode laser off the back of the probe and using a split photodiode to measure the probe beam displacement. The AFM images presented are false-colour images in which the heights (deflections) are represented on a colour scale. The images of dried SiQDs (1 μg mL^{-1} SiQDs in DCM) on the top of clean mica showed

approximately spherical particles. Such an image of SiQDs is presented in **Figure 3.4**. Line sections across these features were used to determine the particle heights and a histogram of particle heights was compiled from 59 SiQDs . **Figure 3.4** presents the size of SiQDs, which was in the range of 2.5 to 25 nm in the selected area. The size in the range of 5-7.5 nm represented the dominant size of SiQDs and included 76% of the SiQDs measured in the samples (59 particles). The histogram is shown in **Figure 3.5.**

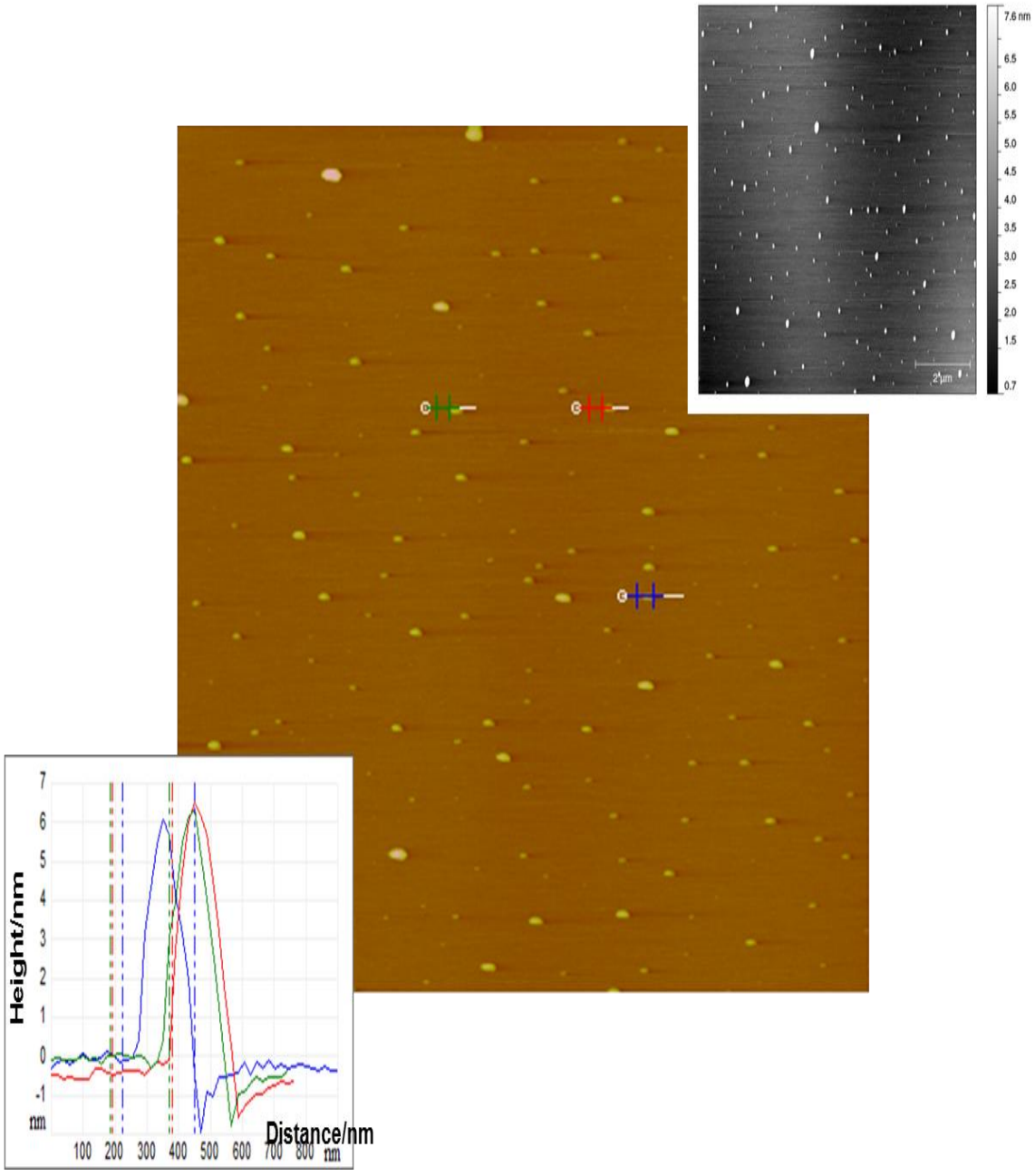

Figure 3. 4 The particle shape image of SiQDs and the particle size cross section of SiQDs measured using TappingMode AFM. The colour scale represents height and the inset shows the actual heights of three selected particles indicated by the red, green and blue crosses which are all about 6 nm in height. The full image width is 10 microns.

.

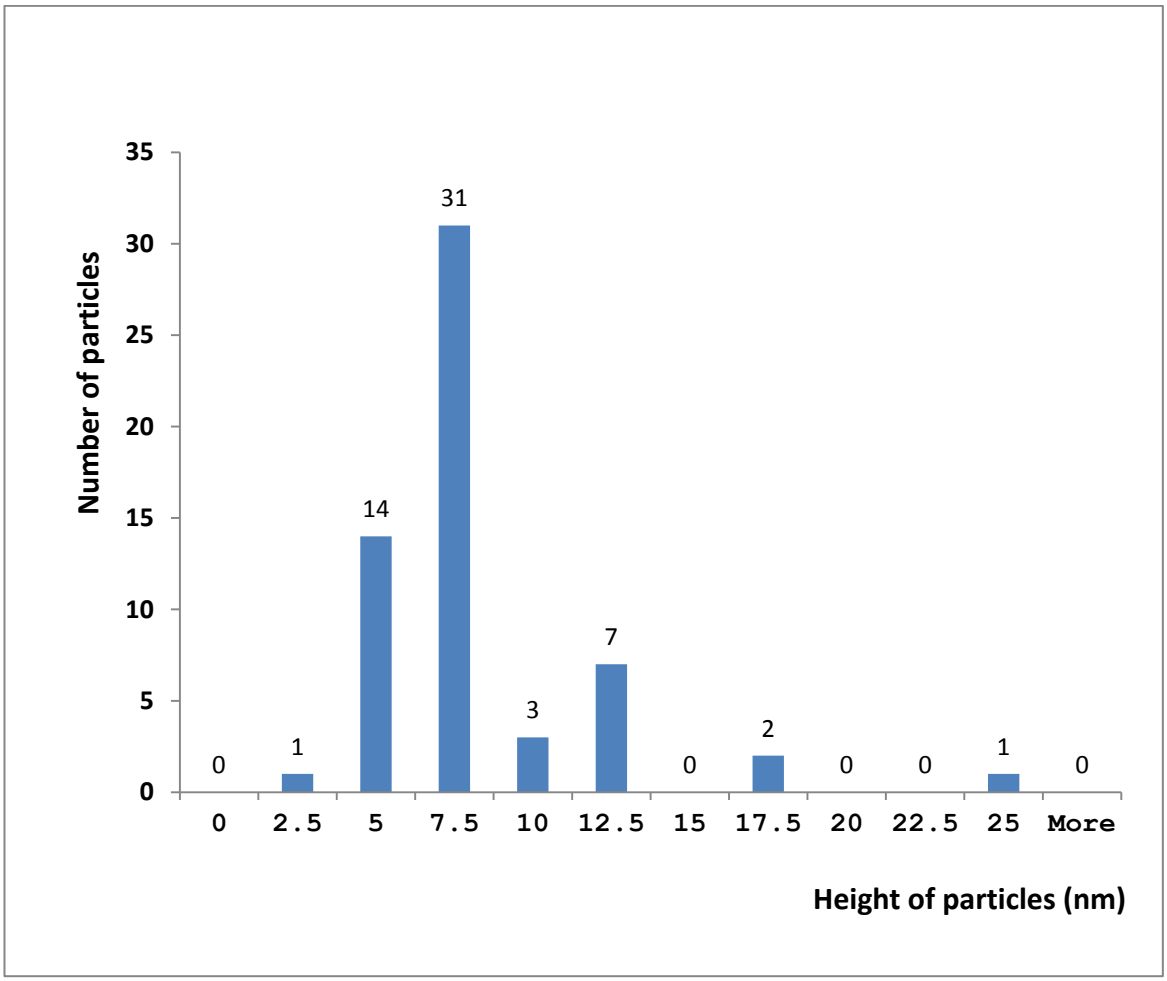

Figure 3. 5 Histogram presents the particles size range of 59 SiQDs. The mean diameter was in the range 5 to 7.5 nm. The particle height data were obtained using TappingMode AFM.

3.3.3 Purification of SiQDs

3.3.3.1 UV-vis Absorption spectroscopy

UV-Vis absorption spectra of 1.25 and 10 μg mL $^{-1}$ SiQDs were measured in DCM solution. The absorption spectrum was scanned from lower energy 800-nm to high energy 200-nm excitation wavelengths. SiQDs showed increasing absorption towards higher energy above about 400-nm excitation wavelength and showed maximum absorption at 230-nm excitation wavelength (this is not a true maximum in the sample absorption, but rather a limitation arising from absorptions in the solvent and cuvettes). The absorption spectra of 1.25 and 10 μg mL^{-1} SiQDs in DCM for excitation wavelength range of 200-800 nm are shown in **Figure 3.6.**

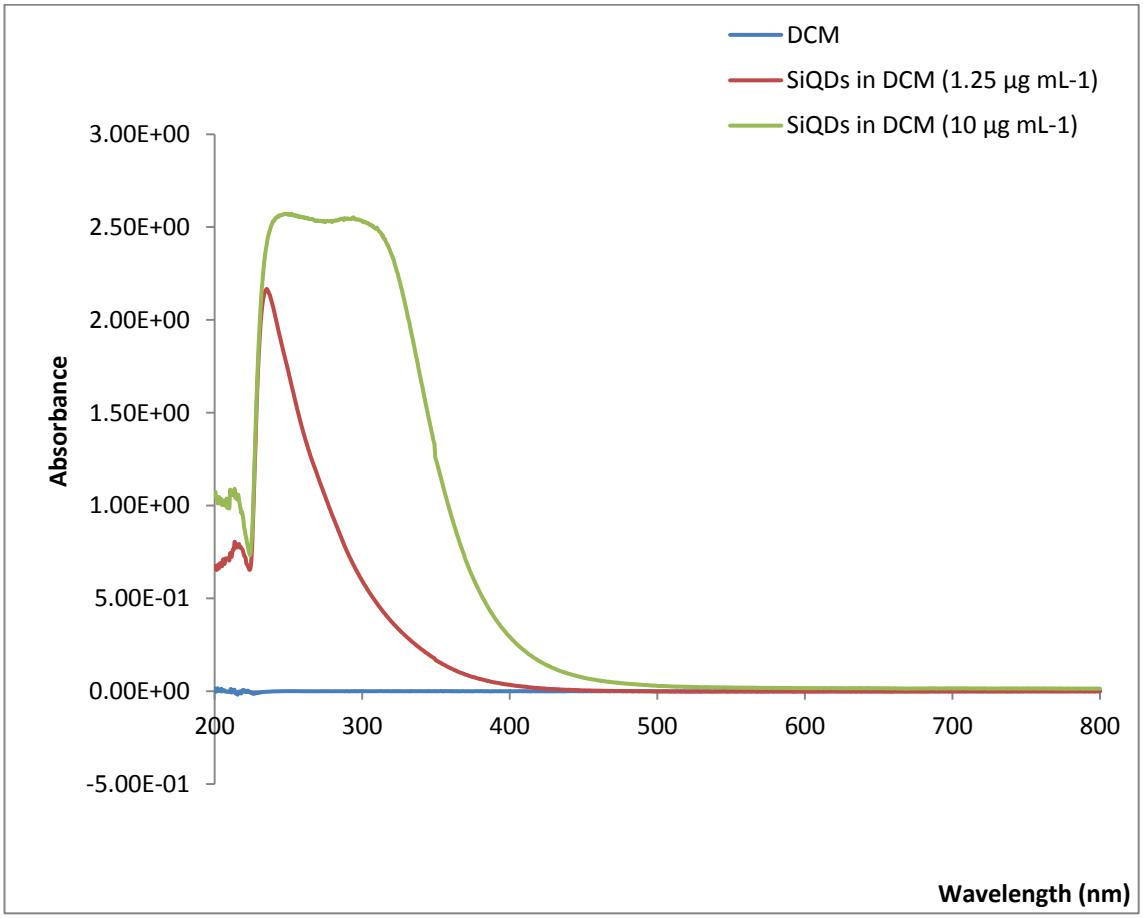

Figure 3. 6 UV-vis absorption spectra of the alkyl-capped silicon quantum dots (SiQDs) in dichloromethane (DCM) with the concentration of 1.25 µg mL $^{-1}$ and 10 µg mL $^{-1}$. The absorbance was measured using a UV-vis spectrometer, Cary model 100.

3.3.3.2 Emission spectroscopy

The fluorescence spectra of 1.25 and 10 µg mL $^{-1}$ SiQDs were measured in DCM using a Spex FluoroMax/GRAMS 32 with 330-nm excitation. Fluorescence spectra were recorded between 400 and 850 nm. SiQDs in DCM showed a maximum emission peak at approximately 620 nm with excitation wavelength 330 nm. The fluorescence spectra of 1.25 and 10 µg mL^{-1} SiQDs in DCM collected between 400 and 850 nm with 330-nm excitation wavelength are shown in **Figure 3.7.**

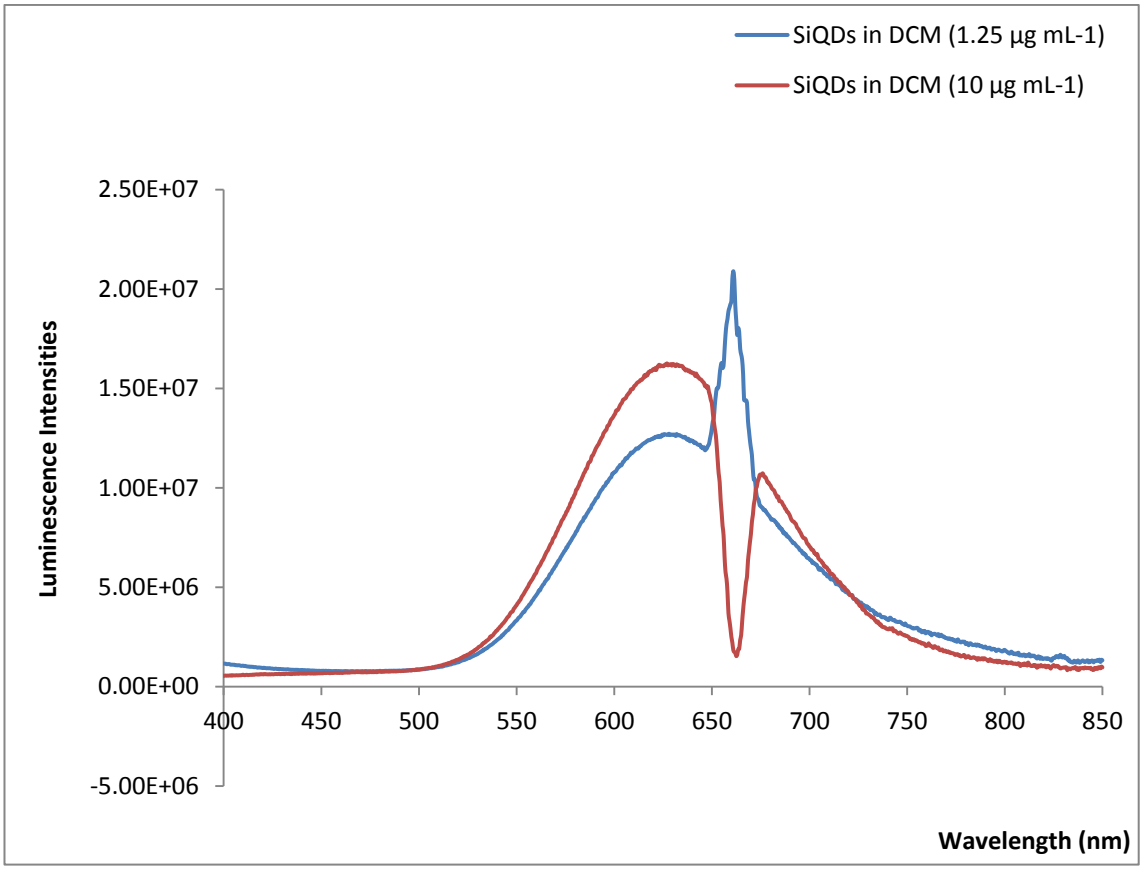

Figure 3. 7 Emission spectra of alkyl-capped silicon quantum dots (SiQDs) dispersed in dichloromethane (DCM) with the concentrations of 1.25 µg mL $^{-1}$ and 10 µg mL $^{-1}$. The luminescence intensities were measuring using emission spectroscopy, Spex FluoroMax/GRAMS 32 with excitation 330 nm. Note: the feature at 660 nm is second order scattering from the excitation wavelength and not a property of the sample.

The fluorescence spectra of SiQDs shown in **Figure 3.5** is typical; the peak absorption is in the red-orange region and the peak wavelength is invariant to the wavelength used for excitation (Lie et al., 2002) for any given sample, though it may vary between 600 and 670 nm between batches. Previous work suggested that fluorescence is superior to absorption for quantitation because

of the absence of self-quenching effects in SiQD samples(Dickinson et al., 2008).

3.3.4 Quantifying Photochemical Properties and Luminescent Intensity per Mass (mg) of SiQDs

3.3.4.1 UV-vis Absorption spectroscopy

High concentrations of SiQDs were dispersed in organic solvent dichloromethane (DCM) and divided into small amounts: 1 mg dried weight per vial. Each vial which contained 1 mg of SiQDs was used as SiQDs sample for the rest of the project. Serial dilutions of SiQDS were made from SiQDs at concentrations of 0.27, 0.29, 0.31, 0.33, 0.36, 0.40, 0.44, 0.50, 0.57, 0.67, 0.80, and 1.00 mg mL^{-1} in DCM. The absorption spectra of serial dilutions of SiQDs in DCM were measured using UV visible absorption spectroscopy. The absorption spectrum was scanned from lower energy 800-nm to high energy 200-nm excitation wavelengths. SiQDs showed absorption spectra at high energy after 400-nm excitation wavelength and showed maximum absorption peak at 240-nm excitation wavelength. The absorption spectra of serial dilutions of SiQDs in DCM scanning excitation wavelength 200-800 nm are shown in **Figure 3.8.**

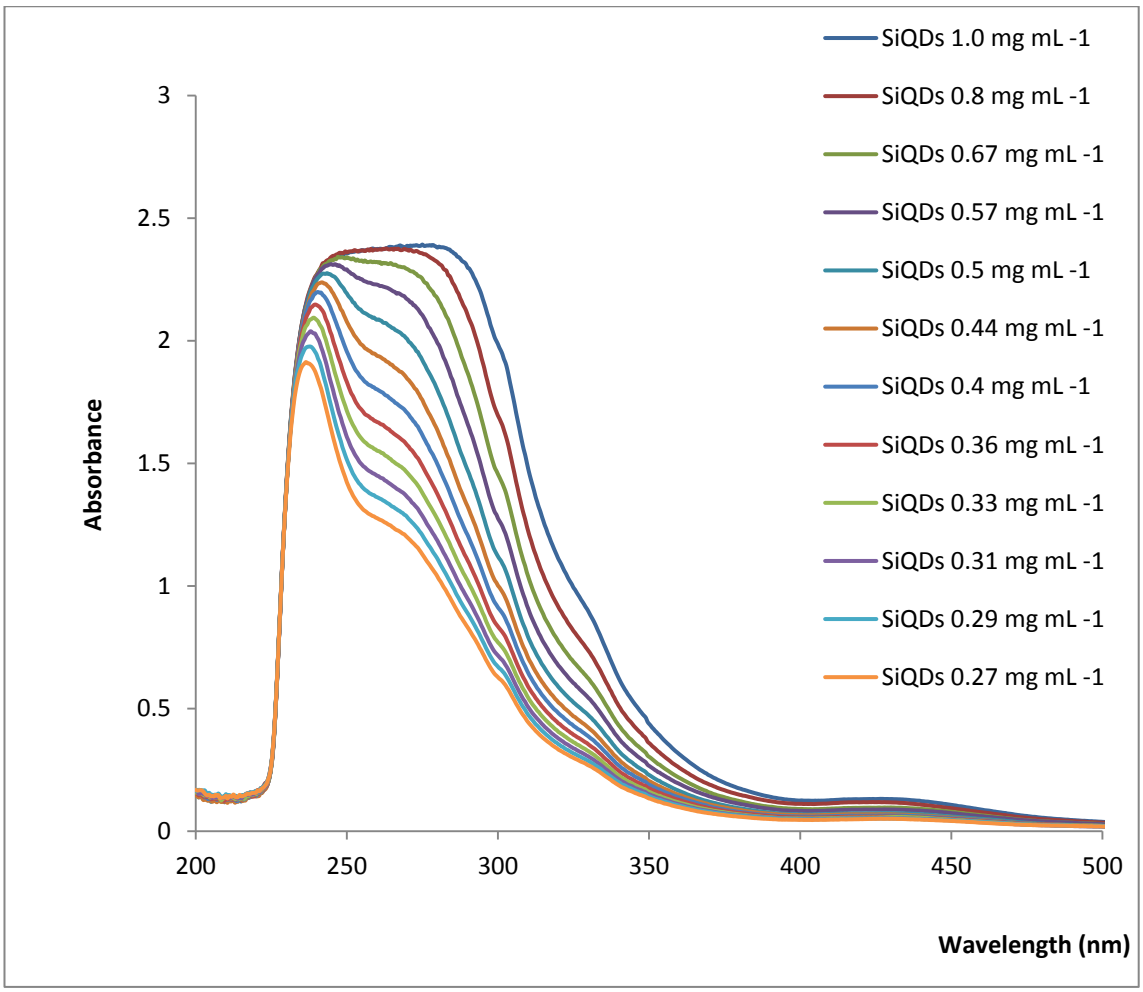

Figure 3. 8 UV-vis absorption spectra of the alkyl-capped silicon quantum dots (SiQDs) in dichloromethane (DCM) with various concentrations measured using a UV-vis spectrometer, Cary model 100.

Although absorption spectroscopy could be used for quantitation, the sensitivity is worse than for fluorescence spectroscopy and the absorption varies in a complex manner with wavelength and concentration. Complete spectrum shows fluorescence more sensitive than absorption. The very high intensity of excitation wavelength is the limitation of absorption.

3.3.4.2 Emission spectroscopy

The fluorescence of serial dilutions of SiQDs in DCM at concentration 0.27, 0.29, 0.31, 0.33, 0.36, 0.40, 0.44, 0.50, 0.57, 0.67, 0.80, and 1.00 mg mL^{-1} were measured using a Spex FluoroMax/GRAMS 32 fluorimeter with 365-nm excitation. Fluorescence spectra were recorded between 400 and 850 nm. SiQDs in DCM showed maximum emission peak approximately 670 nm with excitation wavelength 365 nm. High quality with purification and mono size distribution in each concentration of SiQDs showed only one peak for entire spectrum. The fluorescence spectra of serial dilutions of SiQDs in DCM collected between 400 and 850 nm with 365-nm excitation wavelength are shown in **Figure 3.9.**

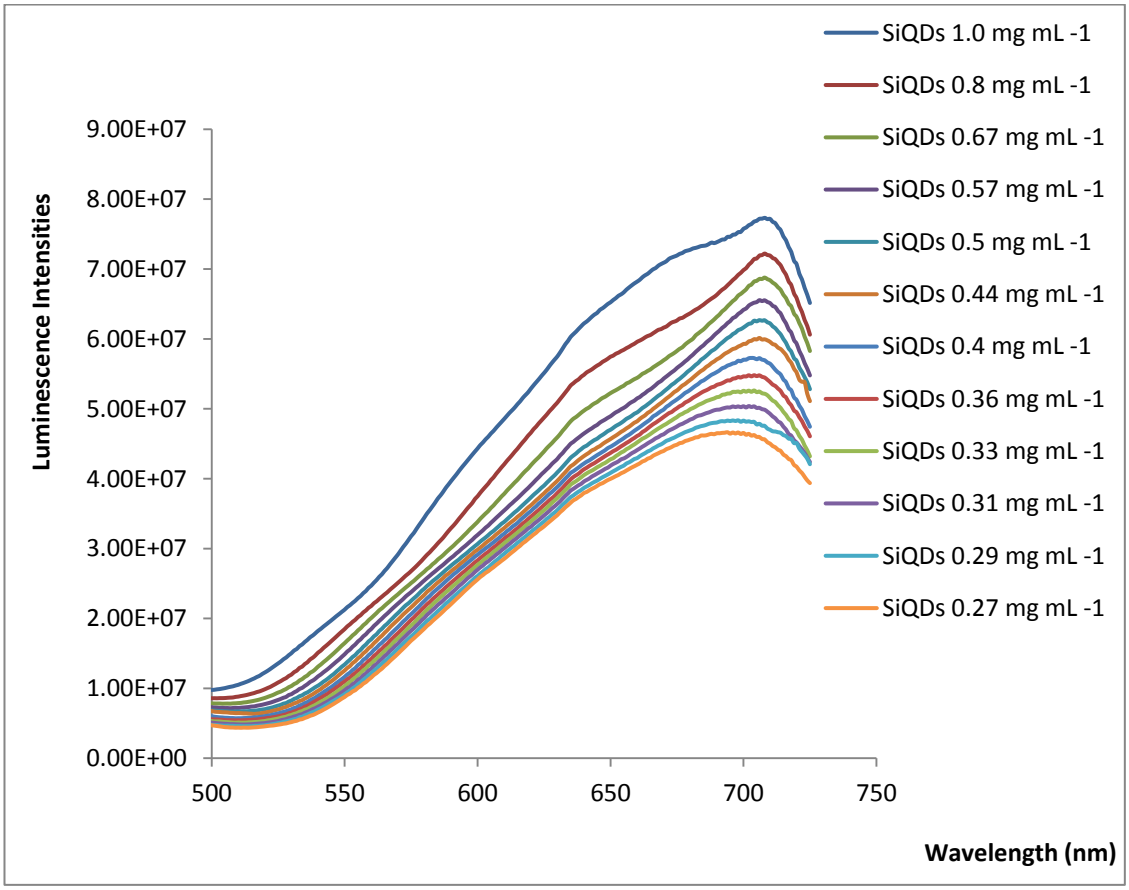

Figure 3. 9 Emission spectra of alkyl-capped silicon quantum dots (SiQDs) dispersed in dichloromethane (DCM) with various concentrations measured using an emission spectrometer, Spex FluoroMax/GRAMS 32 with an excitation wavelength of 365 nm. The rest of luminescence intensities after 730 were not included because they are the 2nd order of scattering.

3.3.4.3 Quantitation study of SiQDs

The fluorescence spectrum for each concentration of SiQDs was integrated to obtain spectral intensity for each dilution. The plot of fluorescence intensities against concentration of SiQDs showed that the emission intensity is linear with the concentration of SiQDs **Figure 3.10**.

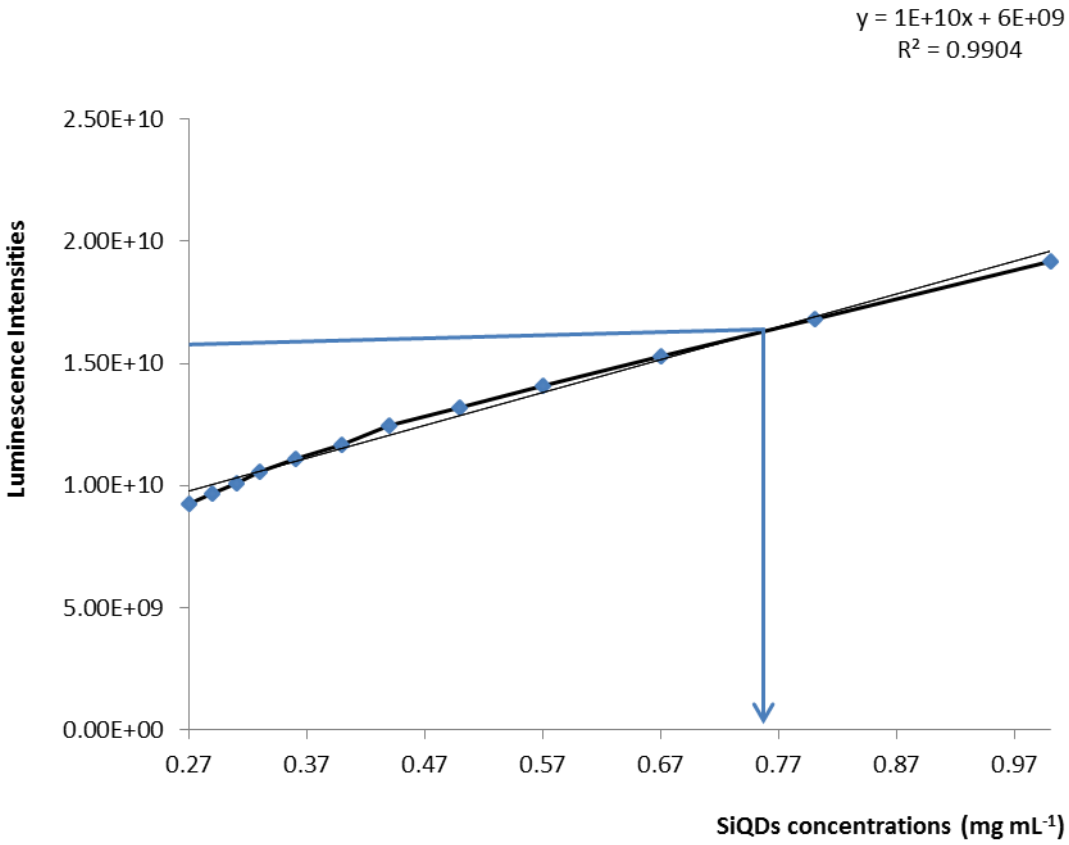

Figure 3. 10 Fluorescence intensities against concentrations of SiQDs, the fluorescence intensities were calculated from emission spectra of alkyl-capped silicon quantum dots (SiQDs) dispersed in dichloromethane (DCM) in various concentrations measured using emission spectroscopy, Spex FluoroMax/GRAMS 32 with an excitation wavelength of 365 nm. The concentration of SiQDs in any sample was calculated by measuring their fluorescence and using the calibration curve in this figure.

3.3.5 Photochemical Properties Studies of SiQDs in Physiological Solutions

3.3.5.1 UV-vis absorption spectroscopy

The absorption properties of SiQDs were studied in various physiological solutions. The SiQDs at a concentration of 0.2 µg mL^{-1} in 1% (v/v) cremophor were dispersed in phosphate- buffered saline (PBS), Krebs solution, complete RPMI medium with phenol red and 10% (v/v) foetal Bovine serum (FBS), and complete DMEM medium with phenol red and 20% (v/v) FBS. The absorption spectra of SiQDs in different physiological solutions were measured using UV visible absorption spectroscopy over the wavelength range of 800-200 nm. The SiQDs at concentrations 0.2 µg mL^{-1} in physiological solutions showed weak absorption at wavelengths greater than 400 nm. Physiological solutions containing phenol red dye and protein (FBS) also showed second and third peaks of absorption spectra at 560 nm for the phenol red dye and at about 260 nm for the proteins present. The absorption spectra of SiQDs in physiological solution are shown in **Figure 3.11.**

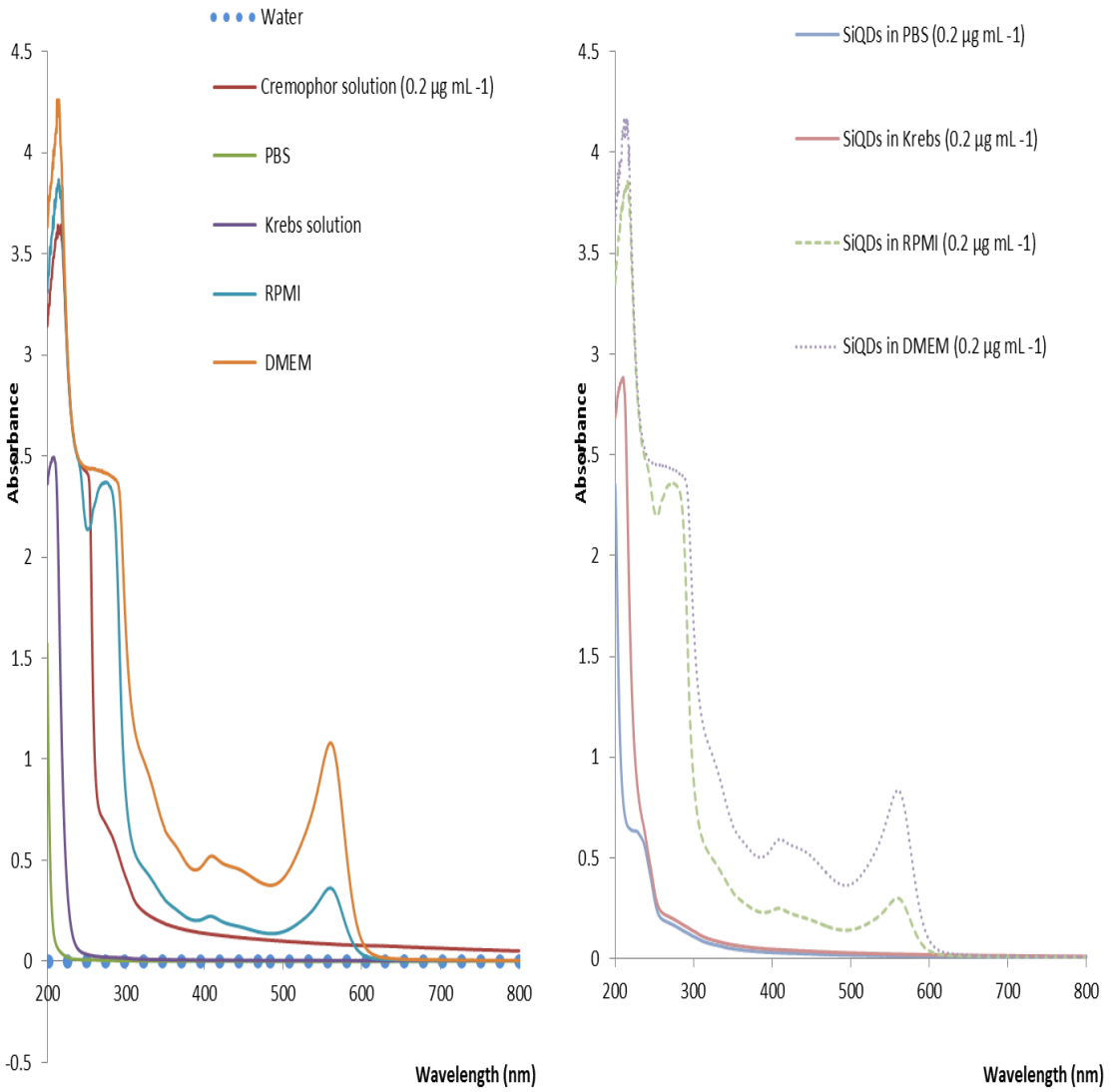

Figure 3. 11 UV-vis absorption spectra of alkyl-capped silicon quantum dots (SiQDs) measured using UV-vis spectroscopy, Cary model 100. The 0.2 µg SiQDs in 1% volume: volume (v:v) cremophor was dispersed in various physiological solutions.

An important conclusion from **Figure 3.11** is that phenol red may interfere substantially with the absorption of light by SiQDs and therefore SiQD internalisation experiments carried out in later chapters use phenol red-free media whenever appropriate.

3.3.5.2 Emission spectroscopy

The fluorescence properties of 0.2 µg mL^{-1} SiQDs in various physiological solutions were measured using fluorescence spectroscopy Spex FluoroMax/GRAMS 32 with 365-nm excitation. Fluorescence spectra were recorded between 400 and 850 nm. SiQDs in PBS and Krebs showed emission spectra in the range of 560-700 nm. Physiological solution containing SiQDs with phenol red dye or phenol red and protein showed broad emission spectra in the range of 400-700 nm. The fluorescence spectra of 0.2 µg mL^{-1} SiQDs in various physiological solutions collected between 400 and 850 nm with 365-nm excitation wavelength are showed in **Figure 3.12.** Again, there is some overlap between phenol red and the SiQDs in the emission spectra which is the reason phenol red-free media were used in the experiments reported in later chapters wherever appropriate. In particular, experiments in which quantitative measurements of the emission of SiQDs were required used such dye-free media.

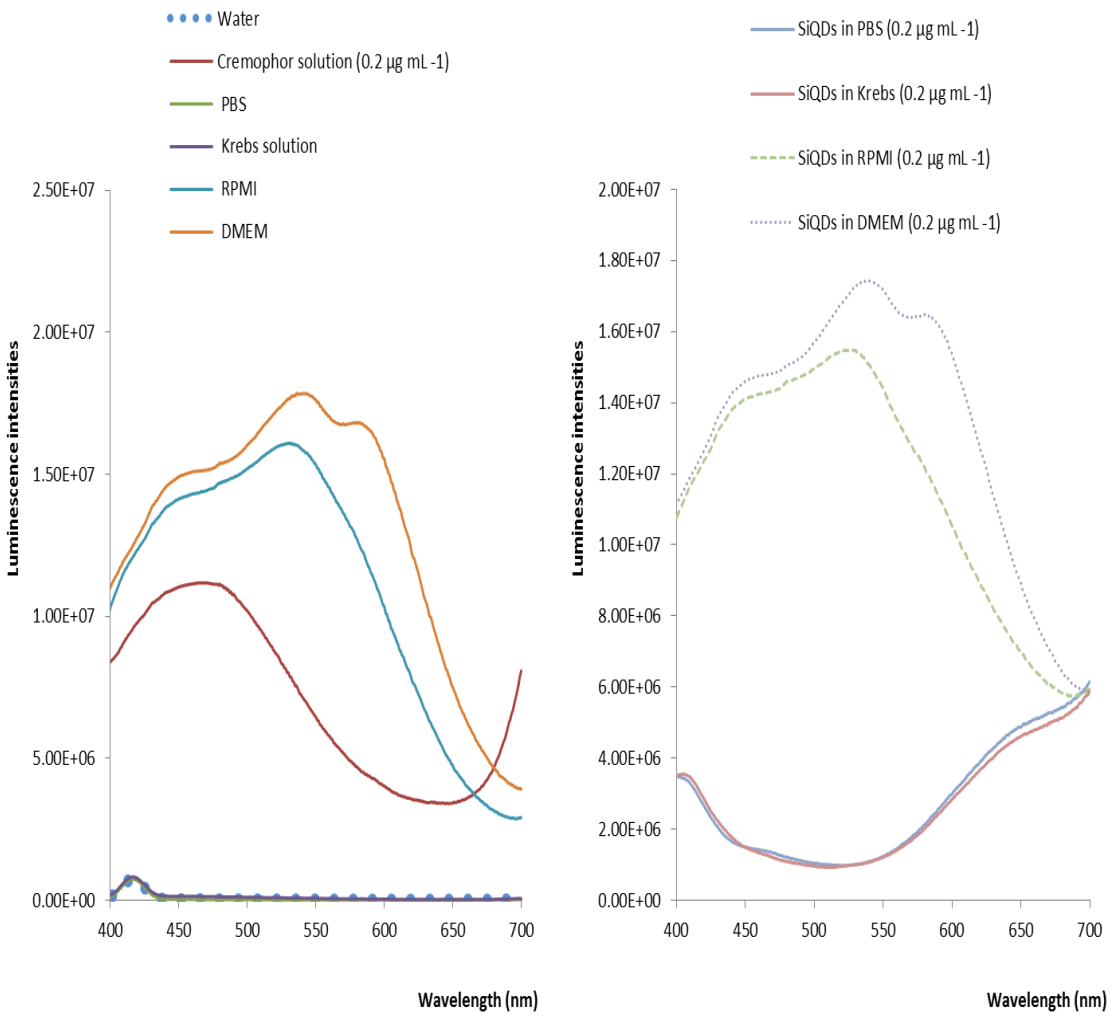

Figure 3. 12 Emission spectra of alkyl-capped silicon quantum dots (SiQDs) measured using emission spectroscopy, Spex FluoroMax/GRAMS 32 with excitation wavelength 365 nm. The 0.2 µg SiQDs in 1% volume: volume (v: v) cremophor was dispersed in various physiological solutions. The fluorescence of SiQDs at 620 nm is masked in the case of the RPMI and DMEM because these media contain phenol red; the PBS and Krebs do not and the SiQD fluorescence is more clearly distinguished.

3.3.6 Luminescent Morphology, Particles Distribution, and Aggregation Studies of SiQDs in Physiological Solutions

3.3.6.1 Scanning Confocal Microscope

Fluorescence images of 1 mg mL^{-1} SiQDs in 0.7% (v/v) cremophor solution and drying on the top of a clean glass slide are shown in figure 3.11. The images were collected by confocal microscope (Leica TCS SP2, UK) with the 488 nm line of an Argon/Krypton ion laser as the excitation light. SiQDs showed strong luminescence and the particles tended to aggregate on the top of coverslip (**Figure 3.13).** The objects observed by fluorescence microscopy are large aggregates of SiQDs, unlike the higher resolution AFM images in which individual SiQDs can be seen.

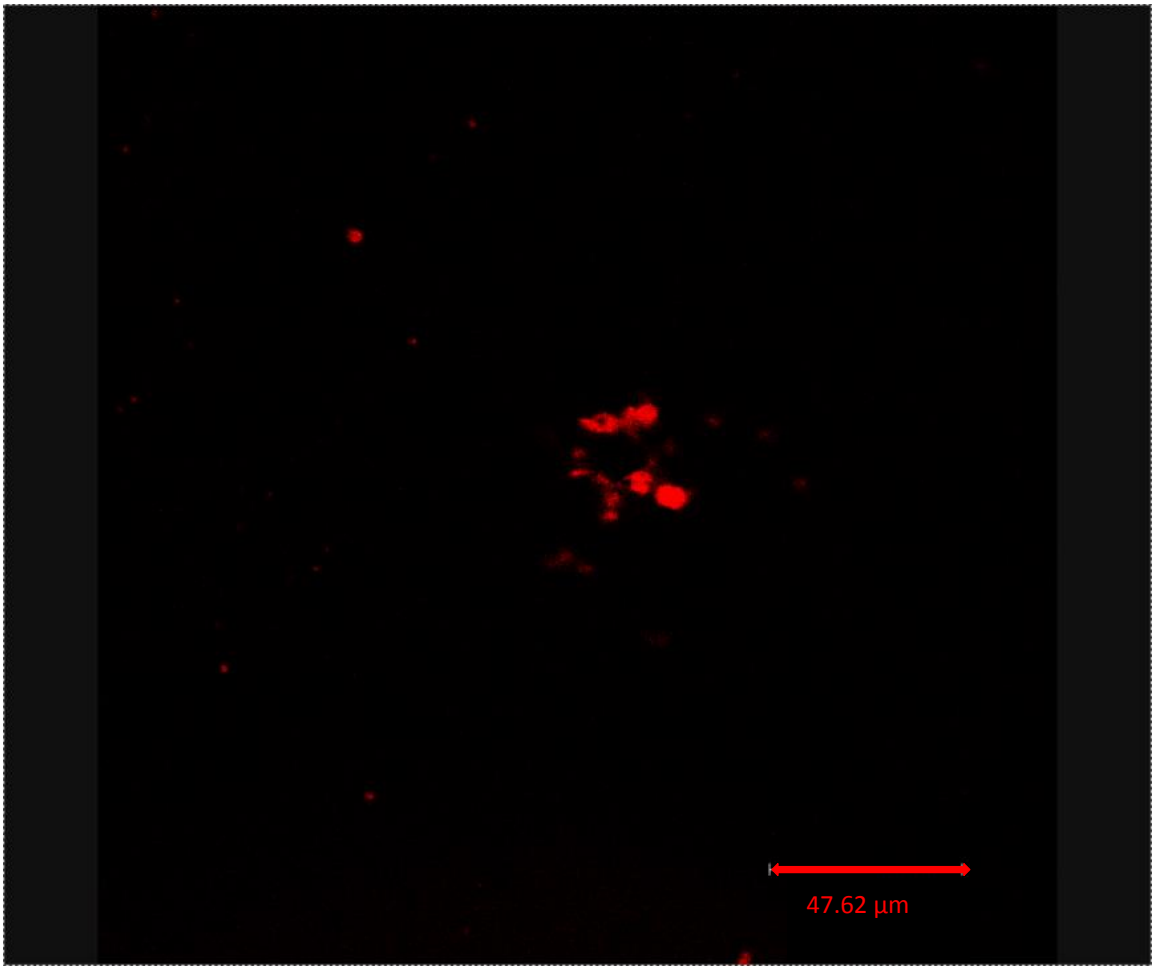

Figure 3. 13 Luminescent image (x1000 magnifications) of SiQDs captured using Confocal Laser Scanning Microscope, Leica TCS SP2, Spectral Confocal and Multiphoton Microscope. The SiQDs suspension solution 50 µL of 100 µg ML^{-1} in 50 µL organic solvent diethyl ether was dispersed in phenol red free medium and dried on the top of slide.

3.3.6.2 Epi-fluorescene Microscopy

Fluorescence images of 100 µg mL^{-1} and 1 mg mL^{-1} SiQDs in 50 µL organic solvents diethyl ether were dispersed in complete medium without phenol red detection and observed using an epifluorescence microscope. 50 µL of SiQDs suspension solution on the top of slide and covered with coverslip showed strong luminescence and exhibited less particle aggregation. The image of strongly luminescence SiQDs dispersed in culture medium captured using fluorescent microscope is shown in **Figure 3.14-15.**

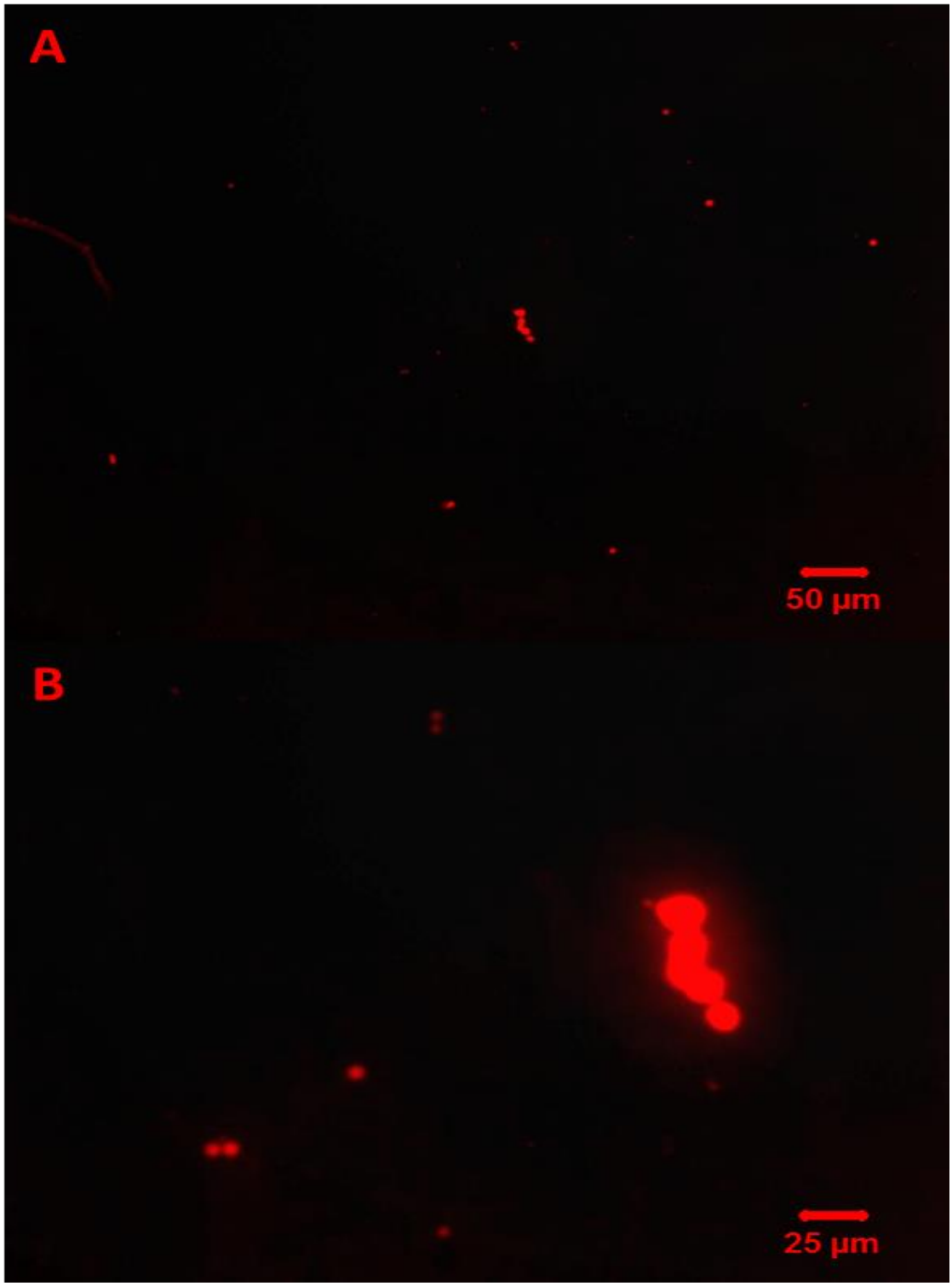

Figure 3. 14 Luminescence image (100 x magnifications) (**A**) and luminescence image (400 x magnifications) (**B**) of SiQDs captured using Luminescence microscopy (Leica Laborlux). SiQDs 100 µg ML^{-1} in 50 µL organic solvent diethyl ether was dispersed in phenol red free medium.

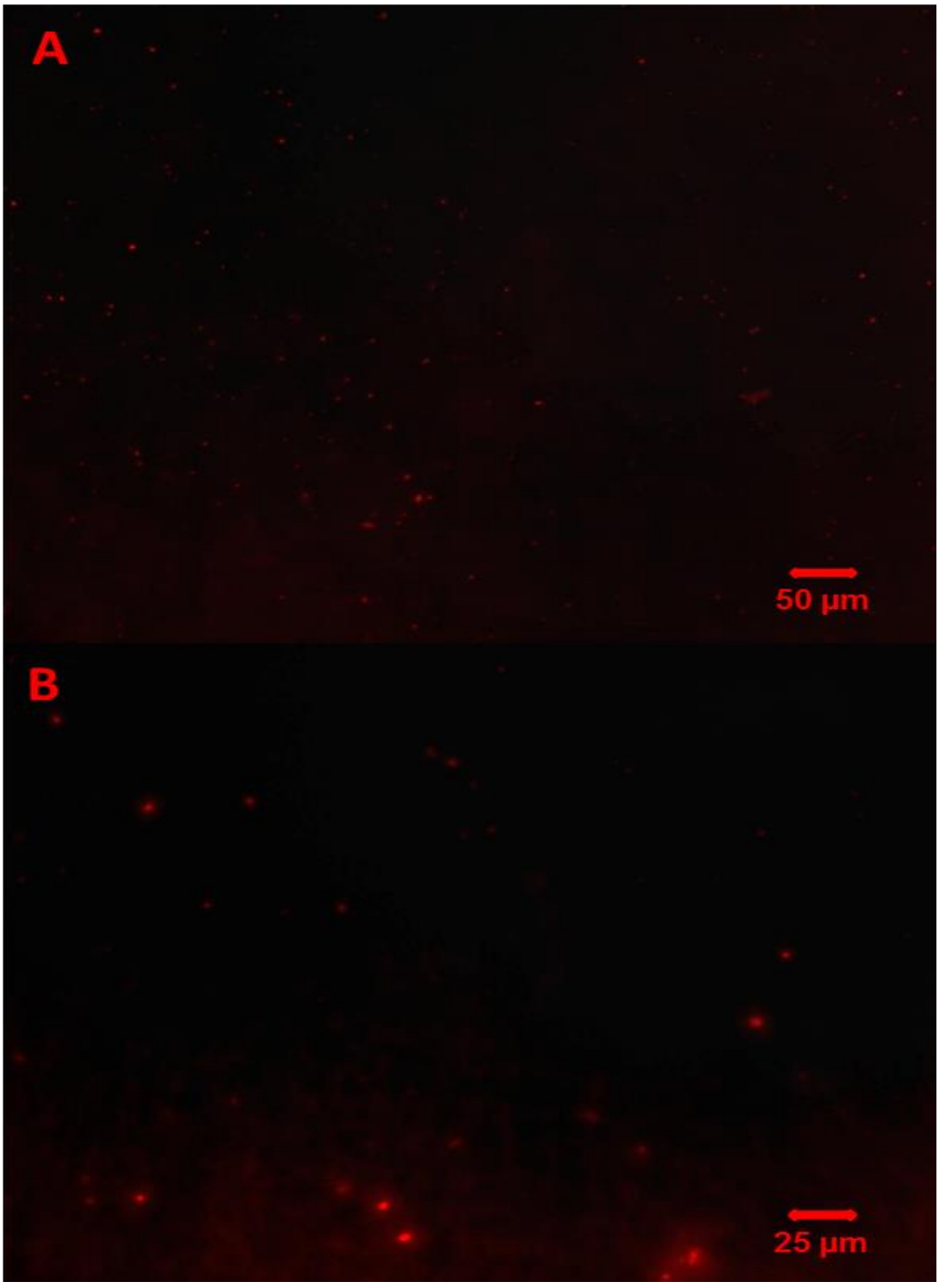

Figure 3. 15 Luminescence image (100 x magnifications) and luminescence image (400 x magnifications) of SiQDs captured using Luminescence microscopy (Leica Laborlux). SiQDs 1 mg ML^{-1} in 50 µL organic solvent diethyl ether was dispersed in phenol red free medium.

3.3.6.3 Confocal Raman Microscope

Fluorescence images of SiQDs inside treated IGE cells with 0.2 µg mL^{-1} SiQDs dispersed in complete medium for 1 hour (preliminary studied) were measured with a confocal Raman microscope using an argon ion laser (488 nm) as excitation source (WiTec model CRM 200, Ulm, Germany). SiQDs accumulate inside the cell and SiQDs showed strong luminescence after internalisation by the cell. The image of strong luminescence of SiQDs inside the cell is shown in **Figure 3.16-19.**

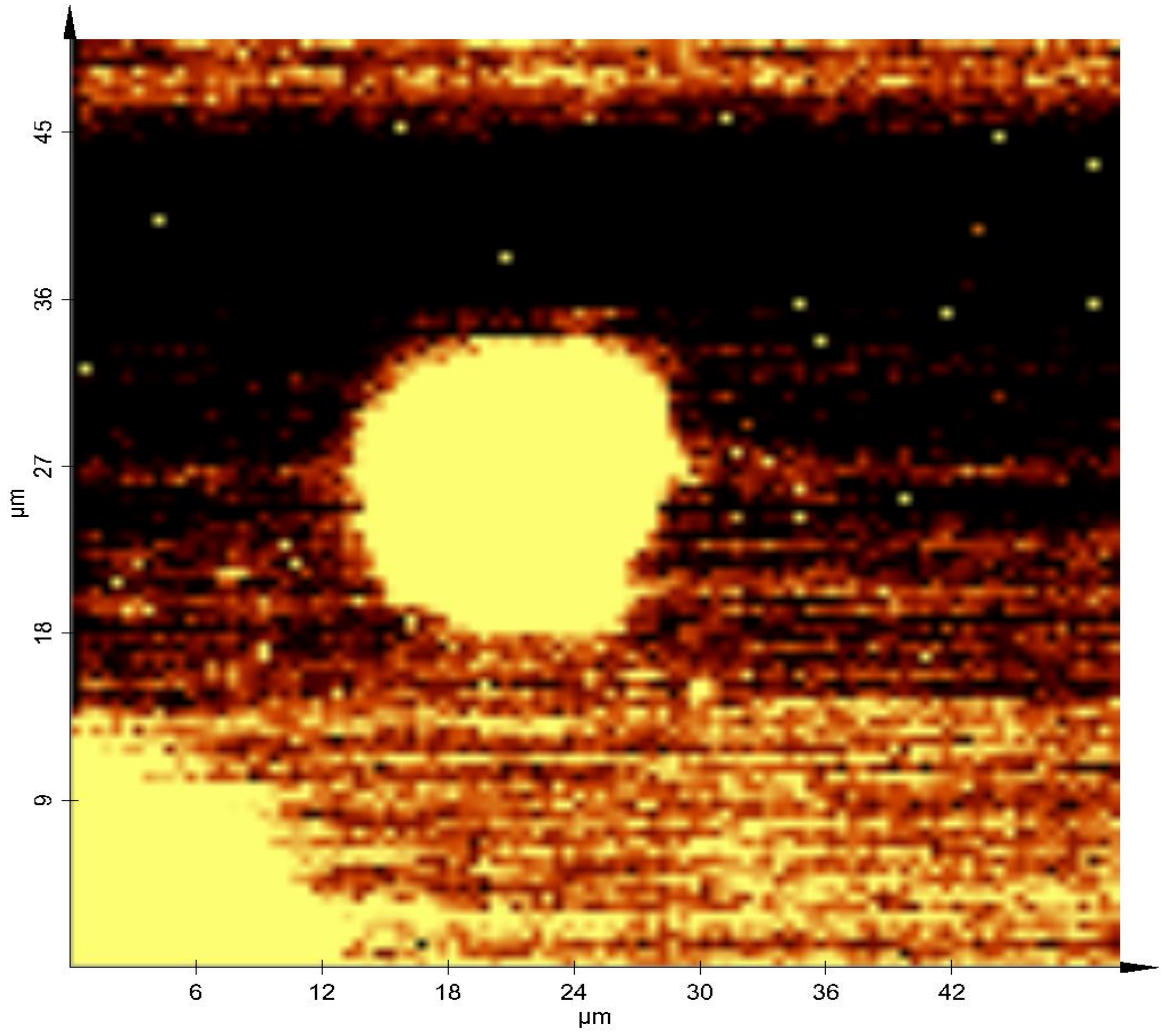

Figure 3. 16 The original image of SiQDs inside the IGE cells captured using confocal microscope. The starving cells had been incubated with 0.2 µg mL $^{-1}$ SiQDs for 1 hour.

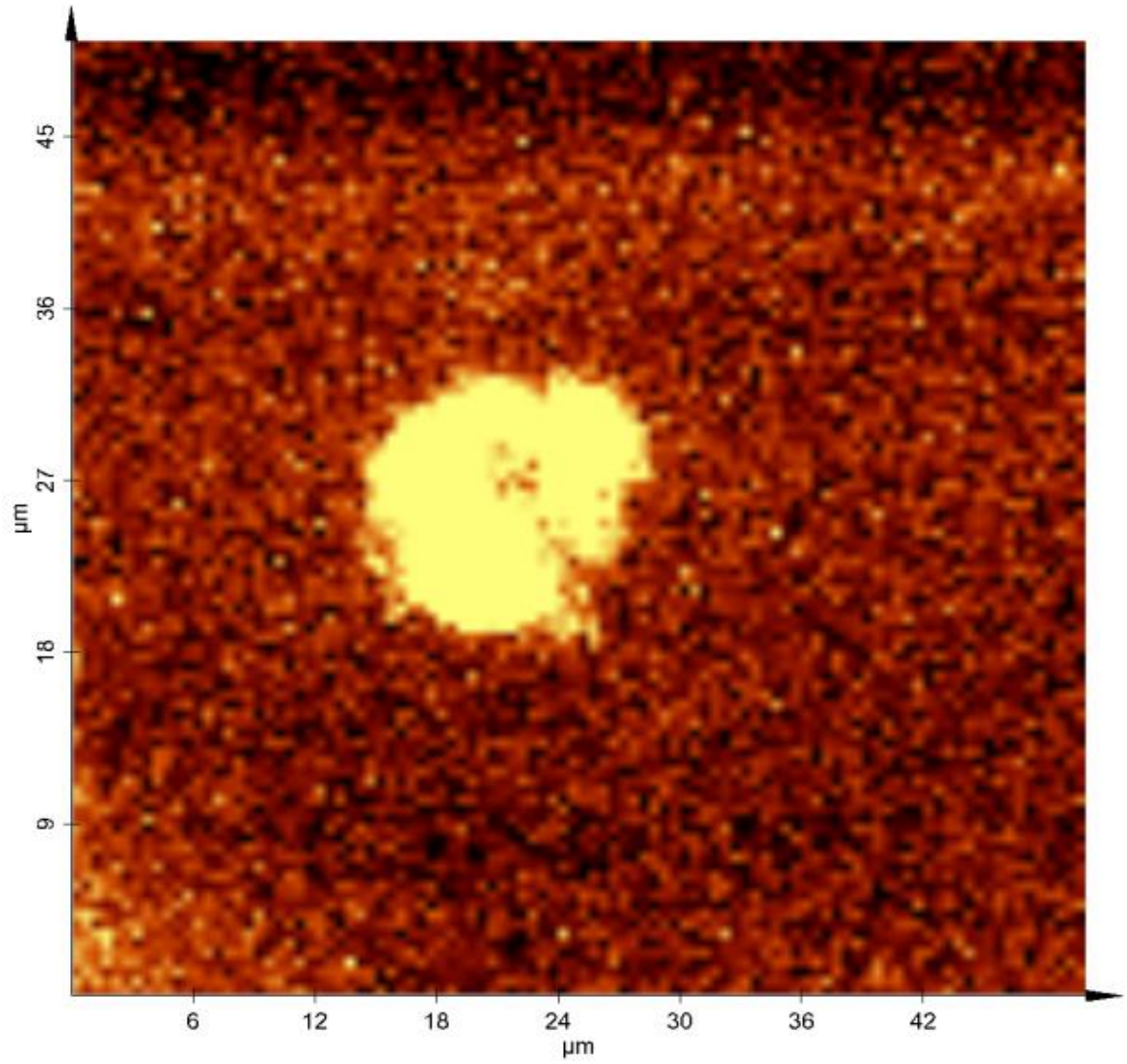

Figure 3. 17 The luminescence image of SiQDs inside the IGE cells captured using confocal microscope. The starving cells had been incubated with 0.2 µg mL^{-1} SiQDs for 1 hour.

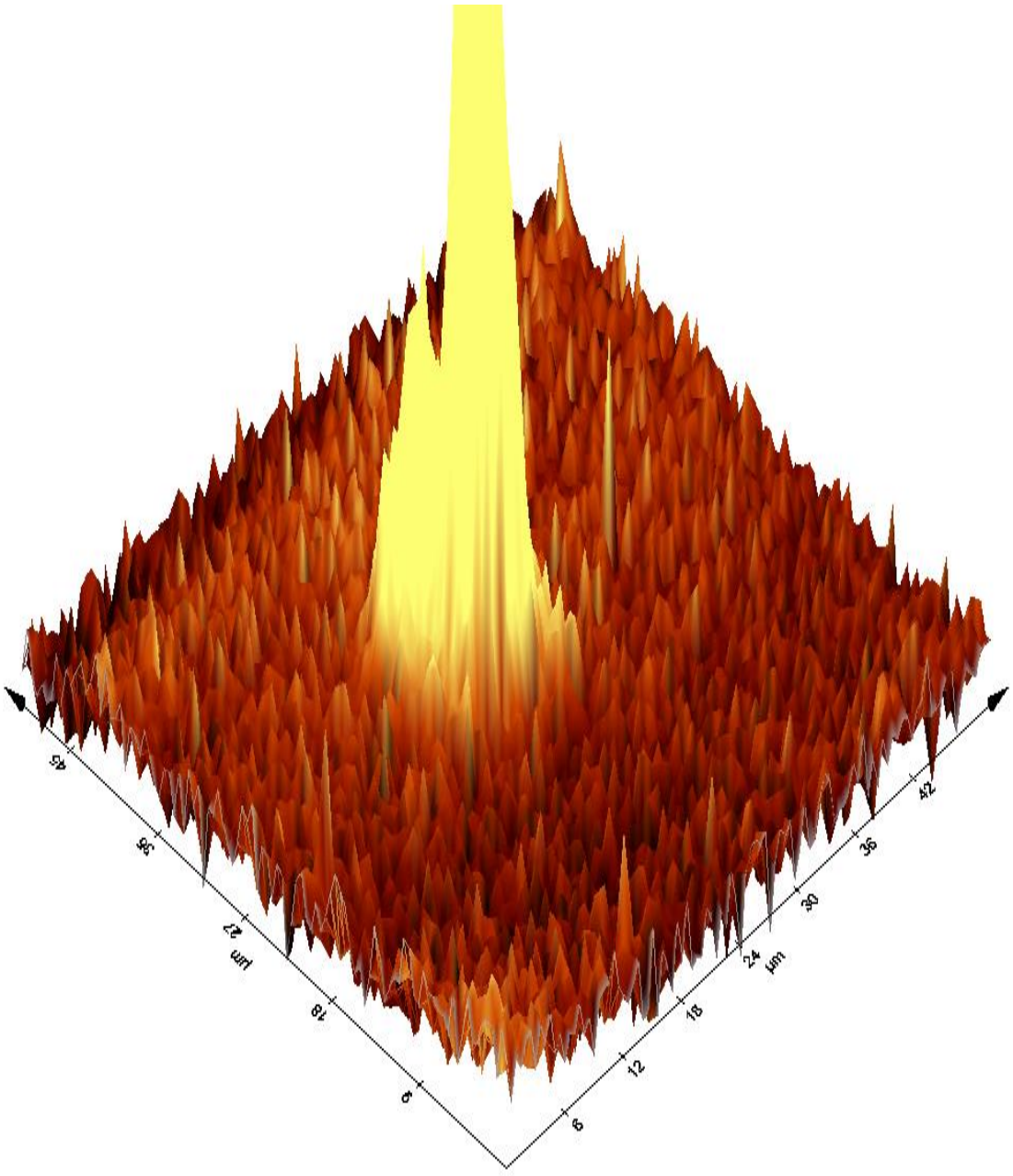

Figure 3. 18 The three dimensional luminescence image of SiQDs inside the IGE cells captured using confocal microscope. The starving cells had been incubated with 0.2 µg mL $^{-1}$ SiQDs for 1 hour.

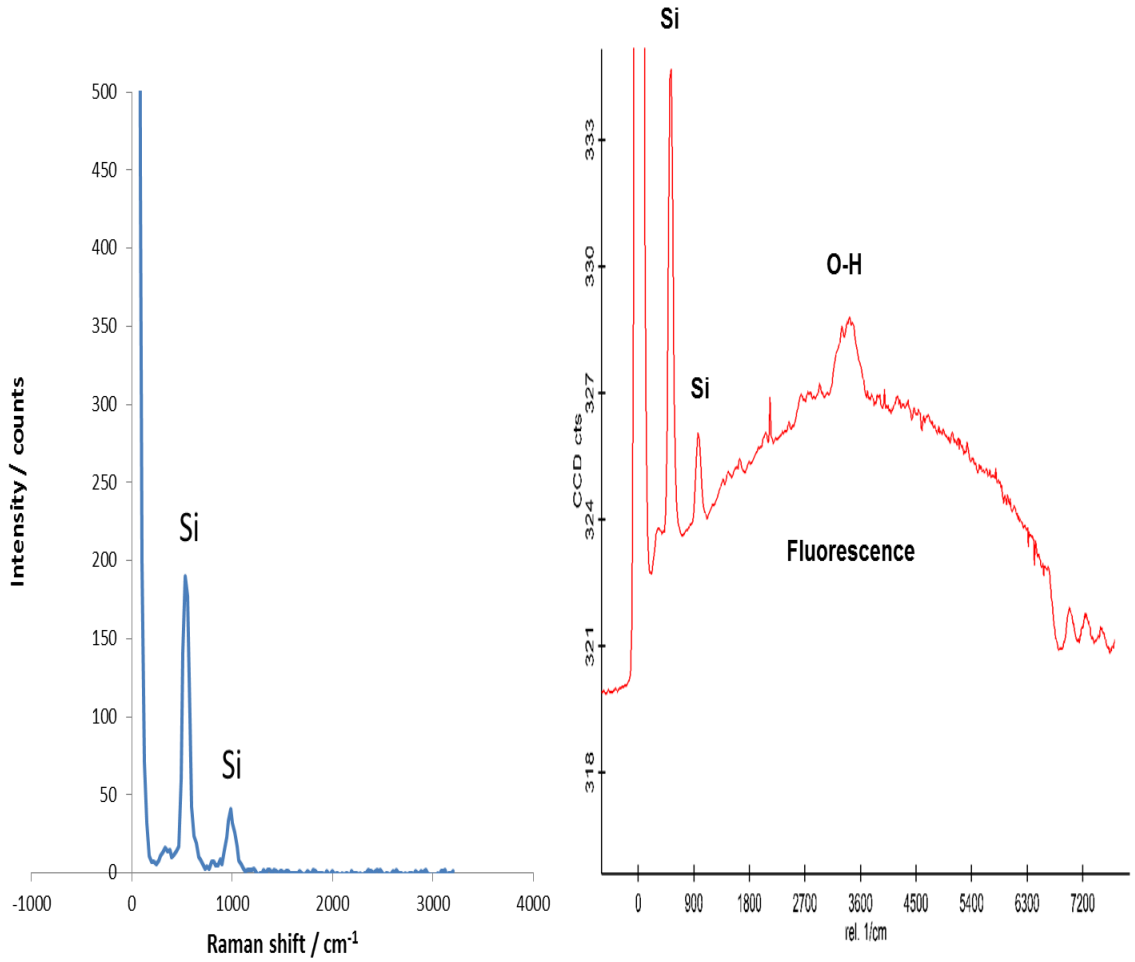

Figure 3. 19 The Raman & luminescence spectrum of SiQDs inside the IGE cells measured using confocal microscope. The starving cells had been incubated with 0.2 µg mL $^{-1}$ SiQDs for 1 hour. The left-hand spectrum is the Raman spectrum of a clean Si wafer, the right hand spectrum shows the broad fluorescence of the SiQDs, the reflected laser light at 0 cm^{-1}, the Si Raman peaks at 520 and 950 cm^{-1} and O-H Raman stretching modes near 3500 cm^{-1}.

3.4 Discussion

Luminescent probes are the major tool applied in many studies of cell organelles and cell function. Consequently various organic dyes have been introduced and widely used in cell biology and biomedical science. However the organic dyes still have some limitations. Typically organic dyes have low stability in physiological conditions and are highly photo sensitive (O'Farrell et al., 2006). The intensity and colour of luminescence of both organic dyes and quantum dots (QDs) both depend on their electronic structure (O'Farrell et al., 2006), however QDs have controllable properties which are determined largely by their radius and may be tuned more easily. QDs show the potential to overcome the difficulties of organic dyes under physiological condition and imaging with high intensity excitation light as in confocal experiments (Michalet et al., 2005). However the toxicity aspect is still a concern for QDs application in life science as the typical QDs are composed of elements in groups II-VI, III-V of periodic table and many of them contain heavy metals, especially Cd. Therefore silicon QDs are one type of QD that is particularly attractive because Si is known to be metabolised to relatively harmless silicate species (Park et al., 2009).

To control the size of semiconductor (silicon) particles and exploit the quantum confinement effects is challenging because as well as the particles' stability, one must also control the polydispersity of the size distributions. Lars H. Lie and colleagues, 2002 successfully prepared alkyl-capped silicon quantum dots (SiQDs). They prepared strong luminescent SiQDs from silicon wafer with high current densities in hydrofluoric (HF)-ethyl alcohol solution followed by a reflux in anhydrous toluene with undecene (Lie et al., 2002). Consequently SiQDs revealed narrow size distribution and were stable in aqueous solutions as well as water insoluble, their stability is a consequence of the strong Si-C bond between the particle surface and the undecyl (C_{11}) capping reagent. However SiQDs were easy to prepare as a clear colloidal solution in organic solvents and dispersed in aqueous media to make monodidperse distribution colloidal. SiQDs in organic solvents for instance dimethyl sulfoxide (DMSO), diethyl ether, and tetrahydrofuran can make clear colloidal solution in aqueous media (Dickinson et al., 2008). The aqueous dispersion SiQDs showed linear correlation between

luminescent intensities and concentration. They also tolerate media pH changing (Dickinson et al., 2008). SiQDs showed strong luminescent inside tumour derived cell lines as well as low cytotoxicity (Alsharif et al., 2009).

In this study, SiQDs were prepared by a minor modification of the methods of Lars H. Lie and colleagues, 2002. The method used is described in detail by Chao et al and was successful in producing narrow size distributions of SiQDs with mean diameters in the range of 5 to 7.5nm (diameter of particle + cap, the diameter of the Si core is about 2.5 nm). The sizes of the SiQDs are smaller than the Bohr radius of the bulk materials and therefore they show strong quantum confinement effects with unique optical properties (Shirahata, 2011). They were confirmed by the onset of absorption of light at wavelengths below 400 nm and the emission of orange photoluminescence in the range 600-650 nm typically. Additionally SiQDs in aqueous media showed narrow size distribution, and low flocculation with strong intensities luminescent characterised by using fluorescent and confocal microscopy. In addition, SiQDs which had been incubated with epithelium cell were internalised and revealed strong luminescent detected using confocal microscope inside the cell.

In summary, the mean SiQDs diameter was obtained from AFM height measurements and was in the range of 5 to 7.5 nm. This is similar to previous work (Chao et al., 2007, Alsharif et al., 2009). Also the image of SiQDs which had been capped by AFM revealed a roughly spherical shape. SiQDs which had been dispersed in DCM showed a yellowish, clear solution with high luminescence. Dispersion of the SiQDs in ether or DCM was found to be the simplest accurate method to divide a given sample into equal portions for biological studies. These solvents have a high vapour pressure and evaporate quickly to leave dry SiQD samples and therefore do not contaminate the biological systems (see toxicity data in later chapters). The low concentration of SiQDs in organic solvent such as diethyl ether and dispersed in physiological solutions without foetal Bovine serum (FBS) exhibited high luminescent intensities compared with the complete solution with FBS. Alkyl-capped SiQDs revealed strong emission with a maximum wavelength of around 650 nm and it was found that a 1 cm^{-2} of 20 silicon chips can produce up to 10 mg of SiQDs. A uniform and successful size distribution of SiQDs in physiological solution was

also measured using confocal microscopy and fluorescence microscopy. The SiQDs which had been internalisation by the cell showed strong luminescent intensities measured using confocal Raman microscopy. It revealed that photochemical properties of SiQDs were durable to cell metabolism (preliminary studied 1 hour).

Chapter 4. Cellular Internalisation Studies: Imaging and Cellular Localisation of Alkyl-Capped Silicon Quantum Dots (SiQDs)

4.1 Introduction

Fluorescent organic dyes have several limitations which are revealed in experiments associated with high energy and long exposure time; in particular they are susceptible to photo-oxidation and fading (O'Farrell et al., 2006). In addition, the fluorescent properties of organic dyes may not be stable in different physiological solutions because of protonation or other chemical interactions (Invitrogen, 2005, O'Farrell et al., 2006). Quantum dots or fluorescent semiconductor nanoparticles have drawn the attention of many researchers because of their stability and brightness. Furthermore quantum dots also have unique photophysical properties; the colour of the fluorescence can be changed by tuning the particle size and Q-dots of different fluorescent colours can be excited by the same wavelength. These properties are advantageous for multicolour detection using only one excitation wavelength (Jaiswal and Simon, 2004).

Despite this, the standard cadmium selenide particles do show some cytotoxicity in long duration experiments and therefore other materials, particularly silicon quantum dots, are being investigated as an additional, safer choice for the fluorescent probe (O'Farrell et al., 2006, Martin, 2013). Silicon quantum dots are promising fluorescent probes with small overall diameter, low cytotoxicity effects, strong fluorescence, and, appropriately capped, are stable under aqueous conditions.

In addition to being a safer alternative QD with properties resulting from quantum confinement, Si QDs also have a much simpler structure than other quantum dots because an organic monolayer can be used to both cap and stabilise the inorganic core as well as facilitating conjugation to biomolecules via standard organic chemistry (Sailor and Lee, 1997). Changing the layer capping on the silicon core can turn on and off the photoluminescence, allowing for tuning of chemical and physical characteristics (Sailor and Lee, 1997); (Bateman et al., 1998). SiQDs have been used for cell specific target labelling, while other applications, including use in drug discovery, diagnostics and genetic disease have also been proposed but require further study. Wang and colleagues (2004) developed a multiple layer capping of SiQDs with alkyl-linker and oligonucleotides. These systems produce a SiQD probe with sequence-

specific binding to target DNA (Wang et al., 2004). Cellular interactions of SiQDs were studied by Shiohara and colleagues (2011); the group showed that allylamine capped silicon nanocrystals can be used as a biocompatible biological markers. The fluorescent amine terminated silicon nanocrystal was internalised by a human-derived tumour breast cell line and accumulated in lysosomes as confirmed by confocal fluorescence (Shiohara et al., 2011).

A new application of SiQDs was developed by Erogbogbo and colleagues (2010) to produce a multifunctional probe. Micelles were used to encapsulate a mixture of SiQDs and Iron oxide QDs. The composite object allows both fluorescence imaging and exploitation of magnetic effects (Erogbogbo et al., 2010). In a similar fabrication as that of Erogbogbo et al, SiQDs were combined with a fluorescent enhancer and encapsulated within micelles. In this case, SiQDs were combined with an anthracene-based dye followed by micelle-encapsulation. Fluorescence of the SiQDs was excited via energy transfer from the attached dye (Erogbogbo et al., 2012).

In an effort to improve stability and increase applications of SiQDs for commercial products and biological applications, SiQDs have been coated with polymer, styrene and 4-vinylbenzaldehyde using miniemulsion polymerisation techniques. The polymer encapsulated SiQDs tolerated alkaline conditions and emitted strong luminescence (Harun et al., 2011). SiQDs have also been encapsulated with the polymer Pluronic F127 (containing the block copolymer P85 (PPO)). The F127 encapsulated SiQDs were internalised via caveolae-mediated endocytosis and targeted at the endoplasmic reticulum; they were successfully used to image the ER in live cells in long duration studies (Shen et al., 2011).

Dextran-coated silicon quantum dots have been used in positron emission tomography (PET). PET is a powerful nuclear imaging technique for investigating nanomaterial probe distribution deeply inside animal and human bodies. The radioactive copper ($^{64}Cu^{2+}$)-labelled and dextran-coated SiQDs show exceptional fluorescent stability and quantitative PET images (Tu et al., 2011). Due to lack of toxicity and the absence of heavy metals, SiQDs have been increasing used in in vivo studies. Micelle-encapsulated SiQDs with various end terminal groups: methoxy, amine, folate, and transferrin groups

have been used by Erogbogbo and colleagues, 2011 to image different kinds of tumours, their spreading stage and localisation (Erogbogbo et al., 2011b). One dimensional (1D) silicon nanostructures were studied by Zhang and colleagues (2012). The internalisation of folate-functionalised silicon nanotubes was observed to be accelerated, and on accumulation in immortalised Chinese hamster ovary cells (CHO) these nanostructures showed strong fluorescence (Zhang et al., 2012). In order to improve aqueous dispersibility, SiQDs have been coated with allylamine. The amine-terminated SiQDs were stable and resistant against aging in alkaline conditions; however, they produced adverse effects on a human liver derived cell line (HepG2) (evaluated cytotoxicity using the MTT assay (Ahire et al., 2012)).

In a recent study by Hajjaji and colleagues, 2014, SiQDs were used as a thermal probe. These new applications of the alkyl-capped silicon quantum dots show that novel ways of employing silicon nanoparticles may yield valuable and increasing applications in the future (Hajjaji et al., 2014).

In spite of much progress in silicon quantum dot (QDs) applications studies, there are not many studies that focus on basic information concerning how cells interact and internalise SiQDs. There are a few, but not many studies concerning the basic safety information of silicon nanoparticles. The expected low cytotoxicity of SiQDs (which has been confirmed in a few studies (Alsharif et al., 2009), is based on the absence of heavy metals and the known metabolism of bulk silicon which is degraded and eliminated from organism in the form of silicic acid (Park et al., 2009). However, to increase the applications of silicon particles in life sciences, it remains essential to obtain direct cytotoxic profile and to study the mechanism of internalisation of SiQDs.

Alkyl-Capped Silicon Quantum Dots (SiQDs) are a type of semiconductor nanoparticle. SiQDs comprise nanocrystalline silicon that is surrounded by C_{11} alkyl monolayer. The alkyl monolayer protects the silicon core from oxidation and stabilises the particle in an aqueous environment (Alsharif et al., 2009). This is necessary because Si has a tendency to react with water and oxygen to form, eventually, SiO_2 or silicates. The hydrophobic character of the alkyl monolayer makes the SiQDs water-insoluble, but they can be dispersed in organic solvents such as dichloromethane (DCM) and diethyl ether (ether) to

make homogeneous solutions (Dickinson et al., 2008). SiQDs in DCM and ether produce a yellowish, clear suspension. The serial dilutions of SiQDs show a linear correlation of emitting intensity against concentration. This is useful for quantitation and another advantage over molecular dyes which show strongly nonlinear intensity concentration calibrations because of intermolecular interactions. SiQDs in DCM showed a strong orange fluorescence maximum at 620 - 670 nanometres (nm) for excitation energies below about 500 nm.

The SiQDs synthesised in this study have a mean diameter in the range 5-7.5 nanometre (nm); this figure includes the stabilising capping monolayer of hydrophobic undecyl-chains. A homogenous suspension of SiQDs with narrow size distribution can nevertheless be prepared in aqueous solutions by first suspending SiQDs in organic solvents. A small amount of solution is then rapidly mixed with aqueous solutions or even physiological media. Ether or Cremophor were preferred vehicles to achieve the dispersal of SiQDs in aqueous media, the former because it's high volatility means that after dispersal, the ether rapidly evaporates and therefore no toxic effects are observed from the organic solvent. The latter was chosen because it is widely used in pharmacology for administration of hydrophobic drugs. SiQDs in physiological solution such as phosphate buffered saline (PBS), Krebs solution, and cell culture medium without phenol red and foetal Bovine serum (FBS) also emit fluorescence at 620 – 670 nm, but it is generally preferable to work in phenol-red free media to avoid interference from the absorption of that dye (see Chapter 3). Although SiQDs in physiological solutions showed similar fluorescence spectra to those for dispersions in organic solvents, the fluorescence signal was generally lower simply because of the dilution required to achieve dispersal in aqueous media.

The work reported in this chapter is concerned with the fluorescent properties of SiQDs in physiological solutions, their use as fluorescent stains in experiments with cultured cells and confirmation of their internalisation by human cells (CACO-2). Optical images of CACO-2, which had been treated with physiological solution containing SiQDs, were captured using epifluorescence and confocal microscopy. Moreover, the SiQDs fluorescence spectra were analysed using a confocal Raman microscope with spectrograph to confirm SiQDs localisation inside the cell. In this study CACO-2 was used as a model

in which to explore the uptake and interaction of SiQDs with cells using fluorescence imaging. CACO-2 cells were derived from tumour colon cells and commonly used by other workers in studies of nanoparticle cytotoxicity (Ruizendaal et al., 2009). The CACO-2 cell line was chosen as a model for the interaction of nanoparticles with the gastrointestinal tract, a major route for the exposure of humans to nanoparticles (oral route).

4.2 Methods

4.2.1 Cellular Internalisation Studies Using SiQDs and Observation with an Epi-Fluorescence Microscope

To quantify internalisation and demonstrate visualisation of alkyl-capped silicon quantum dots (SiQDs) inside human cells, the human-derived colon tumour cells (CACO-2) were treated with SiQDs for 1 and 4 hours. In addition some experiments with longer term exposure of 14 days to look for chronic effects were made. The CACO-2 were cultured as described in Section 2.3 but in Dulbecco's modified Eagle's medium (DMEM) complete medium without phenol red in 75 cm^2 culture flasks (filter cap) (T75). For visualisation of the cellular fluorescence, (short time studies) $5x10^3$ cells mL^{-1} of CACO-2 were cultured overnight on cleaned coverslips using 70% (v/v) ethyl alcohol. After 24 hours, the cells were treated with freshly prepared 0.2 µg mL^{-1} SiQDs from a stock solution of 1 mg mL^{-1} SiQDs in 0.7% (v/v) cremophor solution in phenol red-free medium for 1 and 4 hours. The treated cells were washed 3 times with phosphate-buffered saline (PBS). To visualise SiQDs inside the living cells, the coverslip was taken out from the plate and placed on the top of the slide with the cells on the top side. Then the coverslip was sealed with 50 µL Mowiol mounting medium and another cleaned coverslip. The mounted slides were visualised using an epi-fluorescence microscope (Leica Laborlux) with excitation provided by a mercury arc lamp and a 300-400 nm bandpass filter which selects mainly the 365 nm line of the mercury lamp.

To visualise the optical images of cells after 14 days 'chronic' exposure, 5% (v/v) of 70-80 % confluence of CACO-2 (10^3 cells mL^{-1}) were cultured in culture flasks (filter cap), treated surface area 25 cm^2 (T25) overnight. After 24 hours, the cells were treated with various concentrations of freshly preparation SiQDs at 0.5, 5, and 50 µg mL^{-1} from a stock solution of 1 mg mL^{-1} SiQDs in 10 µL

diethyl ether (ether) in phenol red-free medium. The cells were treated with SiQDs for 14 days and the medium were replaced with a fresh preparation of SiQDs suspension every two days. After 14 days the cells were washed with PBS 3 times. Then the cells were removed from the flasks using trypsin solution. The cell pellets were then collected and suspended in 500 µL PBS. To visualise SiQDs inside the cells, 50 µL of the cell suspension was mixed with 50 µL Mowiol mounting medium and 50 µL of the mixture dropped on the top of a clean slide. The slide then was covered with clean coverslips. The cell slides were visualised using an epifluorescence microscope (Leica Laborlux) with excitation provided by a mercury arc lamp and a 300-400 nm bandpass filter which selects mainly the 365 nm line of the mercury lamp.

4.2.2 Cellular Internalisation Studies Using SiQDs and Detection with High Resolution Scanning Confocal Microscope

To quantify internalisation and visualisation of alkyl-capped silicon quantum dots (SiQDs) inside human cells, CACO-2 cells were treated with SiQDs for 0.5,1, 2 and 4 hours. The CACO-2 were cultured as described in Section 4.2.1. For optical images of short time studies $5x10^3$ cells mL^{-1} of CACO-2 were cultured on cleaned coverslips overnight. After 24 hours the cells were treated with freshly prepared 0.2 µg mL^{-1} SiQDs from stock solution 1 mg mL^{-1} SiQDs in 0.7% (v/v) cremophor solution in phenol red free medium for 0.5, 1, 2 and 4 hours. The treated cells were washed 3 times with phosphate-buffered saline (PBS). To visualise SiQDs inside the living cells, the coverslip was taken out from the plate and placed on the top of a glass slide with cells on the top side. Then the coverslip was sealed with 50 µL Mowiol mounting medium and covered with another cleaned coverslip. The mounted slides were imaged using a confocal microscope (Leica TCS SP2,UK) with the 488 nm line of an Argon/Krypton ion laser as the excitation light.

4.2.3 Spectral Analyses of SiQD Internalisation Using Confocal Raman Microscope

To quantify internalisation and visualisation of alkyl-capped silicon quantum dots (SiQDs) inside human cells, CACO-2 cells were treated with SiQDs for 1 hour. The CACO-2 were cultured in Dulbecco's modified Eagle's medium (DMEM) as described in Section 4.2.1. For optical images of short time studies $5x10^3$ cells mL^{-1} of CACO-2 were cultured on cleaned silicon wafers overnight.

After 24 hours the cells were treated with freshly prepared 0.2 µg mL^{-1} SiQDs from stock solution 1 mg mL^{-1} SiQDs in 0.7% (v/v) cremophor solution in phenol red free medium for 1 hour. The treated cells were washed 3 times with phosphate buffered saline (PBS). To visualise SiQDs inside the living cells, the wafer was taken out from the plate and placed on the top of the slide. The slides were visualised and images captured using a confocal microscope (CRM200, Witec, Ulm, Germany) with the 488 nm line of an argon ion laser (35 mW output power) as the excitation light as well as detected luminescence/Raman spectrum.

4.3 Results

4.3.1 Cellular Internalisation Studies Using SiQDs and Observation with Epi-Fluorescent Microscope

To characterise cellular internalisation of SiQDs inside human derived tumour cells over short and long exposure times, CACO-2 were treated with SiQDs for periods of 1, 4 hours and up to 14 days. Internalisation of SiQDs by CACO-2 was confirmed using an epi-fluorescence microscope (excitation ~365 nm from Hg Lamp). Fluorescent images were overlaid on the bright field optical images using ImageJ software; this facilitates localisation of the fluorescence and, with control experiments, allows the SiQD fluorescence to be distinguished from background. The SiQD fluorescence signal dominates the background and is shown as a red false colour representing the intensity of fluorescence (the CCD camera in the microscope is monochrome) **(Figure 4.1)**. The overlaid fluorescence images of CACO-2 treated with SiQDs for 4 hours showed stronger luminescent of SiQDs when compared with 1 hour treated cells and control cells. CACO-2 treated with SiQDs for 4 hours showed strong luminescence (red spots in **Figure 4.1 E&F**) while 1 hour-treated cells showed some fluorescence, but not strongly localised (weak, blurry red colours in **Figure 4.1 C&D**). The CACO-2 treated with SiQDs for 14 days showed the brightest luminescence indicating that the cells continue to internalise the SiQDs for long periods with no apparent harmful effect on the cell morphology. The SiQDs internalised by CACO-2 appear to localise around membranes, but there is some fluorescence dispersed in the cytoplasm. This is perhaps expected because of the highly lipophilic nature of the alkyl capping on the

SiQDs. Bright fluorescence from SiQDs internalised by CACO-2 and overlaid optical images are shown in **Figure 4.1 and Figure 4.2**.

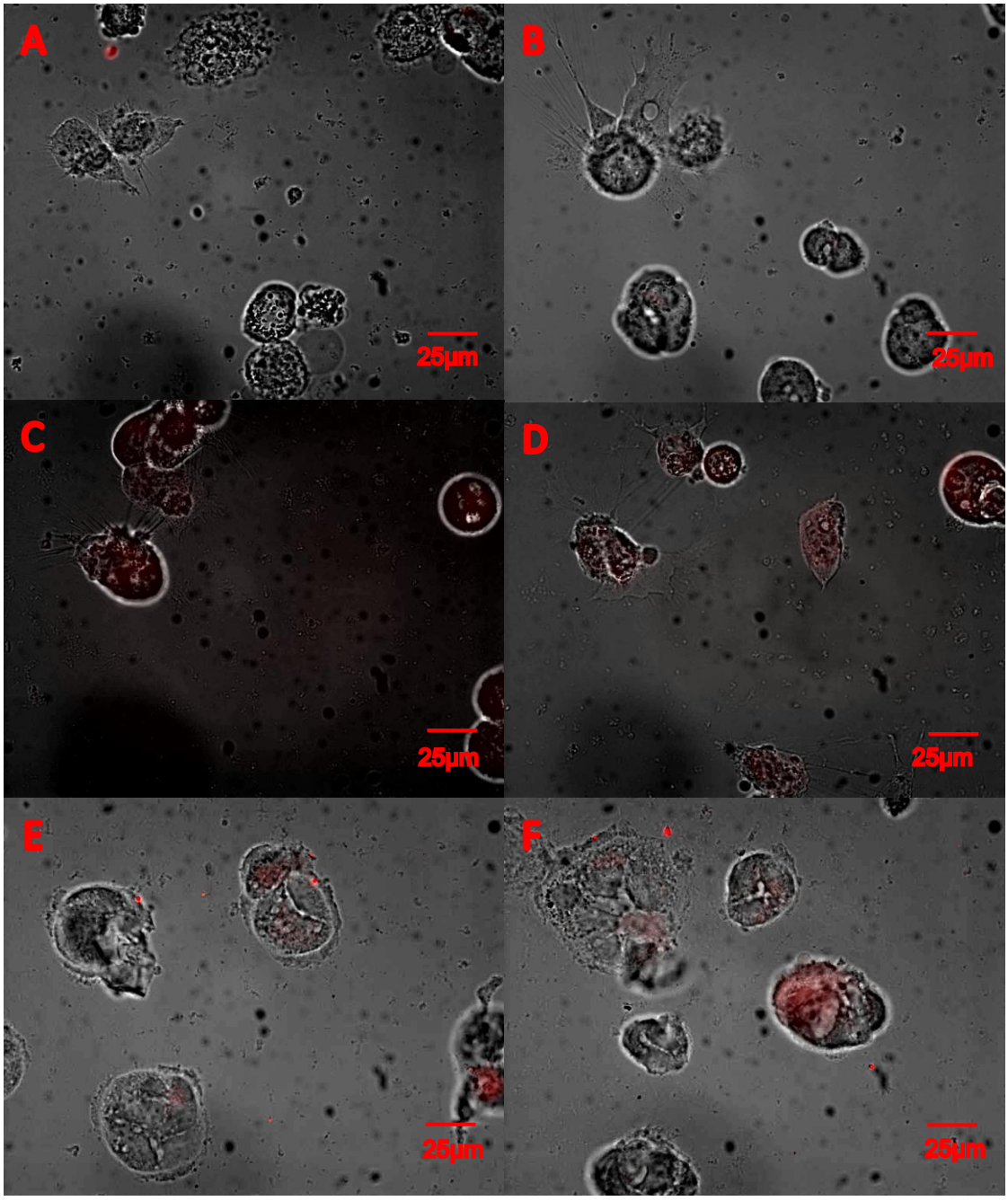

Figure 4. 1 The CACO-2 cell images were captured using an Epi-fluorescent microscope with excitation light of wavelength 300-400 nm and x400 magnification. The bright field and fluorescent field of the same image were overlaid using ImageJ software (//IMAGEJ.NIH.GOV/IJ/). **A**, and **B** are the overlaid images of CACO-2 without exposure to SiQDs. **C** and **D** are the overlaid images of 1 hour-treated (0.2 µg mL^{-1}) CACO-2 internalised SiQDs. **E** and **F** are the overlaid images of 4 hours-treated (0.2 µg mL^{-1}) CACO-2. The red colour and red dots represent fluorescence from SiQDs.

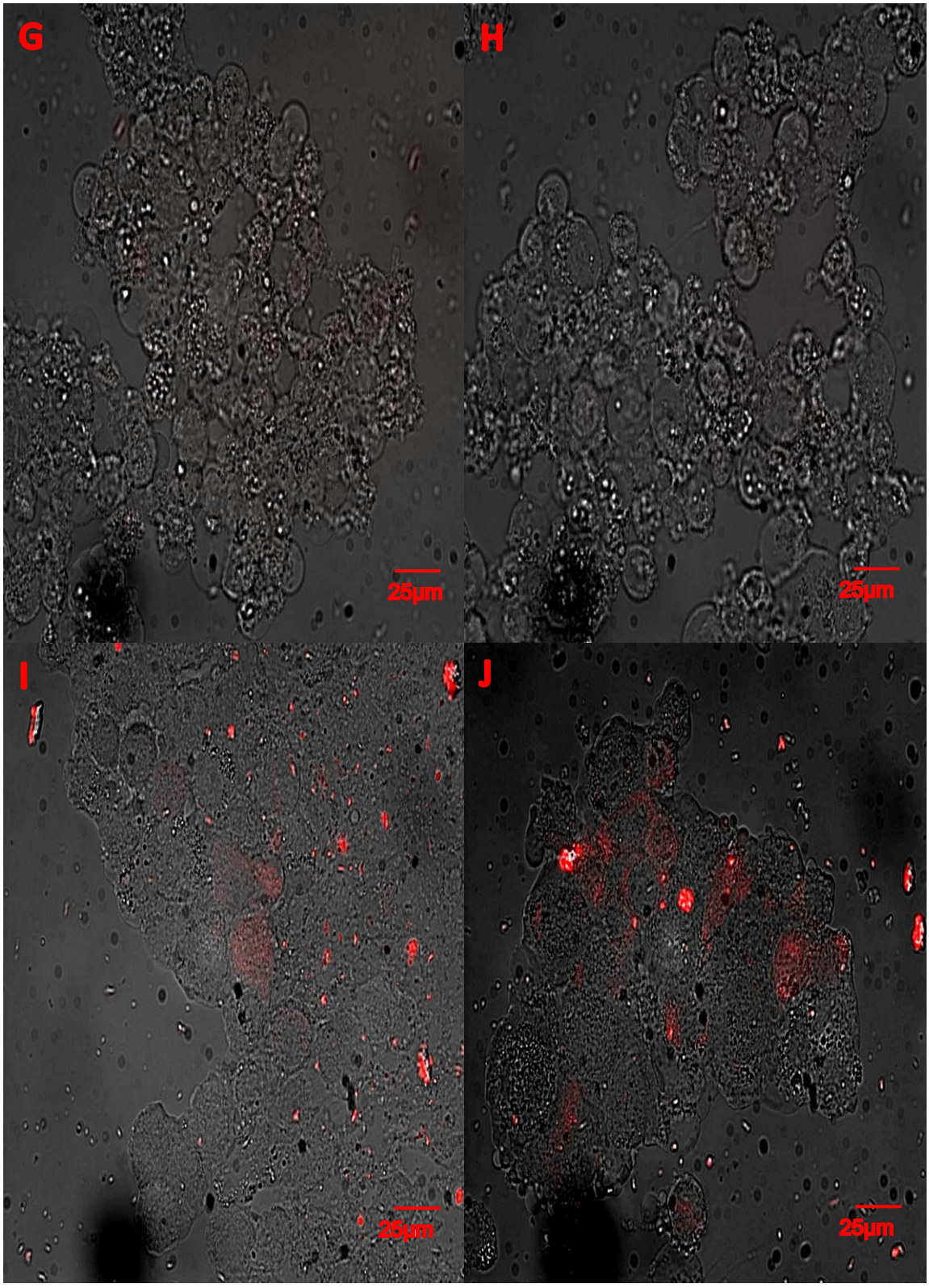

Figure 4. 2 The CACO-2 cell images captured using an Epi-fluorescent microscope with excitation wavelength 300-400 nm and x400 magnification. The bright field and fluorescent field of the same image were overlaid using ImageJ software (//IMAGEJ.NIH.GOV/IJ/). **G** and **H** are the overlaid images of CACO-2 without SiQDs. **I** and **J** are the overlaid images of 14 days treated (50 µg mL^{-1}) CACO-2 internalised SiQDs. The red colour and red dots represent the fluorescence of SiQDs.

4.3.2 Cellular Internalisation Studies Using SiQDs and Detection with High Resolution Scanning Confocal Microscope

Additional fluorescence imaging studies of CACO-2 internalised SiQDs were performed with a high resolution confocal microscope. CACO-2 which had been treated with SiQDs for 0.5, 1, 2, and 4 hours showed strong luminescent compared to the cellular autofluorescence background **(Figures 4.3-4.6)**. Again, the images of SiQDs fluorescence inside CACO-2 were consistent with localisation mainly at cell membranes and the cell cytoplasm. Although the small amount of SiQDs was used to incubate the CACO-2 with very short time 0.5 hour the SiQDs internalised CACO-2 showed strong luminescent with red spots detection with high resolution microscope, confocal. The fluorescent images of SiQDs internalised CACO-2 at 0.5, 1, 2, and 4 hours captured using confocal microscope are showed in **Figure 4.3-4.6.**

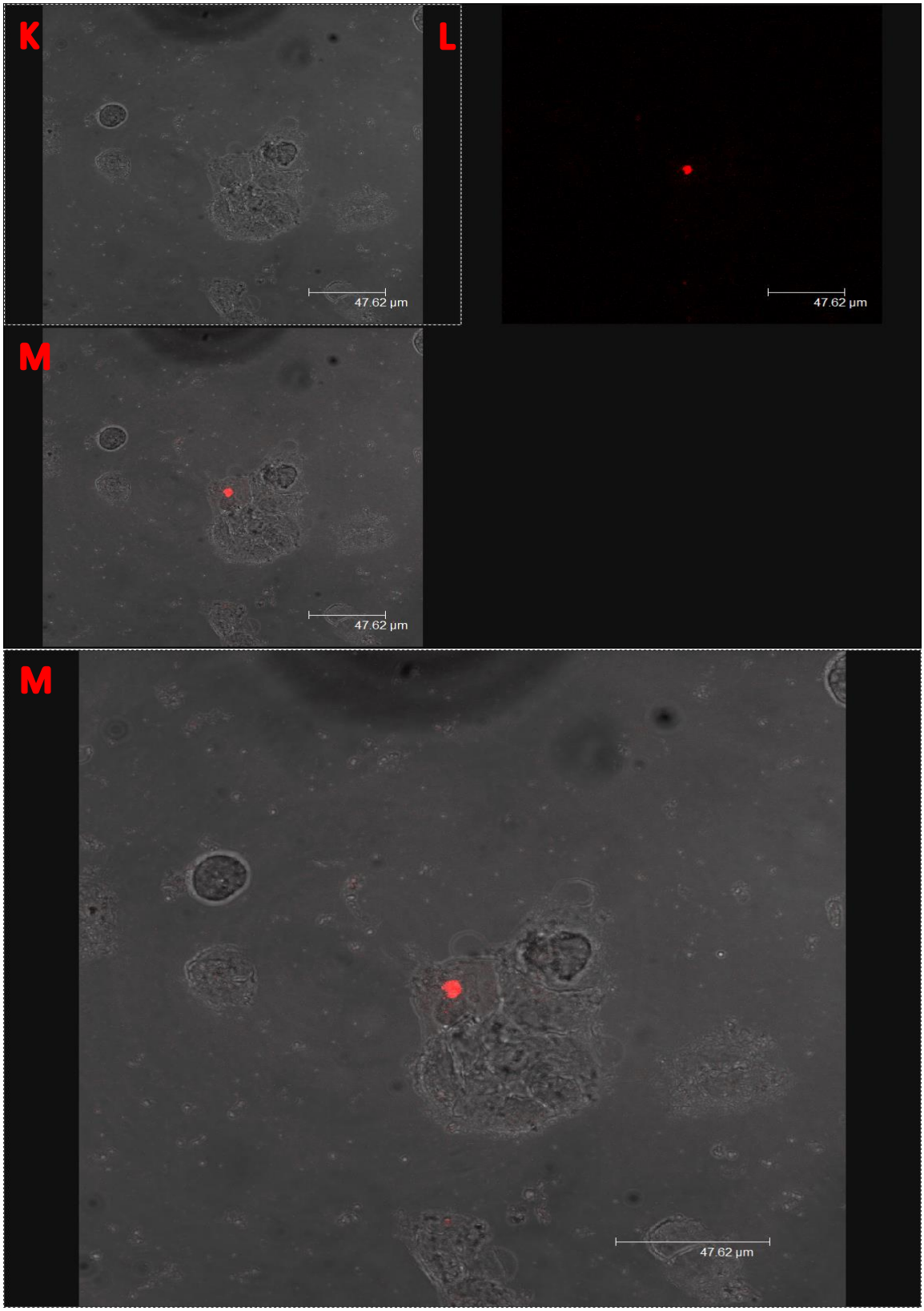

Figure 4. 3 The CACO-2 cells bright field and fluorescent field images were captured using a confocal microscope with an excitation wavelength 488 nm and x1000 magnification. **K** is the bright field image of CACO-2 treated with 0.2 µg mL^{-1} of SiQDs for 0.5 hour. **L** is the fluorescent field image of **K.** **M**, **M** is the overlaid images of **K** and **L**, CACO-2 internalised SiQDs. The red dots represent fluorescence from SiQDs.

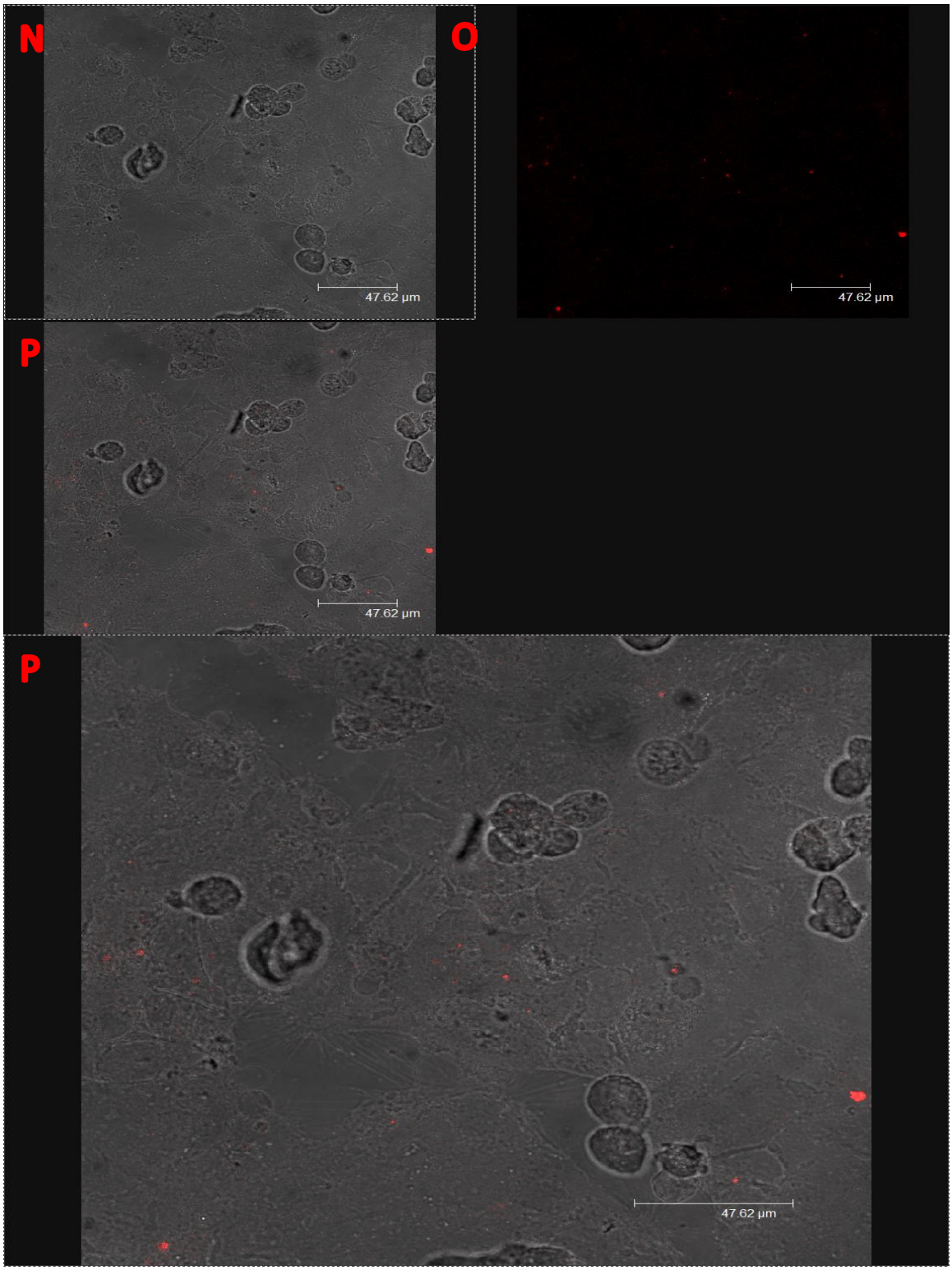

Figure 4. 4 The CACO-2 cells bright field and fluorescent field images were captured using a confocal microscope with excitation wavelength 488 nm (1000 (oil) X magnification). **N** is the bright field image of CACO-2 treated with 0.2 µg mL^{-1} of SiQDs for 1 hour. **O** is the fluorescent field image of **N.** **P**, **P** is the overlaid images of **N** and **O**, CACO-2 internalised SiQDs. The red dots represent fluorescence from SiQDs.

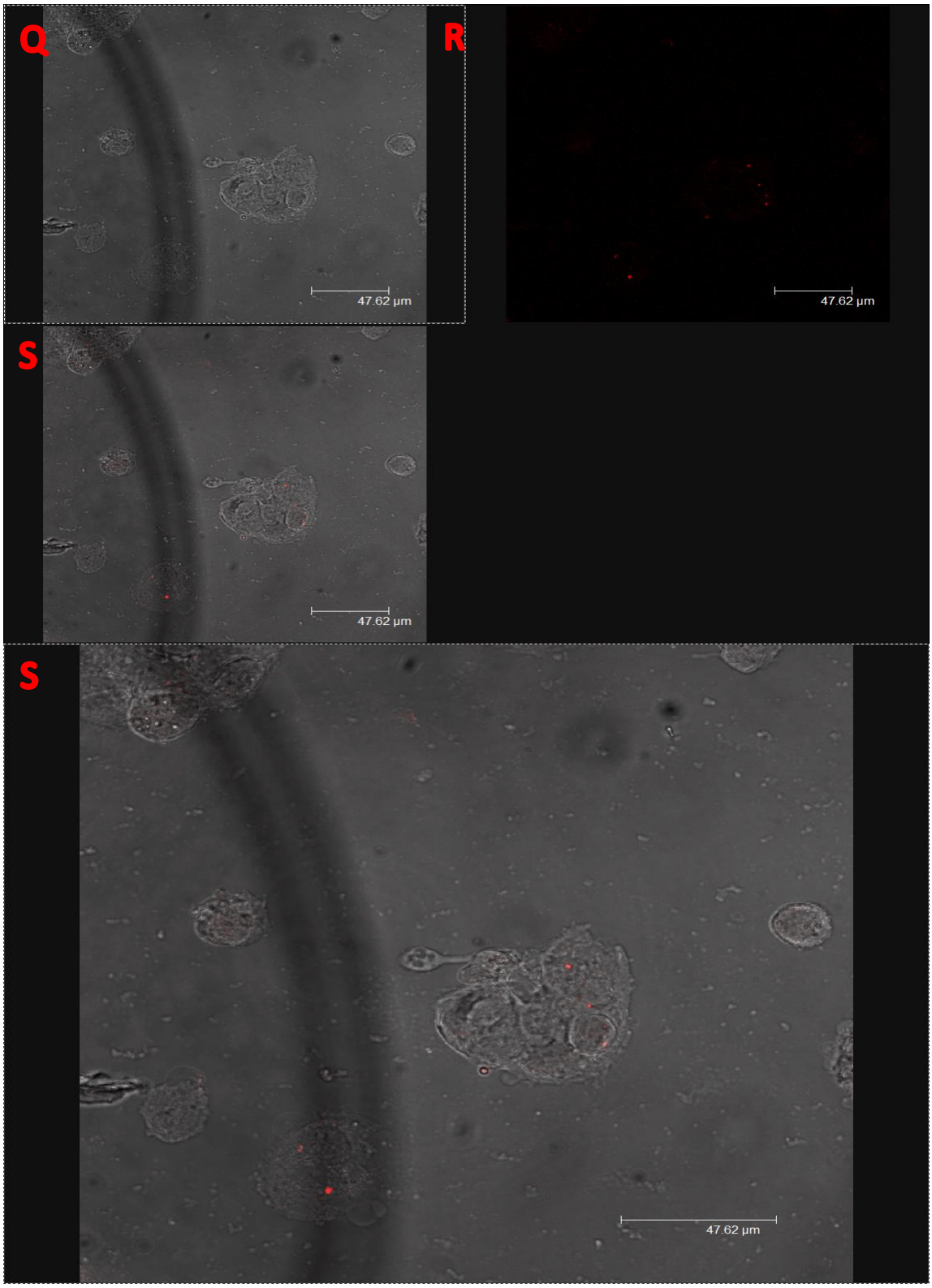

Figure 4. 5 The CACO-2 cells bright field and fluorescent field images were captured using scanning microscope with excitation wavelength 488 nm (1000 (oil) X magnification). **Q** is the bright field image of CACO-2 treated with 0.2 µg mL^{-1} of SiQDs for 2 hours. **R** is the fluorescent field image of **Q.** **S**, **S** is the overlaid images of **Q** and **R**, CACO-2 internalised SiQDs. The red dots represent fluorescence from SiQDs.

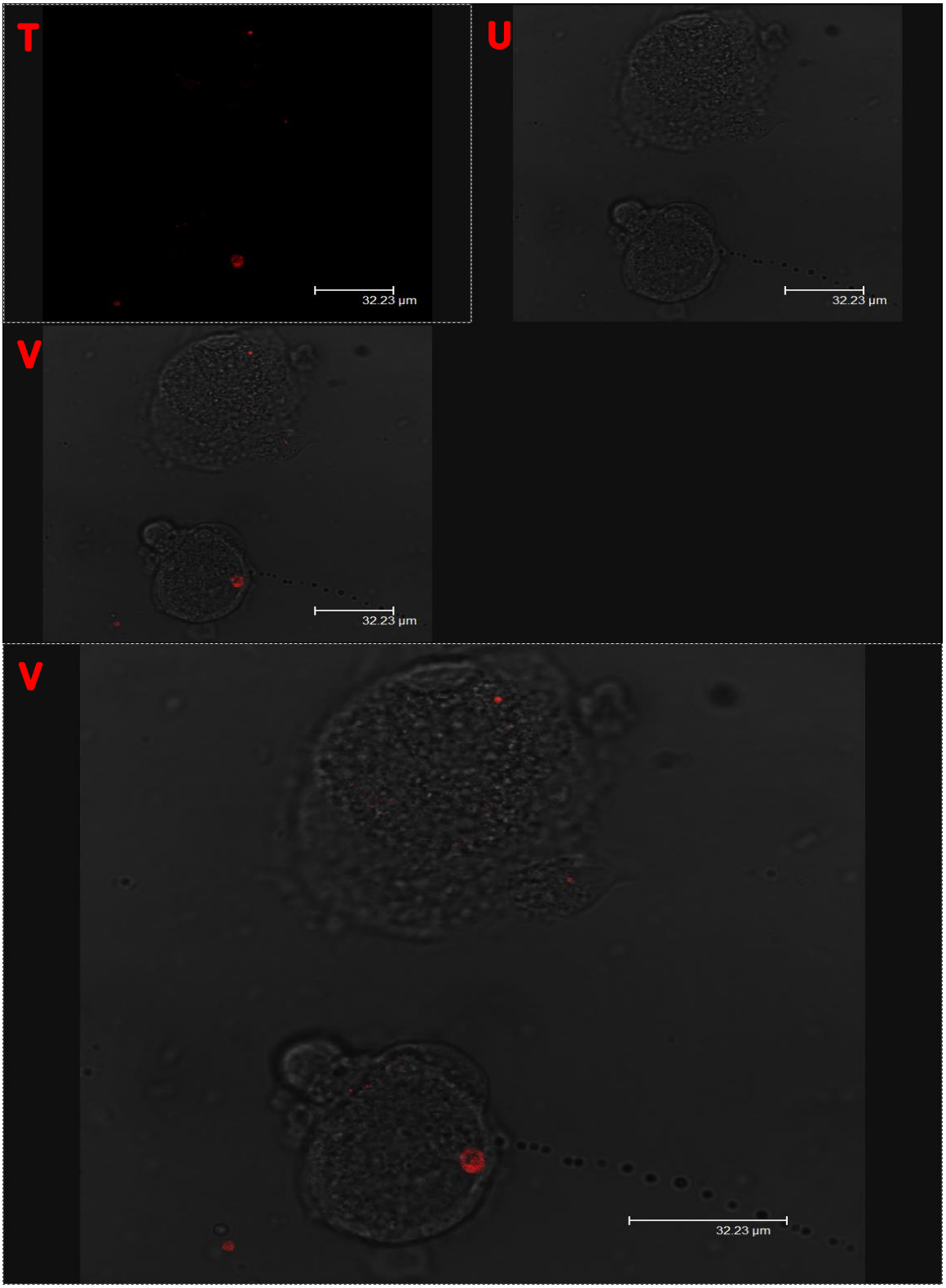

Figure 4. 6 The CACO-2 cells bright field and fluorescent field images were captured using scanning microscope with excitation wavelength 488 nm (1000 (oil) X magnification). **T** is the bright field image of CACO-2 treated with 0.2 µg mL^{-1} of SiQDs for 4 hours. **U** is the fluorescent field image of **T.** **V**, **V** is the overlaid images of **T** and **U**, CACO-2 internalised SiQDs. The red dots represent fluorescence from SiQDs.

4.3.3 Quantitative Analyses of SiQDs Internalisation Using Confocal Microspectroscopy

To confirm that the fluorescence images represent SiQDs internalised by CACO-2, the confocal microscope was used to capture luminescence spectra of the fluorescence reported in **Figures 4.3-4.6**. CACO-2 cells were starved to avoid high background fluorescence. The cells were cultured in 10x dilution of foetal Bovine serum (FBS) of regularly complete medium. Likewise, prevent precipitation and aggregation of SiQDs in the culture medium when contained high concentration of FBS). The starved CACO-2 showed strong fluorescence, dominating the background and revealed luminescence-Raman spectral features characteristic of SiQDs (orange-red emission with a large Stokes shift – the difference between excitation and emission wavelengths). The luminescence/Raman spectra of SiQDs internalised CACO-2 are present in **Figure 4.7 – 4.8.**

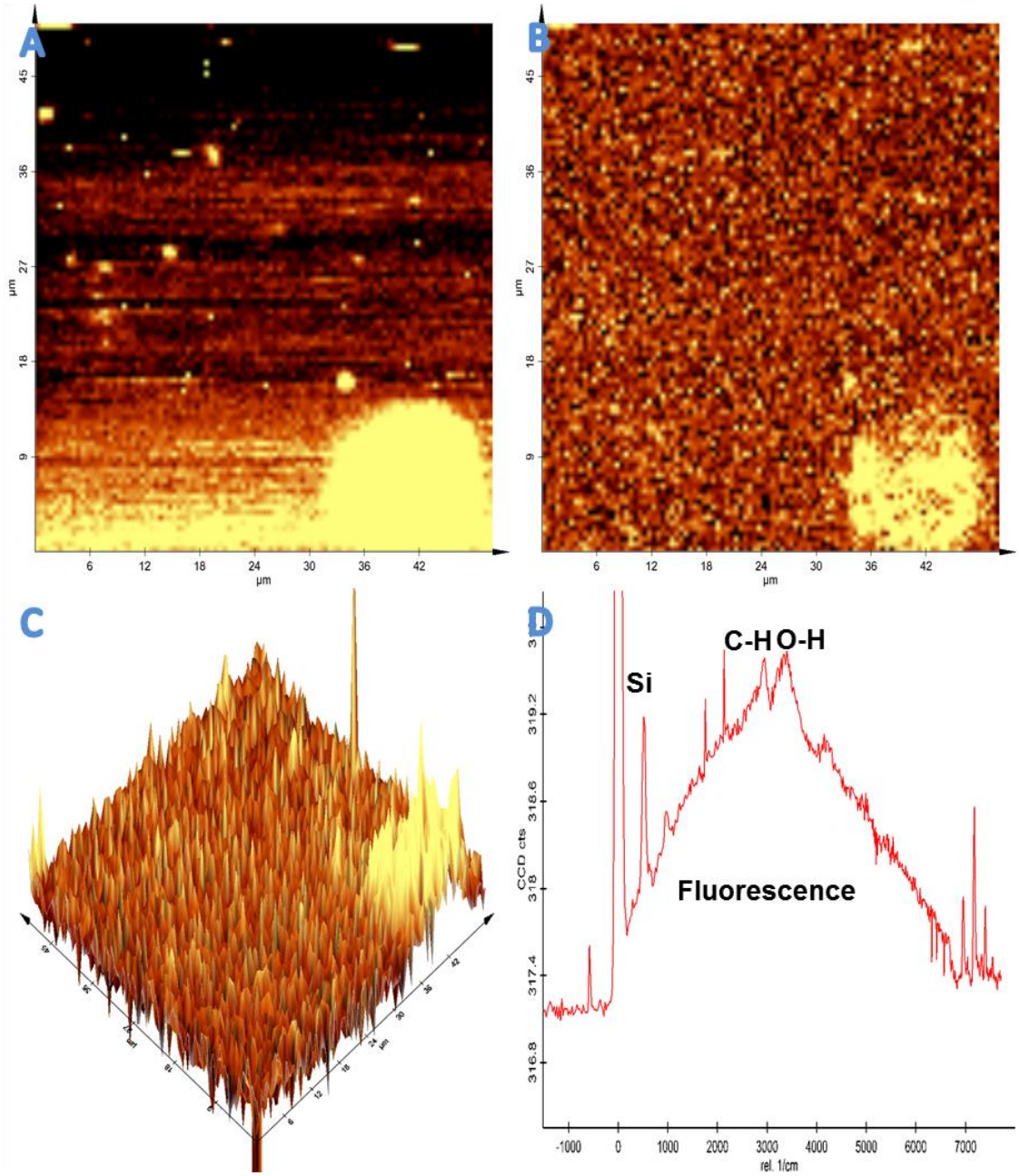

Figure 4. 7 The confocal fluorescent spectral images at an excitation wavelength of 488 nm of SiQDs inside starving CACO-2 which had been treated with 0.2 µg mL^{-1} for 1 hour. **A** is the original luminescence image of CACO-2 internalised SiQDs. **B** is the one dimensional luminescence image of **A. C** is the three dimensional luminescence image of **A. D** is the luminescence/Raman spectra of SiQDs inside CACO-2. The bright yellow colour is a false colour that represents the intensity of emission from SiQDs. In image (a) the colour scale represents the total intensity of the whole spectrum, including the elastically-scattered (reflected) light at 0 cm^{-1}. The intensity shown at each pixel of (b) & (c) is the integral of the spectrum in (d) over the range of wavenumbers from 200 to 7000 cm^{-1} from the excitation line (0 cm^{-1} in relative wavenumbers).

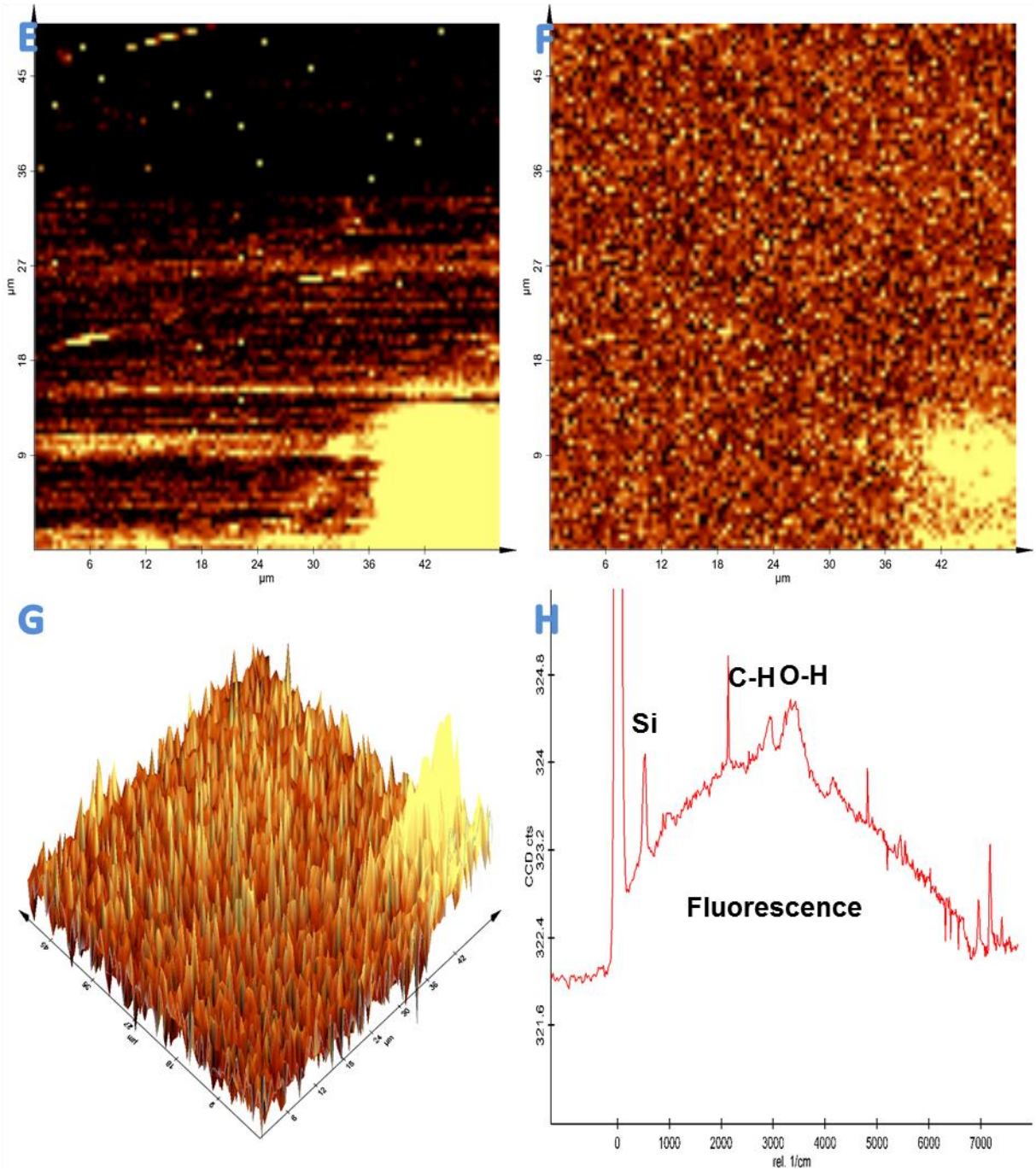

Figure 4. 8 The confocal fluorescent spectrum images at excitation wavelength 488 nm of SiQDs inside starving CACO-2 which had been treated with 0.2 µg mL^{-1} for 1 hour. **E** is the original luminescence image of CACO-2 internalised SiQDs. **F** is the one dimensional luminescence image of **E.** **G** is the three dimensional luminescence image of **E. H** is the luminescence/Raman spectra of SiQDs inside CACO-2. The bright yellow colour is a false colour that represents the intensity of emission from SiQDs. In image (e) the colour scale represents the total intensity of the whole spectrum, including the elastically-scattered (reflected) light at 0 cm^{-1}. The intensity shown at each pixel of (f) & (g) is the integral of the spectrum in (d) over the range of wavenumbers from 200 to 7000 cm^{-1} from the excitation line (0 cm^{-1} in relative wavenumbers).

4.4 Discussion

Fluorescent semiconductor nanocrystals or quantum dots (QDs) are well known in the electronic field for optoelectronic applications such as diodes, lasers, and solar cells (Mastronardi et al., 2012). Typical QDs are composed of elements of groups II and VI, IV and VI or III and V of the periodic table (Erogbogbo et al., 2011a). QDs reveal superior optical properties such as broad excitation spectra, size dependent emission, brightness, and high photostability (Erogbogbo et al., 2011a). Their unique optical properties of QDs have increased applications in other fields apart from electronic applications such as biology and medical as biological labelling or fluorescent probes. The application of QDs in biology and medical fields arise from their suitability for confocal microscopy: their stability and bright fluorescence help resolve difficulties related to cell auto-fluorescence with high background noise and the fading of luminescent molecular dyes in long-time imaging experiments. However, cytotoxicity remains a concern for QD applications in biology and medical fields because QDs exhibit unique physicochemical properties and behave differently from the bulk materials. The methodologies for safety evaluation in bulk materials do not necessarily apply to QDs. In particular, some QDs contain heavy metals such as cadmium which may leach from the particles and is known to be cytotoxic (Derfus et al., 2004).

Alternative SiQDs which do not contain heavy metals are being sought, Lie et al, 2002 developed a technique to produce SiQDs without any heavy metals (Lie et al., 2002). This study employed alkyl-capped silicon quantum dots (SiQDs) which were synthesised by a modified version of the Lie technique. The SiQDs are composed of a silicon core and stabilised with an organic n-alkyl (C_{11}) monolayer (Alsharif et al., 2009). SiQDs are strongly hydrophobic because of this surface termination and are easily suspended in organic solvents. These suspensions show intense luminescent under excitation with $\lambda_{ex} < 550$ nanometre (nm). SiQDs suspended in organic solvents can also be used to prepare clear (non-turbid) lyophobic colloids in aqueous or physiological media (Dickinson et al., 2008). The application of SiQDs as fluorescent labels and their potential in the life sciences were investigated by Alsharif et al, 2009. They found that SiQDs were internalised by tumour-derived cell lines and non-tumour cells using a confocal fluorescence microscope. The internalisation was more dominant (faster) in tumour cells particularly in HeLa cells. In addition the SiQDs

showed a lack of acute toxicity (Alsharif et al., 2009). The studies reported in this thesis have also shown evidence of internalisation of SiQDs in CACO-2 - a model of the gastrointestinal tract.

Stable SiQDs in organic solvents showed strong luminescent under excitation $\lambda_{ex} < 550$ nm, however when SiQDs were dispersed in aqueous or physiological solutions the luminescent intensities were slightly compromised (Erogbogbo et al., 2012). Previous work (Dickinson et al., 2008) showed that alkyl-capped SiQDs are very slowly oxidised in aqueous media (over a period of several days) with shifts in the emission maxima of their fluorescence spectra. Our studies in CACO-2 which had been treated with SiQDs at concentrations as low as 0.2 μg mL^{-1} confirmed the optical properties of SiQDs inside the CACO-2 cells using epi-fluorescence and confocal microscopy. The SiQDs internalised by CACO-2 showed strong luminescence over the background as well as the characteristic SiQD fluorescence/Raman spectra inside the cells.

In summary, concentrations of SiQDs as low as 0.2 μg mL^{-1} dispersed in physiological solution showed detectable internalisation of SiQDs by the human colon-derived tumour cell line, CACO-2. Luminescence was detected after 0.5 hour exposure using confocal microscopy. In addition, work with starved cells showed that these internalised SiQDs more vigorously as confirmed by **Figure 4.7- 4.8** images **D** and **H** show fluorescence spectral of SiQDs inside CACO-2 conformation that SiQDs were internalised is available in Chapter 6 in the discussion of the flow cytometry data.

The CACO-2 cells which had been started to grow from the frozen stock in phenol red free culture medium and continued to culture in that medium as well as collected cells using phenol red-free trypsin showed a minimum autofluorescent background and revealed strong fluorescence of SiQDs inside the cells.

Cremophor EL is widely used to improve solubility of water insoluble chemicals, in particular for drug solubility and absorption (Kiss et al., 2013). Cremophor can also be used to prepare solution dispersion of SiQDs in physiological solutions for studying internalisation of SiQDs. However cremophor does exhibit some background fluorescence, although the emission from SiQDs is stronger. We did not make extensive use of cremophor in later chapters of this thesis

because it produces suspensions that have a slight turbidity and it showed some adverse effects on endothelial cells (Kiss et al., 2013).

For cell slides preparation, it was found that Mowiol mounting medium was suitable for cell uptake studies of SiQDs. Mowiol, which contains 2 basic chemicals: Mowiol 40-88poly (vinyl alcohol) and Glycerol BioXtra, ≥99% (GC), also has a colourless and sticky texture and showed low background autofluorescence using confocal microscopy with 488 nm excitation.

The CACO-2 internalised SiQDs showed bright fluorescent images and luminescence/Raman spectra of SiQDs inside the cells detected by a confocal Raman/luminescence microscope. The SiQDs internalised by CACO-2 were found to be localised near membranes but with some fluorescence dispersed in the cell cytoplasm.

SiQDs can therefore be used as a fluorescent stain to study cell organelles and cell functions by epi-fluorescence and confocal microscopy.

Internalisation studies of CACO-2 using SiQDs as a fluorescence probe showed evidence of uptake and accumulation of SiQDs inside the cells using both epifluorescence and confocal fluorescence microscopy. Hence it was good evidence for further study to understand the mechanism of internalisation and the potential adverse effects of SiQDs to the cells.

Figures 4.7 and 4.8 show confocal spectral images of a single CACO-2 cell. It is located at the bottom right hand corner of the images **(a)-(c)** and **(e)-(g)**. Each pixel of these images contains a fluorescence spectrum such as **Figure 4.7(d)** and **Figure 4.8(h)**. The false colour scale represents the intensity of detected light across a defined range of wavenumbers in the spectrum. In **(a)** and **(e)** the raw data are shown, which include a contribution from reflected laser light a 0 cm^{-1} relative wavenumbers, i.e. light scattered from the cell or slide without change in wavelength (488nm). The colour scales in **(b)-(c)** and **(f)-(g)** are adjusted to integrate over the range 200-7000 cm^{-1} which removes the contribution of reflected light and the cell is now clearer in the image. Finally, the sample spectra in **(d)** and **(h)** show the characteristic broad fluorescence band of SiQDs with a maximum at about 3000 cm^{-1} or equivalently 570 nm, slightly shorter in wavelength than for SiQDs free in solution, but still with the

typical large Stokes shift between absorption and emission (Lie et al., 2002), (Dickinson et al., 2008). There are also some Raman bands visible in these spectra just below 3000 cm^{-1} and more intense at 3500 cm^{-1}. The latter is simply the water Raman band, but the former is due to C-H stretching vibrations and is most likely associated with components of the cell membrane. The very sharp features which appear in these spectra with no detectable line-width are cosmic ray events recorded by the CCD detector and do not represent Raman or fluorescence bands. Overall, the spectral images demonstrate the origin of the fluorescence as fom SiQDs and confirm their uptake by CACO-2.

The ability of the CACO-2 to internalise the neutral charge SiQDs could extend the application of fluorescent SiQDs more efficiently in cells and also increase the potential use of SiQDs to studies involving cell organelles, cell function and the treatment of disease.

Chapter 5. Potential Cytotoxicity of Alkyl-Capped Silicon Quantum Dots (SiQDs)

5.1 Introduction

In this study, the possible cytotoxicity of alkyl-capped silicon quantum dots (SiQDs) was investigated. The suitability of SiQDs for cell imaging was first investigated by Alsharif and colleagues (Alsharif et al., 2009). The group noted that SiQDs were internalised by tumour derived cell lines and primary cell lines, and also reported cell line dependent internalisation. The endocytosis inhibitors filipin, cytochalasin B, and actinomycin D were used to verify the internalisation mechanism of SiQDs and specific endocytotic processes involving SiQDs internalisation (Alsharif et al., 2009). Cytotoxicity was investigated by undertaking cell viability, cell proliferation and apoptosis studies, ultimately leading to the conclusion that SiQDs do not produce any adverse effects on HeLa and SW1353 cells (human chondrosarcoma). Moreover, various particle sizes and coatings known as mesoporous silicon (Psi) (2-50 μm) or silicon quantum dots (QDs) have been used increasingly in applications of life science as promising oral drug delivery agents (Santos et al., 2010).

Although silicon QDs do not contain any heavy metals and have been classified as low toxicity (Martin, 2013), the literature regarding SiQDs toxicity is sparse and incomplete. Conventional toxicology of chemicals was originally investigated by Paracelsus and shows direct correlation between both concentration and exposure time with an adverse effect (Elsaesser and Howard, 2012). Despite this, SiQDs that show unique photo properties are very small in size, typically ranging between 5 to 7.5 nm which make them very different from bulk material (Hardman, 2006). SiQDs may possess unique adverse effects when the particle size is within this range (Li et al., 2003). Particles smaller than 100 μm may also generate free radicals (Li et al., 2003). Information regarding toxicity of QDs is also important for the development of biological applications using nanomaterials. Optimised imaging and therapeutic potential of nanomaterials require at least four basic characteristics, including internalisation by the target cell, specified localisation, well defined interaction with the cell, and low toxicity with safe metabolic profile (Santos et al., 2013).

Previous SiQDs cytotoxicity studies have been based on the cytotoxicity of the bulk material as there are currently no standard protocols specified for nanomaterial cytotoxicity studies. According to the basic understanding of bulk

materials, the concentrations of SiQDs used for cytotoxicity experiments in the present study were adapted between 0 to 200 µg mL^{-1}. Furthermore, previous studies by Santos and colleagues (2010) evaluated cytotoxicity of microporous silicon at concentrations 0.2 – 4 mg mL^{-1} with the particles size in the range of 1.2 µm -75 µm. The group highlighted that in CACO-2 cells (a model intestinal epithelial cell), the toxic effects of microporous silicon were significantly increased when studied with the small particle size after the cells were treated for more than 11 hours. Moreover, cell damage, apoptosis, and death in the cell line appeared to be influenced in a dose-dependent manner (Santos et al., 2010).

The effect of smaller nanoparticles on human cells is still unclear. A number of approaches can be used to assess this. Measuring cell viability using 2-(4,5-dimethyl-2-thiazolyl)-3,5-diphenyl-2H-tetrazolium bromide (MTT assay) has been widely conducted and is one of the most popular cytotoxicity studies. The MTT assay is sensitive, practical, quantitative, and reproducible. The quantity of end product (formazan) is also directly proportional to the number of the viable cells (Ferrari et al., 1990, Ciapetti et al., 1993). The yellow MTT is metabolised by viable cells using mitochondrial and non-mitochondrial enzymes (Bernas and Dobrucki, 2002). The positive charge of MTT facilitates cellular internalisation and metabolism occurs in intracellular and extracellular producing a dark purple end product of insoluble formazans (dark purple) (Berridge et al., 2005). MTT is metabolised by oxidoreductase dependent reducing agents and happens mainly in mitochondria. The reducing agents are the products of cell respiration such as NADH, NADPH. The cells which low metabolic or high metabolic activities may give false positive or false negative results. Also mitochondrial stress will give an apparent reducing in cells viability.

Additionally, another quantitative measure of cell viability is through determination of ATP inside the cell. ATP is the energy source of all living organisms. ATP is used for many biological processes such as membrane transport and cell motility and also the intracellular ATP content is directly correlated with the number of living cells (Imamura et al., 2009, Kolibab et al., 2012) Quantifying cell viability using the adenosine 5´- triphosphate (ATP) assay or firefly luciferase assay of ATP is a sensitive technique. The chemical reaction behind the assay involves extracting ATP from the cells. In the

presence of luciferin the ATP-luciferin complex reacts with luciferase to emit light which is proportional to the ATP concentration (Hoffner et al., 1999). The ATP assay has been validated by comparing with traditional cell viability count. There is high correlation between ATP content and the conventional viable count method (Jensen et al., 2008).

Through use of multiple cytotoxicity evaluation methods which quantify how nanoparticles interact with human cells, the balancing of reactive oxygen species (ROS) with antioxidant capacity can be determined by measuring ROS content using 2´, 7´- dichlorofluorescein diacetate (DCFH-DA) fluorescine. ROS are by-products of cellular metabolism which often originate from mitochondria activity (Thannickal and Fanburg, 2000). Collectively, ROS form a group of oxidative species: superoxide anion ($O_2^{\bullet-}$), hydroxyl radical ($OH^{\bullet}$), hydrogen peroxide (H_2O_2), singlet oxygen ($^1O_2$), and hypochlorous acid (HOCl) (Manke et al., 2013). Excess levels of ROS generates oxidative stress (OS) which contributes to cellular macromolecule damage (Thannickal and Fanburg, 2000). DCFH-DA is a nonfluorescent dye and is nonpolar. DCFH-DA is able to cross the cell membrane and is converted to nonfluorescent DCFH by intracellular esterases via a hydrolysis reaction (Wang and Joseph, 1999). ROS inside the cell react with DCFH by an oxidation reaction which produces highly fluorescent dichlorofluorescein. The fluorescent product shows linear correlation with ROS concentration (Wang and Joseph, 1999).

In addition, the effect of oxidative stress on DNA can be investigated using the Comet assay. DNA damage may occur even with low cytotoxic effects or negative results from other safety evaluation methods without cell death. The unique properties of nanoparticles could influence their ability to generate unpredictable genotoxic effects (Singh et al., 2009). The Comet assay detects single cell DNA damage using a gel electrophoresis technique (Singh et al., 1988, Speit and Hartmann, 2006); thus, an individual cell can be evaluated. A cell with DNA damage shows the migration of single strand DNA fragments with an appearance similar to a comet shape (Speit and Hartmann, 2006).

In the present study the effects of SiQDs on CACO-2 cells were evaluated. CACO-2 is a human colon derived cell line which is widely used to study nanoparticle cytotoxicity via the oral exposure route (Ruizendaal et al., 2009).

Toxicity evaluation of SiQDs interaction on CACO-2 was performed with various toxicity endpoints: cell morphology evaluation using bright field microscope, potential adverse effects on cell viability detected with MTT assay, quantitative ATP measurement using FLASC assay, determination of oxidative stress condition using DCFH-DA assay, and evaluation of DNA damage potential using the Comet assay.

5.2 Methods

5.2.1 Route of Exposure of SiQDs Internalisation by CACO-2

CACO-2 cells were cultured as described in Section 2.3 but without phenol red in the culture medium. Cells with starting density of 1-2 x 10^5 cells mL^{-1} were treated with SiQDs for 1 and 4 hours in 6, 12, 96 wells-plates, and T25 culture flasks. In addition, some experiments were conducted with longer term exposure of 14 days in order to look for chronic effects.

5.2.2 Cell Morphology Studies

Cell morphology studies were used to examine external morphology changes of the cells using a light microscope with 400x magnification to capture images of CaCO2 cells during the MTT assay.

5.2.3 Potential Adverse Effects of SiQDs on CACO-2 Cell Viability (MTT assay)

To evaluate the cytotoxicity of silicon quantum dots (SiQDs), the 3-(4, 5-dimethylthaiazol-2-yl)-2,5-diphenyltetrazolium (MTT) reduction assay was used to determine any adverse effects on the viability of the cells. CACO-2 cells with density 1-2 x 10^5 cells mL^{-1} were cultured overnight in 96 well and 12 well plates. The cells were then treated with 50 µg mL^{-1} of freshly preparation SiQDs, positive control (15 µg mL^{-1} H_2O_2), and controls (untreated and solvent treated) for 4 and 24 hours. Thereafter the treated cells were washed and incubated with MTT dye (50 µg mL^{-1}) for 2 hours. After 2 hours the MTT solution was removed and the dark purple colour from the cells was dissolved using neat isopropanol. The plates were then incubated for a further 10 minutes. Finally, the solution (0.1 mL) was removed from the 12 well plates and transferred to 96 well plates. The absorbance at 570 nm was measured using a

spectrophotometer (Thermo Scientific Multiskan microplate reader (96 wells plate)). The percentage cell viability was calculated and compared with the control cells. Results were obtained as the mean ± SD of the triplicate independent MTT experiments.

5.2.4 Effect of SiQDs on Intracellular ATP Content

A bioluminescent method was used to measure intracellular ATP content. An adenosine 5-triphosphate (ATP) bioluminescent somatic cell assay kit (Sigma-Aldrich) was used to measure ATP content inside the cells **(Appendix5.1)**. CACO-2 cells were incubated with SiQDs at 100 µg mL^{-1} in culture media for 4 and 24 hours and SiQDs 0.5, 5, or 50 µg for 14 days. As a positive control, cells were also treated with 2,4-dinitrophenol (2, 4 DNP)(ATP production inhibitor) (7 mg mL^{-1}) for 4 and 24 hours. ATP was extracted from CACO-2 cells (50 µL) using somatic cell ATP releasing reagent (FLSAR (100 µL). The extract was decanted in to micro UV cuvettes containing luciferin-luciferase solution and MgSO4 and luminescence read in a fluorescence spectrometer (SpexFluoroMax/GRAMS 32) with the instrument's excitation beam blocked with a piece of black card. The luminescence was read at 560 nm and the luminescence intensities of the samples were compared with positive and negative control group.

5.2.5 Measurement of Oxidative Stress in CACO-2 Cells Treated with SiQDs

To determine the level of ROS inside the cells, 2,7-dichlorodihydrofluoresceindiacetate (H2DCFDA) was used. To measure ROS contents in acute and longer incubation studies, CACO-2 cells which had been incubated with SiQDs at 100 µg mL^{-1} for 4 and 24 hours and SiQDs at 0.5, 5 or 50 µg mL^{-1} for 14 days were incubated with 0.5 mg mL^{-1} H2DCFDA (stock 20 mM in DMSO) in culture medium for 45 minutes. The H2DCFDA cell solutions were transferred to micro UV cuvettes using positive displacement pipetting for accurate aspiration and complete dispensing and immediately the fluorescence was measured at an excitation wavelength of 485 nm with the emission wavelength at 530 nm.

5.2.6 DNA Damage Potential Evaluation of SiQDs in CACO-2 cells

To evaluate the potential for SiQDs to induce DNA damage, CACO-2 cells treated with SiQDs (200 μg mL^{-1}), positive control (cells treated with 15 μg mL^{-1} H_2O_2) as well as control (solvent treated cells) for 4 and 24 hours were used to evaluate DNA damage using single cell gel electrophoresis (SCG) or Comet assay using method of Singh and colleagues (1988). The alkaline Comet assay (pH > 13) measures DNA lesions including single and double DNA beaks (SSBs, DSBs) and alkali-labile site (ALS) (Singh et al., 1988, Tice et al., 2000). The CACO-2 cells were cultured in a T-25 flask at a cell density 5 x 10^5 cells cm^{-2} in 4 mL DMEM medium for 24 hours before treatment. After treatment, the cells were gently harvested from the flask using trypsin and the cell pellets were re-suspended in 1 mL of cool PBS in amber microcentrifuge tubes and stored on ice. In the dark room under dim light, a mixture of equal parts cell suspension and 1% (w/v) low melting agarose in PBS (37 ^oC) was prepared (200 μL in total). The mixed solutions (60 μL) were dropped on the top of pre-coated 1% (w/v) low melting point agarose on SuperFrost microscope slides and covered with coverslips (two areas per slide). The agarose slides were allowed to solidify on ice and then the slides without coverslips were gently immersed into chilled lysing solution (2.5 M NaCl, 100 mM EDTA, 10 mM Tris, Triton X-100 (1% v/v), DMSO (1% v/v)). The slides were left in the lysing solution to liberate DNA. The slides were then transferred into chilled alkaline buffer (300 mM NaOH, 1 mM EDTA, pH > 13) in an electrophoresis tank and left for 30 minutes to allow DNA unwinding. The electrophoresis was performed at constant voltage of 22V, 0.5-0.7 mA for another 30 minutes in the same alkaline buffer. The slides were then placed into chilled neutralising buffer solution (0.5 M Trisma base pH 7.5) to allow the DNA to reconstitute. Finally, the DNA slides were dried and stained with SYBR gold solution (1: 10000 (v/v) in 1X Tris-EDTA (0.1 M Trisma base, 0.05 M EDTA). The following day, the cells were re-hydrated with water and fluorescent cells images, 200x magnification (Olympus U-RFLT50/Olympus CX40) with excitation wavelength 490 nm were counted (50 images for each slide and 2 slides for each treatment). As the glowing cells were counted, the counting capture images were directly connected to the image analysis programme (Comet IV (IN STEM)

and the following parameters recorded: head length, tail length, and head intensity of DNA. The independent Comet experiments were performed in duplicate. Results are the mean ± SD of the two whole cells samples (100 cells) in the two independent experiments.

5.2.7 Metabolic Activity Measurement and measurement of Oxidative Stress CACO-2 cells Treated for 14 Days

For studies of chronic exposure, CACO-2 (10^3 cells mL^{-1}) were cultured in T25 culture flasks overnight. After 24 h, the cells were treated with various concentrations of freshly prepared SiQDs at 0.5, 5, or 50 µg mL^{-1} from a stock solution of 1 mg mL^{-1} SiQDs in 10 µL diethyl ether (ether) in phenol red-free medium. The cells were treated with SiQDs for 14 days and the medium was replaced with a fresh preparation of SiQDs suspension every two days. After 14 days the cells were washed with PBS 3 times and detached using trypsin solution. The cell pellets were then suspended in 500 µL PBS. ATP and ROS production were measured using the FLASC and DCFH-DA assays.

5.2.8 Statistical Analysis

All statistical analysis was performed using SPSS software (IBM Statistics 21). The level of significance for the effects and interactions of particular parameters were calculated using-one-way ANOVA. The results are presented as the means and standard deviation (Mean ± SD). Post Hoc tests were used for the comparison for the significant parameters. A p value ≤ 0.05 was taken as statistically significant.

5.3 Results

5.3.1 Route of Exposure of SiQDs Internalisation by CACO-2

CACo-2 cells were exposed to suspensions of SiQDs. The cells showed SiQDs accumulation with orange fluorescence detected inside the cells using an epi-fluorescent microscope. A typical fluorescent image is showed in **Figure 5.1. (B).**

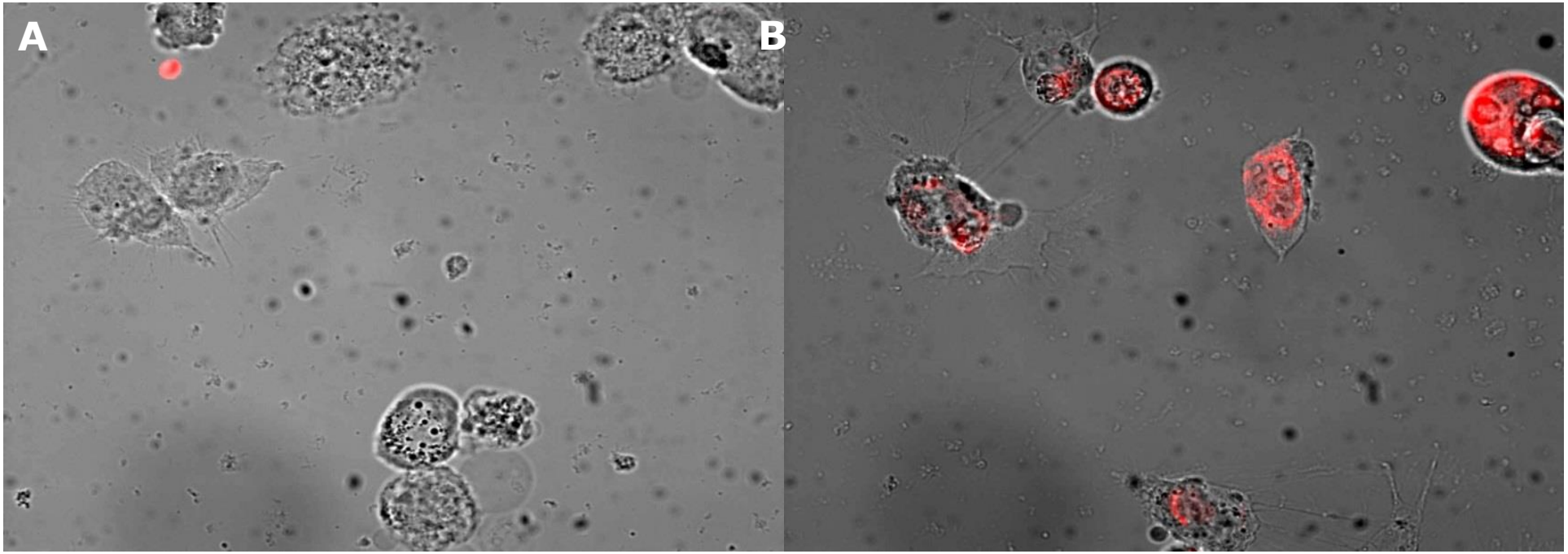

Figure 5. 1 CACO-2 cell images were captured using an Epi-fluorescent microscope with excitation light of wavelength 300-400 nm and 400x magnification. Internalisation studies (**B**) luminescence image of the dots inside Caco2 cells, (**A**) image of the control group. Cells were incubated with the dots (0.2 µg mL^{-1}) for 60 minutes. Red corresponds to the fluorescence from the SiQDs.

5.3.2 Cell Morphology Studies

To detect the effects of 0.1-0.5 % v/v of diethyl ether alone and SiQDs suspended diethyl ether in culture medium (0.1-0.5 % v/v ether) on CACO-2 cell morphology, CACO-2 cells were treated with both solutions for various time points, (0.5, 1, 2, 4, 24 hours or 14 days) and at various concentrations of SiQDs, (0.2, 0.5, 5, or 50 μg mL^{-1}). The images of the control CACO-2 cells and the SiQDs treated CACO-2 cells were captured using a bright field microscope. Images of CACO-2 as shown in **Figures 5.2 and 5.3**, no differences were detected between treated cells and control cells. An image of 50 μg mL^{-1} SiQDs treated CACO-2 for 4 hours is shown in **Figure 5.2 (B),** and images of cells treated with 0.5, 5, and 50 μg mL^{-1} SiQDs for 14 days are shown in **Figure 5.3 (B-D)** and images of the control cells are shown in **Figure 5.2, 5.3 (A)**.

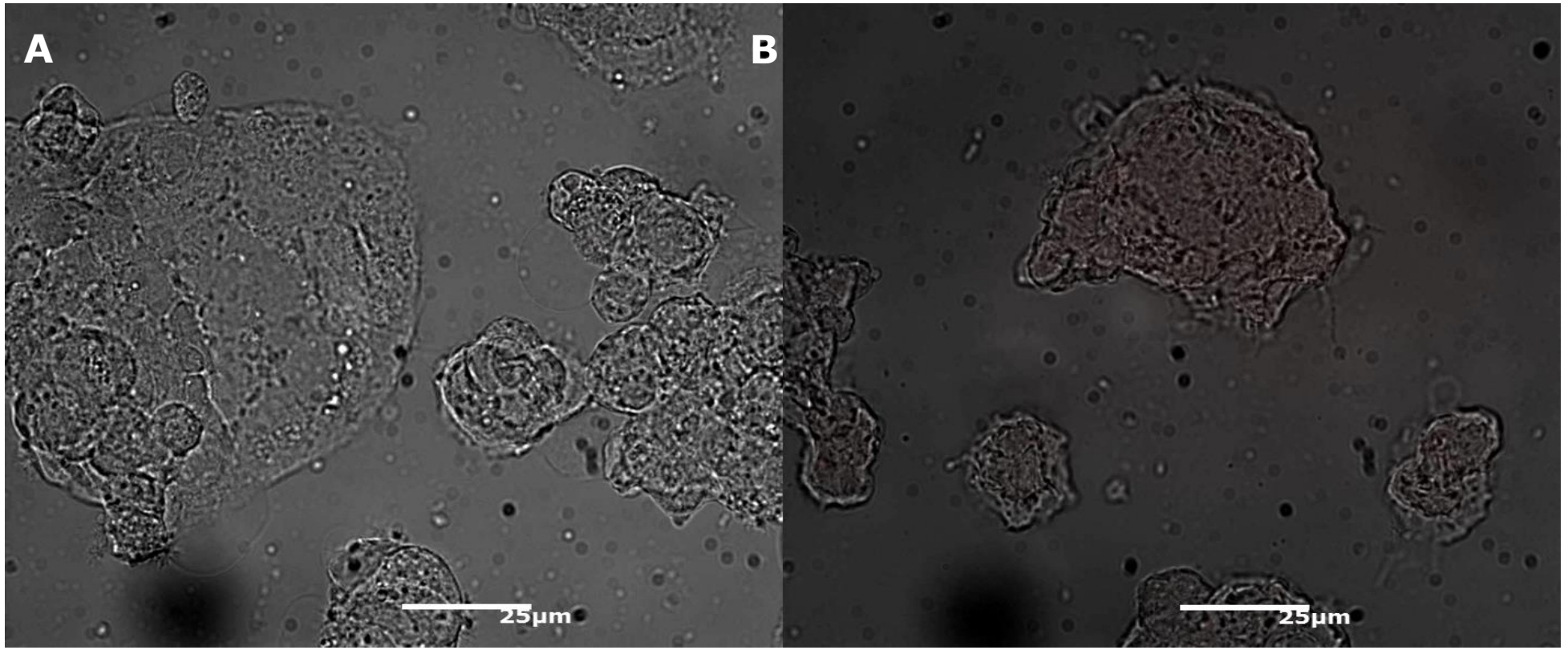

Figure 5. 2 CACO-2 cell images were captured using an Epi-fluorescent microscope with 400x magnification. The bright field image **A** represents the morphology of CACO-2 in the control group (0.1% v/v ether), and image **B** shows the morphology of 4 hours-treated (50 µg mL^{-1}) CACO-2 with SiQDs. The red luminesce of the SiQDs is overlaid on the optical image on the right.

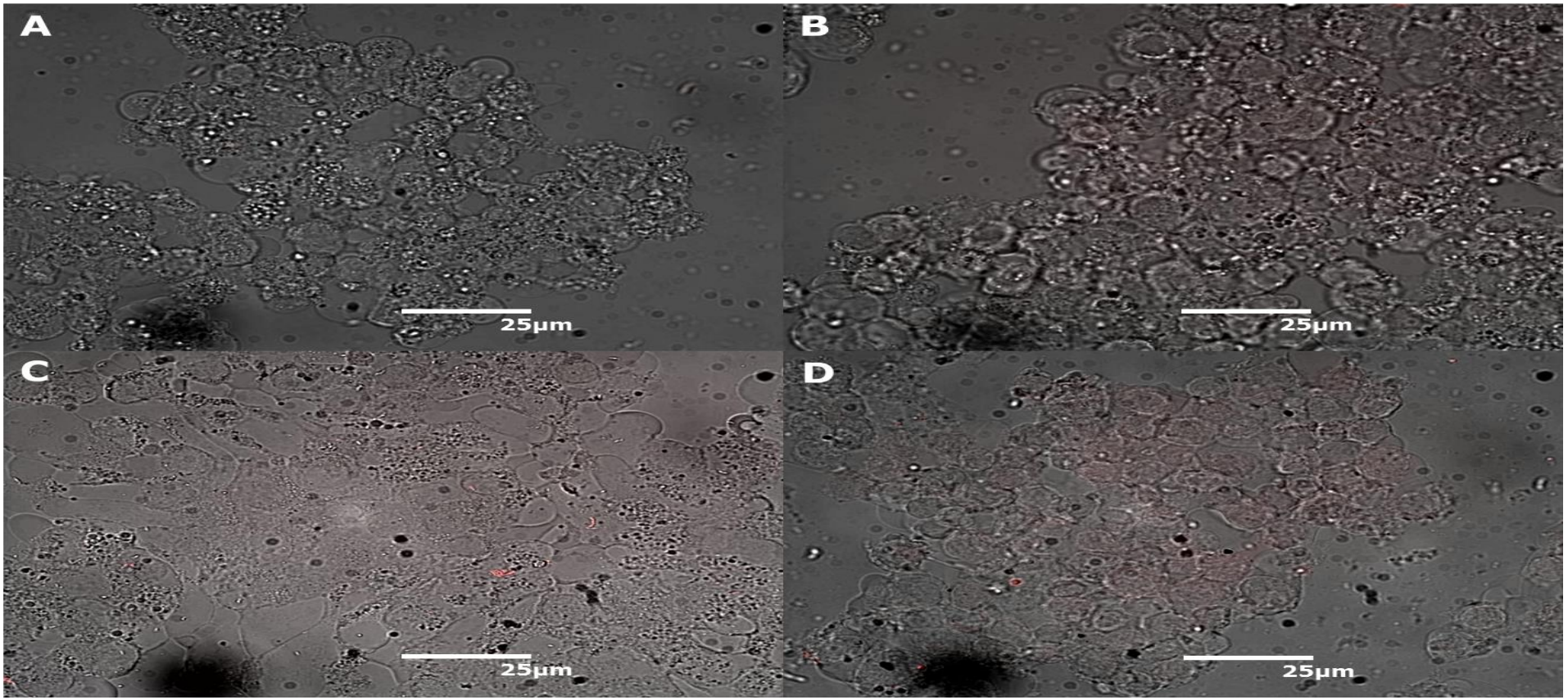

Figure 5. 3 CACO-2 cell images were captured using an Epi-fluorescent microscope with 400x magnification. The bright field image **A** represents the morphology of CACO-2 in the control group (0.1% v/v ether), and image **B, C, and D** show the morphology of 14 Days-treated (0.5, 5, or 50 µg mL^{-1}) CACO-2 with SiQDs, respectively. The red luminesce of the SiQDs is overlaid on the optical images.

5.3.3 Effects of SiQDs on CACO-2 Cell Viability

SiQDs at concentration 50 µg mL^{-1} treated CACO-2 for 4 and 24 hours did not cause any adverse effects on cell viability. The MTT results of the treated CACO-2 showed no difference compared to CACO-2 cells in the control group (**Figure 5.4**). On the contrary, the positive control group (CACO-2 treated with 15 µg mL^{-1} H_2O_2) showed markedly reduced viability when compared with the control CACO-2 cells and SiQDs treated CACO-2 cells **(Figure 5.4).**

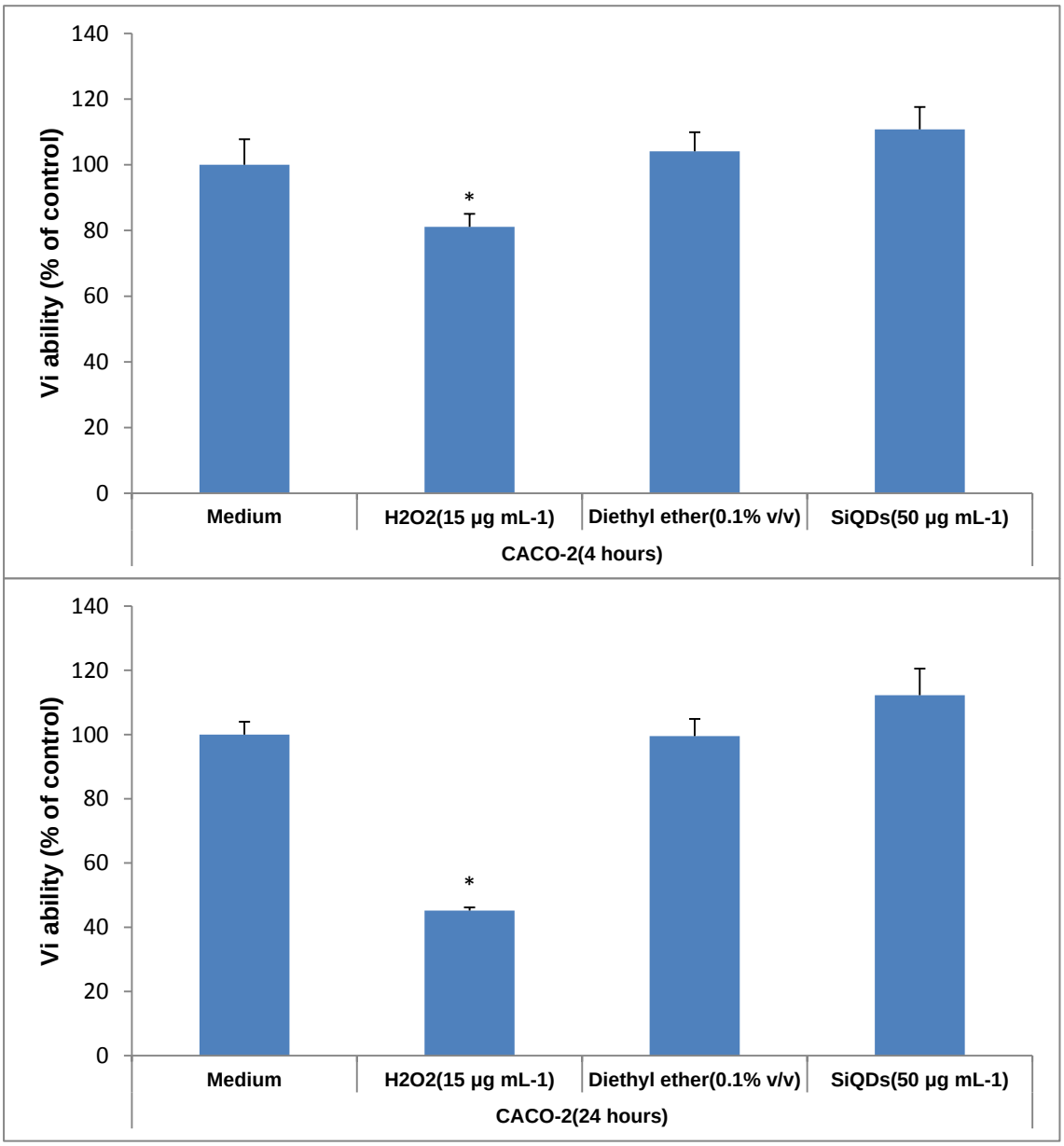

Figure 5. 4 Cytotoxicity studied in CACO-2 after exposed to SiQDs for 4 and 24 hours using MTT assay. Cell viability (% of control) is plotted as means ± SD for n=3 experiments.

5.3.4 Effects of SiQD treatment on cellular ATP concentrations in CACO-2 cells

Measurement of intracellular ATP showed that ATP levels were not significantly different between CACO-2 cells treated with SiQD at 100 µg mL^{-1} and control CACO-2 cells. This was the case for cells treated for 4 -or 24 hours, suggesting that SiQDs had no effect on CACO-2 - ATP production. In contrast, as a positive control (ATP production inhibitor), the ATP content of 2,4-DNP treated CACO-2 was significantly decreased at both 4 and 24 h incubation times (**Figure 5.5)**.

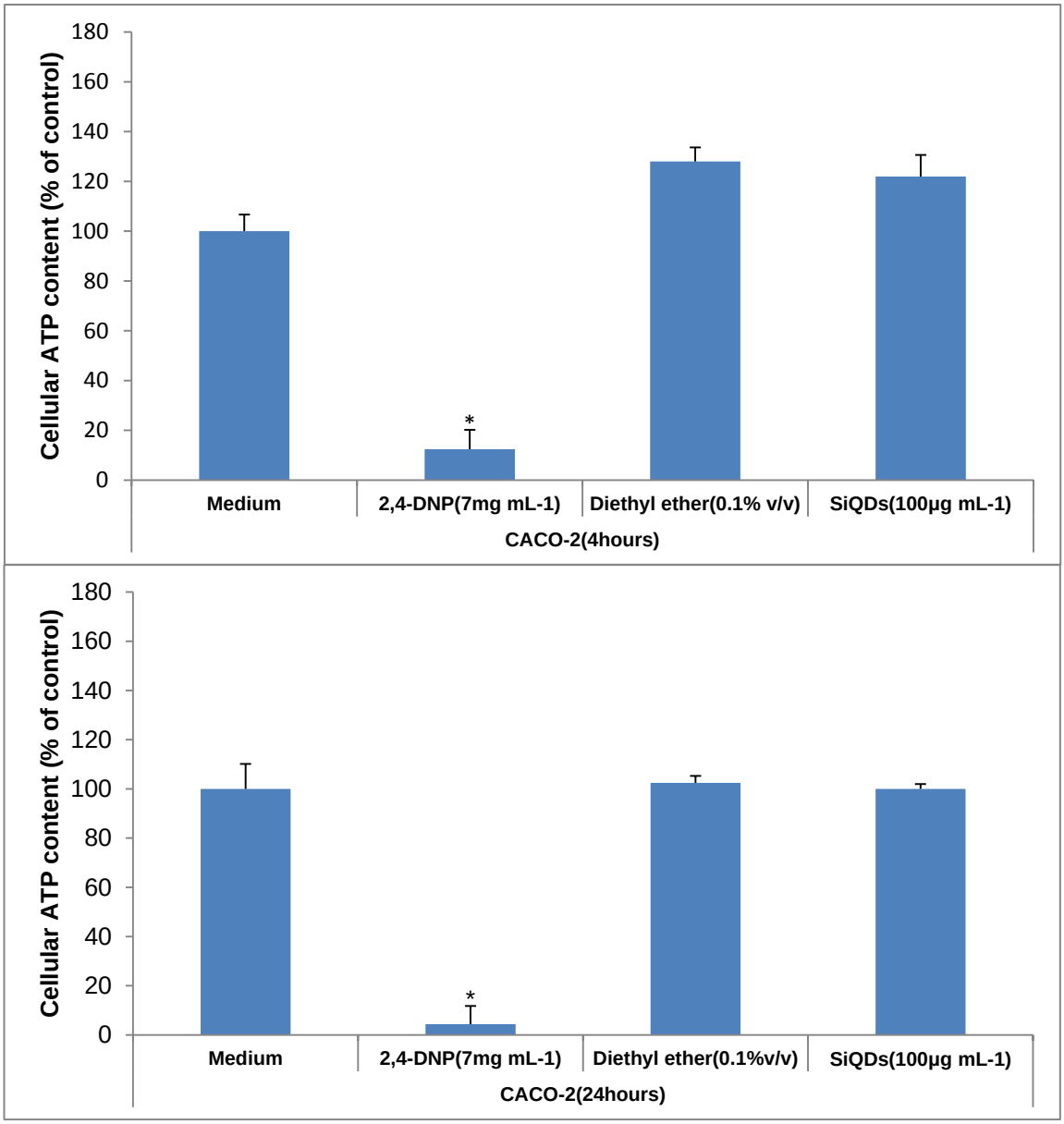

Figure 5. 5 Cellular ATP content measured in CACO-2 cells after exposed to SiQDs for 4 and 24 hours using FLASC (Sigma-Aldrich). The ATP content (% of control) represent with means ± SD for n=3 experiments.

5.3.5 Measurement of reactive oxygen species in CACO-2 cells treated with SiQDs

Using the DCFH-DA fluorescent dye, treatment of CACO2 cells with SiQDs at 100 ug mL^{-1} for up to 24 hours did not result in a significant increase in production of intracellular ROS. On the other hand, H_2O_2 treated CACO-2 cells exhibited much higher ROS concentrations compared to both control and SiQD treated cells. Cellular ROS content inside SiQDs treated CACO-2, control, and H_2O_2 treated CACO-2 is shown in **Figure 5.6**. The vehicle control showed slightly higher ROS production compared to medium after 24 hours.

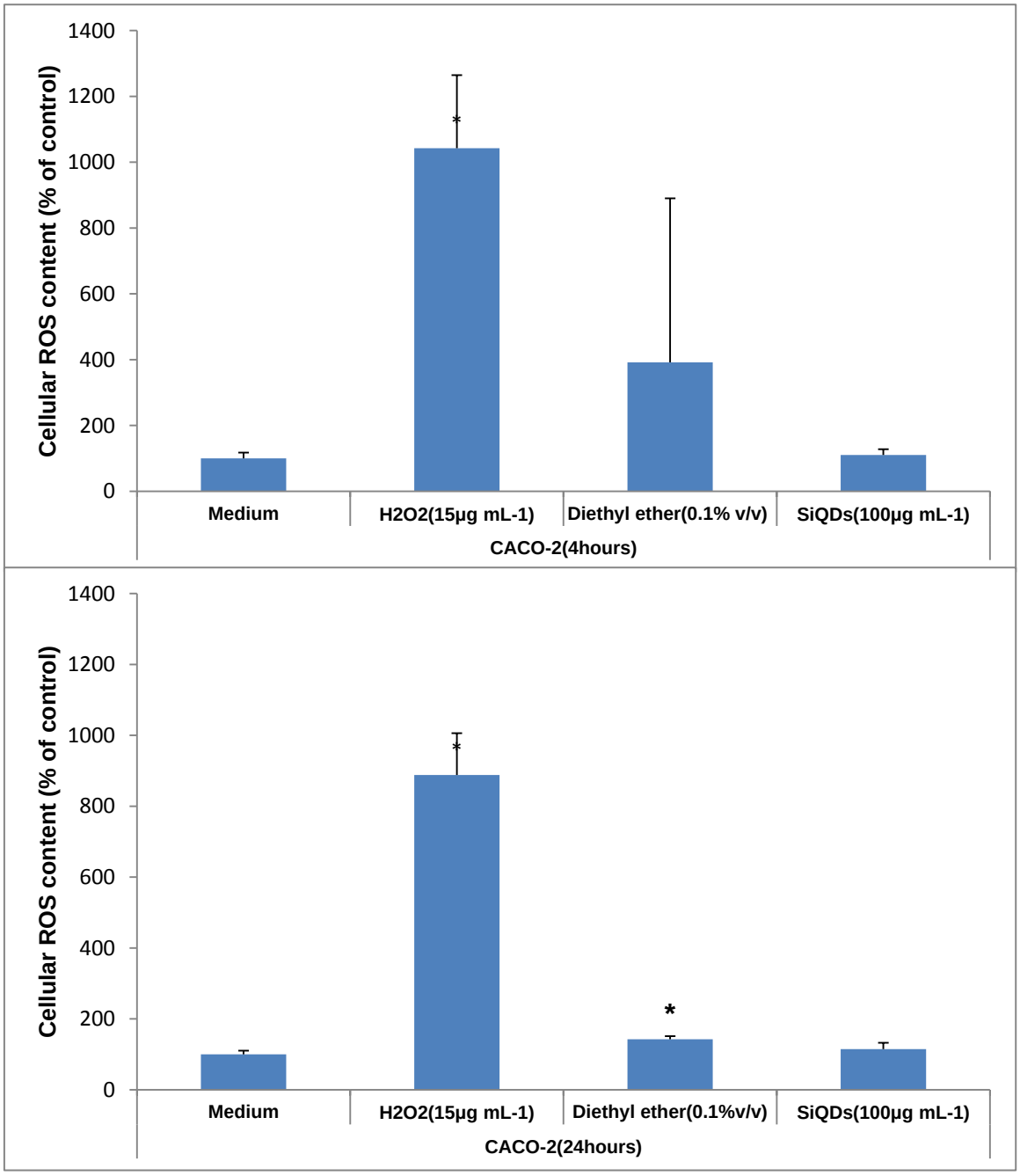

Figure 5. 6 Cellular ROS content measured in CACO-2 cells after exposure to SiQDs for 4 and 24 hours using H2DCFDA (Sigma-Aldrich). The ROS contents (% of control) are indicated as means ± SD for n=3 experiments.

5.3.6 DNA Damage Potential Evaluation of SiQDs in CACO-2

Single cell electrophoresis (Comet Assay) showed that CACO-2 cells treated with 200 μg mL^{-1} SiQDs for 4 or 24 hours did not show any significant change in any Comet parameters when compared to vehicle control. There was a significant decrease in head length at 4 hours compared to vehicle control, but this effect was not present at 24 hours; the SiQD treated cells appear to recover and no significant difference was observed compared to the control. CACO-2 cells treated with the positive control (15 μg mL^{-1} H_2O_2) showed nucleus elongation **(Figure 5.7 A, B)** and marked increases in tail intensity **(Figure 5.8-5.9)** compared to controls.

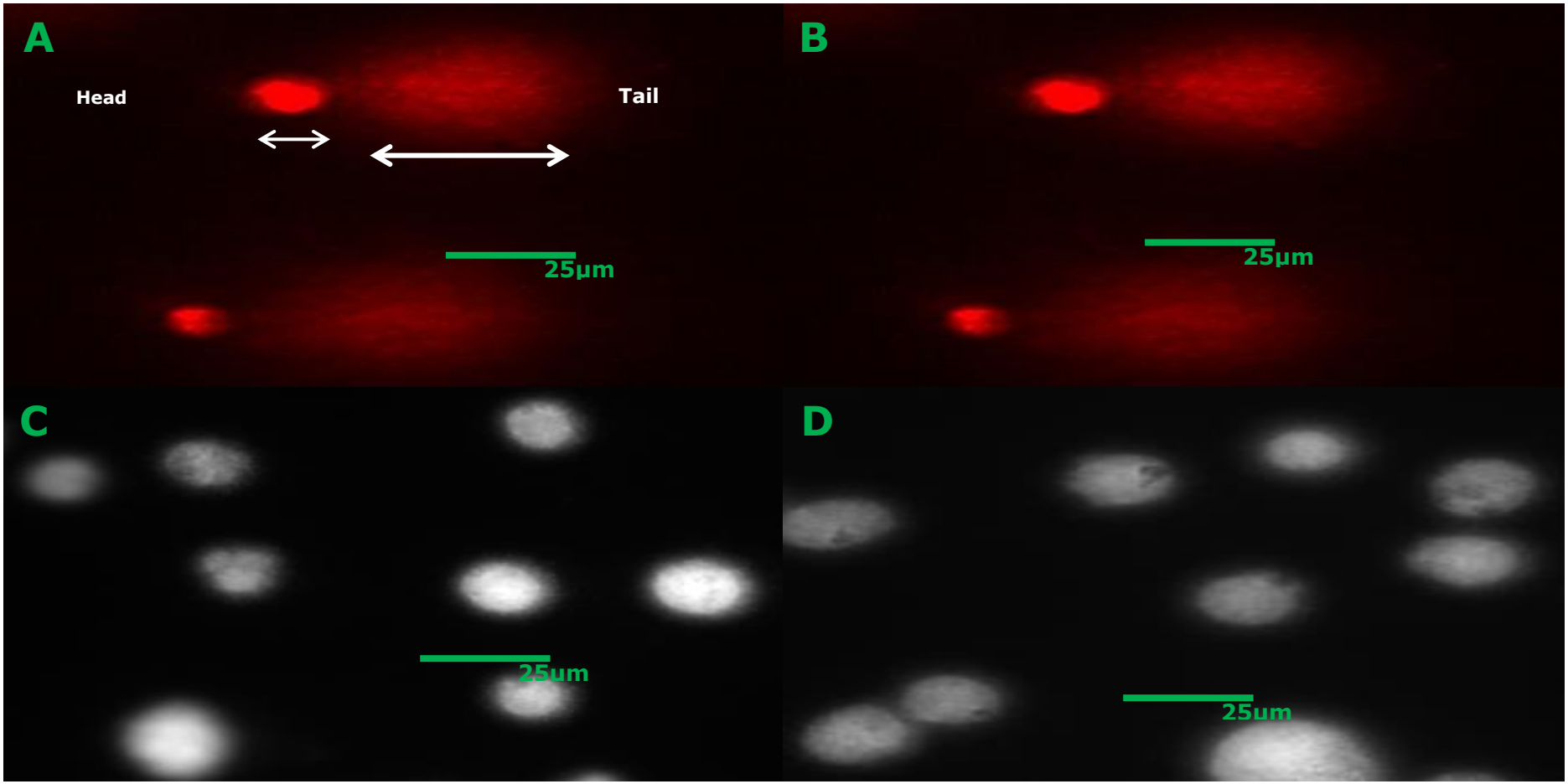

Figure 5. 7 (**A**, **B**) Comet images of CACO-2 cells after exposed to H2O2 (15 µg mL^{-1}) and (**C**, **D**) Images of CACO-2 cells after exposed to SiQDs (200 µg mL^{-1}) for 24 hours using Comet IV (Perceptive, UK).

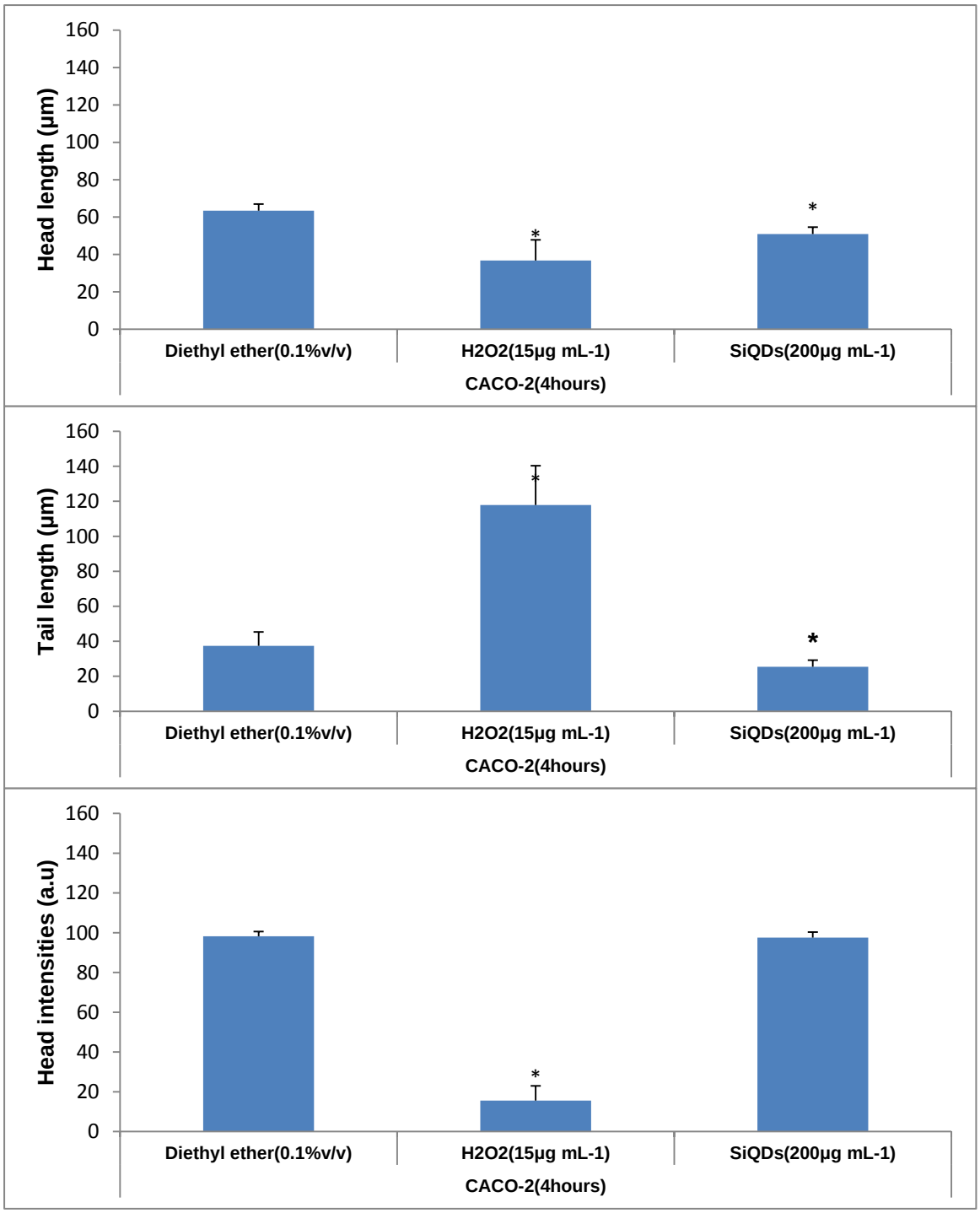

Figure 5. 8 DNA damage in CACO-2 cells after exposed to SiQDs (200 µg mL^{-1}) for 4 hours determined by Comet IV (Perceptive, UK). Head length, tail length and head intensity represent with means ± SD, whole cells experiments (n=2).

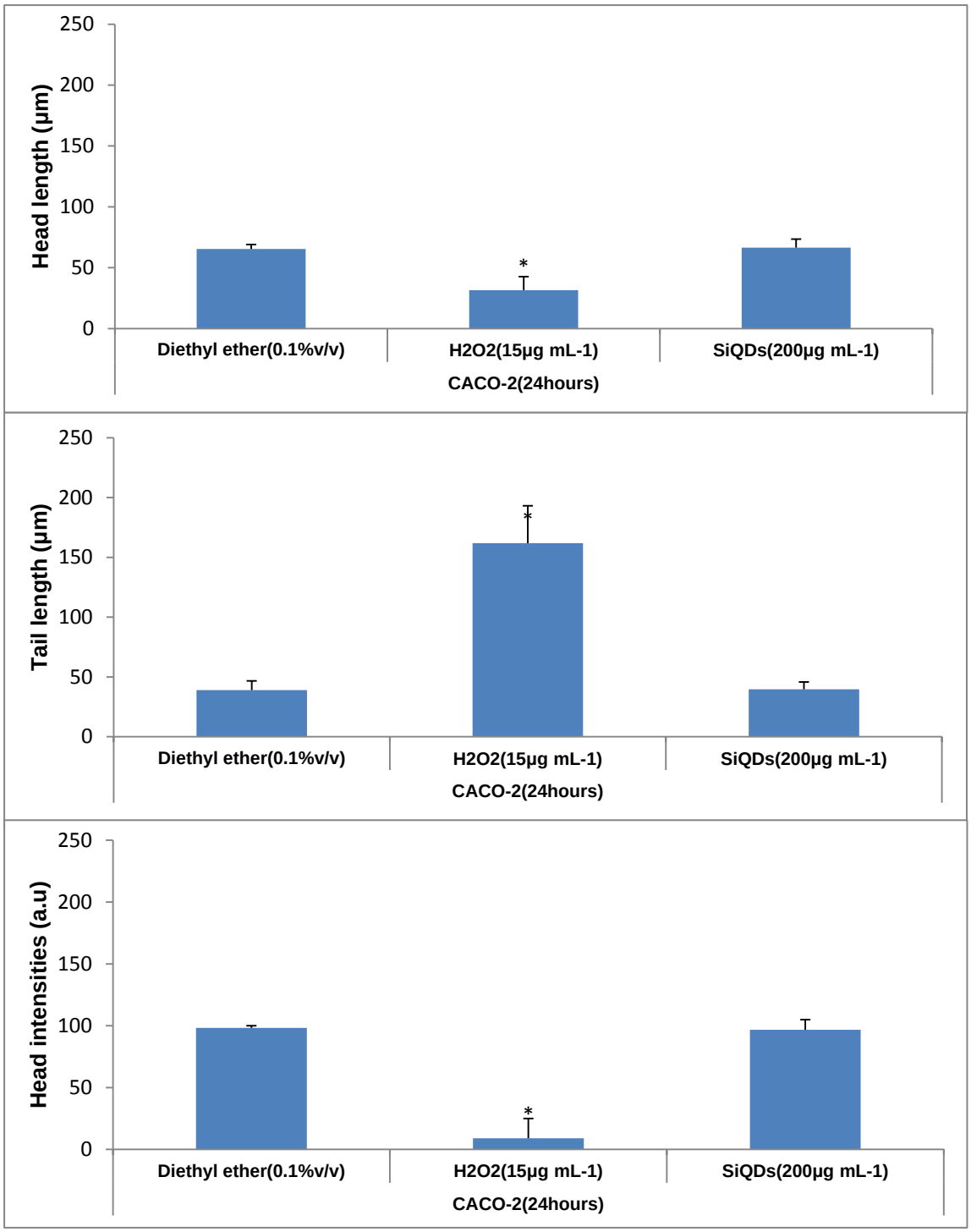

Figure 5. 9 DNA damage in CACO-2 cells after exposed to SiQDs (200 µg mL^{-1}) for 24 hours determined by Comet IV (Perceptive, UK). Head length, tail length and head intensity are indicated as means and SD.

5.3.7 Metabolic Activity Measurement and Validation of Oxidative Stress of Treated CACO-2 for Long Term 14 Days

To evaluate the effects on ATP levels and oxidative stress of long time exposure to SiQDs, CACO-2 cells were treated with 0.5, 5, and 50 μg mL^{-1} SiQDs for 14 days. The FLASC ATP assay and DCFH-DA assay were performed to detect intracellular ATP and ROS content. After 14 days there are no significant differences in the intracellular ATP or ROS concentrations between SiQDs treated CACO-2 cells and control CACO-2 cells **(Figure 5.10-5.11)**.

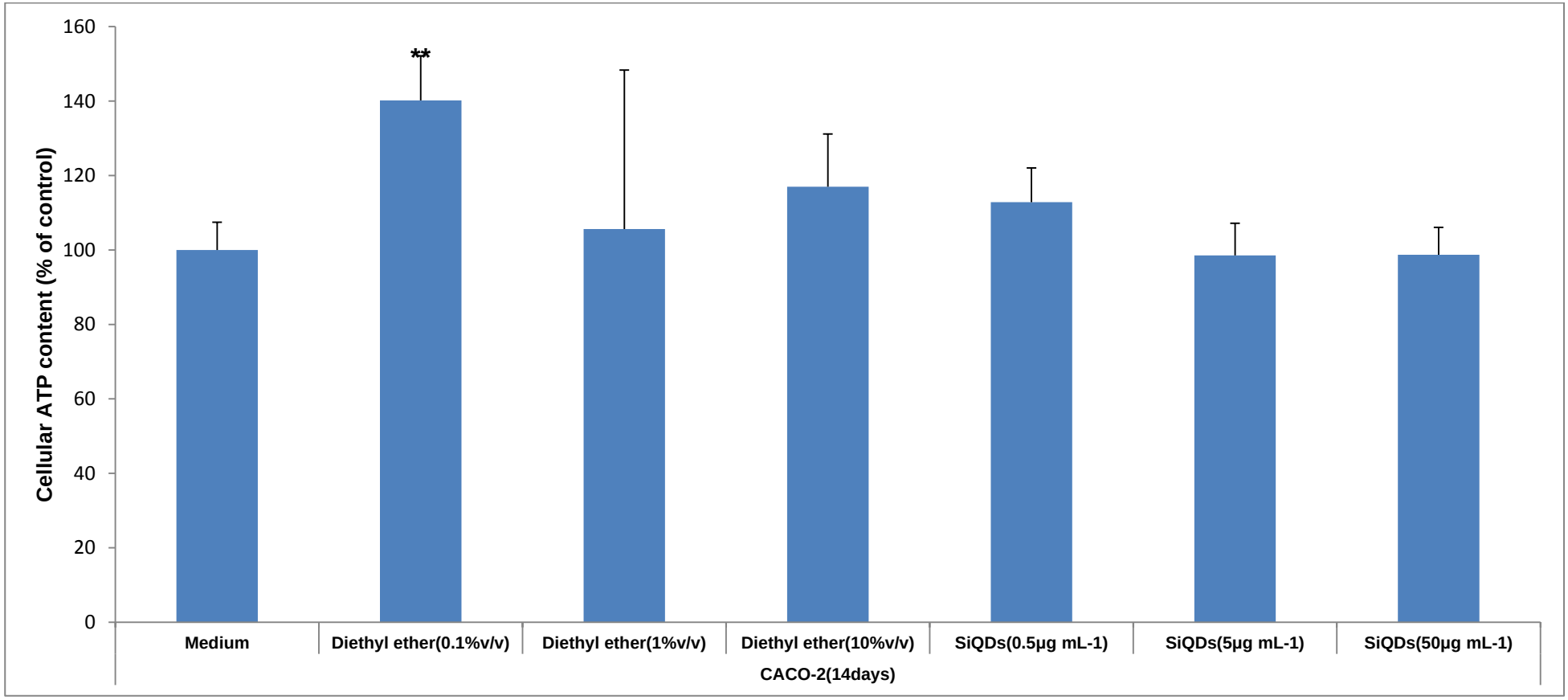

Figure 5. 10 Cellular ATP content measured in CACO-2 cells after exposed to SiQDs for 14 days using FLASC (Sigma-Aldrich). The ATP contents (% of control) are indicated as means ± SD for n=3 experiments.

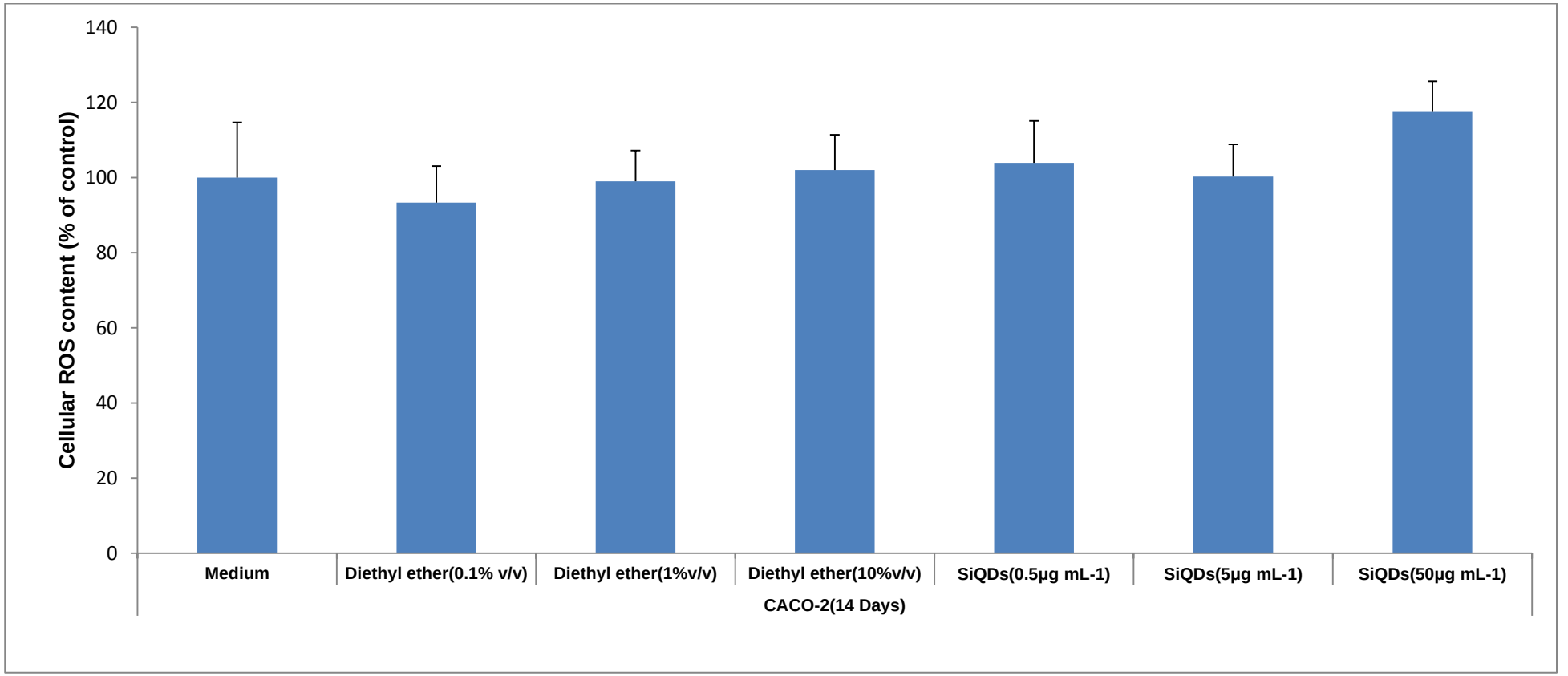

Figure 5. 11 Cellular ROS content measured in CACO-2 cells after exposed to SiQDs for 14 days using H2DCFDA (Sigma-Aldrich). The ROS content (% of control) is indicated as means ± SD for n=3 experiments.

5.4 Discussion

If QDs are to be used as luminescent probes (especially for medical imaging) the safety of these materials is a major concern. Although SiQDs do not contain any heavy metals, safety assessment is still crucial, particularly for nanomaterial applications in life sciences. Despite this, at present there are no standard procedures for nanomaterial safety evaluations. Furthermore, nanomaterials have unique characteristics and properties which differ from bulk material (Singh et al., 2009), (Doak et al., 2012). Particles smaller than Bohr radius might elicit different cellular responses compared to the bulk material (Nel et al., 2006).

The utility of SiQDs as fluorescent probes for cell imaging was demonstrated by Alsharif and colleagues in 2009. They reported that SiQDs could be internalised by both primary and human tumour derived cell lines as shown using confocal microscopy (Alsharif et al., 2009). Accumulations of SiQDs inside CACO-2 cells were also shown using epi-fluorescence and confocal Raman microscopy.

Previously, cytotoxicity evaluations of low concentration of SiQDs have been carried out in HeLa (immortalised epithelial cervical carcinoma) and SW1353 cell lines (chondrosarcoma). At this concentration, SiQDs did not produce adverse effects on HeLa and SW1353 in terms of cell morphological features (membrane sinking or blebbing), cell viability assay (CellTiter-Blue, Promega), cell proliferation assay (MTT), or cell apoptosis assay (DeadEnd Colorimetric TUNEL, Promega). Exposure to SiQDs did not result in membrane damage, decreased cellular metabolism or proliferation or increased cell death (Alsharif et al., 2009).

In the current study, safety of SiQDs was evaluated using cytotoxicity effects models. In particular, CACO-2 cells were used as a model cell system as they are intestinal cells and might be more relevant to human exposure than the HeLa cells and other cells used previously by Alsharif et al. (2009). The MTT assay was first used to investigate cell viability of CACO-2 cells after exposure to SiQDs. According to the results, the concentration of SiQDs leading to cell death is likely to be very high. The cell viability information from the MTT assay alone cannot classify the level of cytotoxicity and assess safety of SiQDs. In

addition another cell viability assay which measures the effect of SiQDs on cellular ability to produce ATP was used. Adverse effects of SiQDs are revealed by the concentration of ATP produced by the cells. High densities and healthy cells generate high concentration of ATP (Jensen et al., 2008, Xia et al., 2008a). In addition, the intracellular effect of SiQDs was investigated using a reactive oxygen species (ROS) assay. Possible DNA damage was assessed using the Comet assay. None of these assays showed toxic effects of SiQDs, either acutely or chronically at the concentrations used (up to 200 μg mL^{-1}). The only evidence of acute effects was found to be that of ether – the vehicle used to disperse the SiQDs – in the cellular ATP content assay. In the presence of ether, the cells generate more ATP for reasons that are not clear.

The unique physicochemical properties of nanoparticles including size, shape, surface, and free radical are all factors attributable to the generation of unique adverse effects in living organisms. Nanoparticles are hypothesised to generate cytotoxicity, oxidative stress, and inflammatory responses (Sayes et al., 2007, Xia et al., 2006, Nel et al., 2006). However, in this study neither cytotoxicity nor increased oxidative stress was detected in CACO-2 cells treated with SiQDs. However, more studies need to be designed for specific safety evaluations relevant to applications of nanoparticles. In order to establish the safety of nanoparticles more information on various aspects such as the interaction of nanoparticles with additional cell lines to mimic the route of administration are needed. The systemic toxicity (in vivo) also needs to be explored.

The phagocytic and non-phagocytic cells, macrophage (RAW 264.7), lung epithelium (BEAS-2B) cells have been used for studying potential cytotoxicity effects of pollutants (particle sizes). Pollutants with ultrafine particles (UFPs) show adverse effects when three well-known oxidative stress markers, heme oxygenase-1 (HO-1) expression, glutathione, and reactive oxygen species (ROS), are investigated. The UFPs have been confirmed to be internalised by those cells by detection with electron microscopy (Li et al., 2003). It is indicated that the size of nanoparticles less than 0.1 μm together with inherent compounds (pollutants: organic carbon and polycyclic aromatic hydrocarbon (PAH) cause oxidative stress in macrophage and lung epithelium cells. The positively charged silicon (Si NP-NH_2) shows more cytotoxic effects and induces high oxidative stress compared with the neutral silicon (Si NP-N_3) while

negatively charge silicon (Si NP-COOH) shows very low cytotoxicity effects in macrophage NR8383 cells (Bhattacharjee et al., 2010). In addition, liver cell lines (HHL-5, HepG2) and embryonic cells (3T3-L1) treated with silicon coated with poly-acrylic acid (PAAc) reveal no adverse effects when cell morphology, cell proliferation, viability, and DNA damage assays are performed (Wang et al., 2012).

Another significant toxic effect of nanoparticles may be on the inflammatory cellular response. This can be studied by looking at potential cytotoxicity effects of nanoparticles in phagocytic cells (Singh et al., 2009). One study investigated macrophage cells (RAW 264.7) treated with two types of silicons with diameter 3 nm (nanodots) and 100-300 nm (microdots) and found some effects on the cellular inflammatory responses. The cells showed internalisation of silicon nanoparticles (3nm) by fluorescence microscopy. However, in that study the nanoparticles were associated with increased cytotoxicity at concentrations above 20 ug mL^{-1} unlike in the current study where SiQDs showed no toxicity at this concentration for CACO-2 cells. Concentrations above 20 ug mL^{-1} were also associated with decreased synthesis of tumour necrosis factors-alpha (TNF-α) and interleukin 6 (IL-6). Microdots with a larger diameter than silicon dots were less toxic to the macrophage cells but induced increased production of IL-6 and TNF-alpha at relatively low concentrations (Choi et al., 2009). Production of cytokines by CACO-2 cells in response to SiQDs was not studied in the current investigation as endogenous levels of these are likely to be very low in these non-immune cells. However, further studies involving investigation of SiQD effects on macrophage cytotoxicity and cytokine production should be performed.

In addition, a pharmacokinetic assessment using an in vivo model is also important to determine the toxicity effects on distribution, clearance and specific organ (Fischer and Chan, 2007, Santos et al., 2013). The first in vivo study of Si nanoparticles coated with dextran has shown that porous Si or Si nanoparticles show low toxicity. The biodegradation product of porous Si is orthosilisic acid ($Si(OH)_4$ and this is removed from the body through renal clearance (Park et al., 2009).

In conclusion, no evidence for toxicity of SiQDs at a concentration of up to 200 ug mL^{-1} in CACO-2 cells was obtained using a range of toxicity tests. These confirm the findings of Alsharif et al. (2009) but using a more physiologically relevant cell line and some additional tests such as assessment of DNA damage and oxidative stress.

Chapter 6. Mechanism of Internalisation of Alkyl-Capped Silicon Quantum Dots (SiQDs)

6.1 Introduction

There is a strong relationship between the lipid content in the cell membrane (plasma membrane), proteins and the internalisation of molecules into the cell. The membrane of eukaryotic cells plays a vital role to separate the cytoplasm from environment as well as forming internal compartments of organelles (Phillips et al., 2009). The plasma membrane also functions as a part of sensory, signalling pathways, controls transport into and out of the cytoplasm, intracellular trafficking and energy metabolism in organelles (Phillips et al., 2009).

Endocytosis is one of the molecular transportation systems (Marsh and McMahon, 1999). The endocytosis processes may be divided into broad categories: phagocytosis and pinocytosis. The pinocytosis process or internalisation from the extracellular medium is the dominant process in all cell types (Seto et al., 2002, Conner and Schmid, 2003). Pinocytosis includes 4 basic mechanisms, macropinocytosis, clathrin-mediated endocytosis (CME), caveolae-mediated endocytosis and clathrin-and caveolae-independent endocytosis (Conner and Schmid, 2003). The main function of endocytosis is vital for cell survival by controlling homeostasis of the cell. The cell uses endocytosis to regulate the lipid and protein composition of the cell membrane (Doherty and McMahon, 2009). In addition, endocytosis is not just vesicular as transport also has a role in regulation of many intracellular signalling cascades as well as mitosis, antigen presenting, and cell migration (Doherty and McMahon, 2009). The cell controls lipid and protein to internalise membrane vesicles constantly. Among vesicular membranes, CME and caveolae-mediated endocytosis are the most extensive characterised because they are sensitive to endocytosis pharmacological/chemical inhibitors for examples chlorpromazine (CP), filipin, and methyl-β-cyclodextrin (MβCD) (Ivanov, 2008). CP is a cationic amphipathic drug which inhibits CME. The CP dose required to inhibit clathrin-mediated endocytosis is in the range of 50-100 μM. However, the concentration of CP for cell studies needs to be used with care as CP also shows multiple interactions on intracellular lipids to increase membrane fluidity. It has some adverse effects on the cytoskeleton including effects on actin dynamics and

micropinocytosis (Ivanov, 2008). The exact mechanism by which CP inhibits CME is still unclear. It was thought to affect the interaction of the clathrin protein and AP2 adaptor complex in formation of the vesicle but recent data suggests the effect of this drug is downstream of clathrin-coated vesicle formation (Daniel et al., 2015). Other endocytosis inhibitors have effects on endocytosis involving caveolins. Filipin and MβCD both affect cholesterol (Ivanov, 2008). Cholesterol and sphingolipids interact with caveolins to form caveolae (Ivanov, 2008). The mechanisms for the inhibitory effects of filipin and MβCD are different. Filipin is a polyene antibiotic and binds directly to cholesterol in the cell membrane. It also binds to 3β-hydroxysterol, a major component of glycolipid microdomains and caveolae of the plasma membrane (Nagasawa et al., 2014). At the low concentration (1 μM), filipin treatment results in flattened caveolae probably due to lack of cholesterol to interact with caveolin. Filipin also has effects on the linkage between cortical F-actin and the plasma membrane but the relevance of this to endocytosis is still not clear (Ivanov, 2008). MβCD is a cyclic heptosaccharide that at 5-10 mM forms soluble inclusion complexes with cholesterol and therefore depletes cholesterol from the cell membrane (Ivanov, 2008). Similar to filipin, this affects the formation of caveolae which are flatter than normal, with caveolin 1 also shown to locate in the wrong area of fibroblast membranes. Comparison between the endocytosis inhibitors CP, filipin, and MβCD reveals that MβCD has broader inhibition effects including effects on CME and fluid-phase endocytosis as well as caveolae-mediated endocytosis (Ivanov, 2008).

The internalisation mechanism of alkyl-capped silicon quantum dots (SiQDs) in human cells was characterised because these materials have potential use as luminescent labels in biology as well as being of fundamental interest for the study of the interaction of nanomaterials with biological systems. SiQDs have unique physico-chemical properties with low toxicity (Alsharif et al., 2009). SiQDs have been proposed as a safe probe for cell imaging (Alsharif et al., 2009, Ahire et al., 2012). SiQDs revealed no evidence of in vitro cytotoxicity with different toxicity end points, cell morphology, apoptosis, and cell viability. They also showed a high rate of internalisation including effects on cancer cells (HeLa, A172 and MCF7) compared with various non-cancer cells (HSF1, HSF2, HM, and A5UG) (Alsharif et al., 2009). Atomic force microscopy (AFM) images

showed that the SiQDs are small approximately spherical particles with diameters in the range of 5 to 7.5 nanometre (nm). They also have a bright orange luminescence, λmax ~ 650nm. Previous studies by Alsharif and colleagues showed that SiQDs are a promising alternative to cadmium selenite (CdSe)-based quantum dots for cell imaging. SiQDs were observed using confocal microscopy to be rapidly internalised after incubation with many cell lines, malignant and non-malignant, though at a slower rate in the primary cells (Alsharif et al., 2009).

Alsharif and colleagues proposed that caveolin-mediated endocytosis might be involved in internalisation of SiQDs into HeLa cells as caveolin and cholesterol are major components of the caveolae (flask-shaped features on the cell membrane). It was found that treatment with filipin significantly decreased the accumulation of SiQDs into HeLa cells (Alsharif et al., 2009). Filipin is a well-known endocytosis inhibitor which operates by binding to cholesterol on the cell membrane (Nagasawa et al., 2014). Recent studies on the genes encoding caveolins have revealed 3 gene families, cav-1, cav-2, and cav-3. The cav-1 and cav-2 genes are co-expressed in many cell types. The last, cav-3, is thought to be only expressed in skeletal muscle (Cohen et al., 2004). The studies described in this chapter are concerned with the uptake of SiQDs by several different cell lines as stated, CACO-2, HepG2, Huh7, and HeLa. They are tumour derived cells from the intestine, the liver and cervical epithelium. The relevance of caveolin to this process is also investigated.

Objectives

1. To measure internalisation of SiQDs using fluorescence method (flow cytometry)
2. To measure the influence of inhibitors of endocytosis process-filipin, chlorpromazine, MβCD
3. To quantify caveolin gene expression in the cell lines

6.2 Methods

6.2.1 Cellular Internalisation Potential of SiQDs in Different Cell Lines

Four different cells, CACO-2, Huh7, HeLa, and HepG2 were seeded in T-25 flasks at a density of 1.5 x 10^5 cells mL^{-1} in the appropriate medium and incubated at 37 ^oC with 5% CO_2. CACO-2 cells were cultured as described in Section 2.4. HeLa, HepG2, and Huh7 cells were cultured in complete RPMI-1640 medium (R7509) with 10% (v/v) FBS instead of Dulbecco's modified Eagle's medium. However, all other cell culture procedures were performed exactly as described for the CACO-2 cells.

After 24 hours the cell medium was replaced with complete medium containing 0.1% (v/v) foetal bovine serum (FBS) and freshly prepared 100 µg mL^{-1} SiQDs in 0.5% (v/v) diethyl ether and incubated at 37 ^oC with 5% CO_2 for 1 hour or 24 hours. In a separate flask, the cells were incubated in the complete medium containing 0.1% (v/v) FBS with no SiQDs but the equivalent volume of diethyl ether. These were used as the control flasks. After 24 hours the culture medium was replaced with PBS and washed 3 times to eliminate the treated samples. Then the PBS was replaced with trypsin and left for 3 minutes. The trypsin reaction was stopped by added complete medium containing 10% (v/v) FBS. To remove FBS the cells suspension was washed using cell washer (BD FACS™ Lyse/Wash Assistant), compatible machine in PBS with precipitation G Force 461G, precipitation time 10 second, wash force 350 g, and wash volume 6400 µL. The precipitation cells suspensions were used for measuring luminescent intensities inside the cell. To compare luminescence intensity of SiQDs inside the cell among various cell types, the luminescence intensities were recorded in each individual cell. In each sample 3,000 events were collected using the BD LSR II flow cytometer. In the BD LSRII system, several excitation and detection wavelengths are available; SiQDs show strong orange-red luminescence and are best detected with low excitation wavelength (355 nm) and at a long detection wavelength (675 nm). The data are presented as luminescence intensities average values (Mean ± SD).

6.2.2 Specific Gene Expression of Caveolin-Mediated Endocytosis, Caveolin 1 and Caveolin 2

RNA preparation

RNA was extracted from the cell lines. Cells at 70-80% confluence were used as the source of the RNA extraction. Cells were washed with phosphate buffered saline (PBS) 3 times. The PBS solution was replaced with a trypsin solution to remove the cells from the plate. To produce a cell pellet, the trypsin reaction with the cells suspension was stopped using cell culture medium containing 10-20% (v/v) foetal bovine serum (FBS) and centrifuged at 1000 G for 5 minutes. The cell pellet was re-suspended in PBS and centrifuged at 1000 G for 5 minutes to obtain a clean cell pellet for RNA extraction. Tri-reagent (Sigma-Aldrich) (1 mL) was added to the cell pellet and pipetted up and down to mix well. The cell suspension was transferred into an RNase-free screw cap 1.5 mL micro centrifuge tube and incubated at room temperature for 10 minutes to allow the reagent to dissociate the nucleoprotein complexes. After 10 minutes 100 µL of 1-bromo-3-chloropropane was added and mixed well by hand till the suspension solution became a milky pink colour; it was then incubated at room temperature for another 10 minutes. Then the suspension was centrifuged at 12000 G and 4 ^{o}C for 10 minutes. After centrifugation, the cell suspension revealed 3 different layers. The first layer on the top was a clear RNA-containing solution, the middle, opaque layer contained the DNA and the third layer in the bottom was the dark pink solution comprising mainly protein. The first layer (500 µL) was collected and placed into a new RNase-free micro centrifuge tube. To precipitate the RNA, 500 µl of isopropanol was added to the tube and mixed well using vortex. Then the solution was incubated at room temperature for 10 minutes. After 10 minutes the RNA was separated from the solution by centrifugation at 12000 G and 4 ^{o}C for 10 minutes. The isopropanol was carefully decanted and the white RNA pellet was collected. To clean the pellet and get rid of the remaining isopropanol, the pellet was re-suspended in 75% (v/v) ethanol in RNase-free water and vortexed till the pellet moved out from the bottom of the tube. To collect the RNA, the suspension was centrifuged at 7500 G, 4^{o}C for 5 minutes. After centrifugation the 75% (v/v) ethanol was carefully decanted and left the RNA pellet dried at room temperature for 10 minutes. After 10 minutes the RNA pellet was re-suspended in 50 µL RNase-free water and mixed well using vortex. The RNA solution was stored at -80 ^{o}C and checked for purity using a Nanodrop spectrophotometer ND-1000 (Thermo Scientific) before performing cDNA synthesis. The RNA solution absorbance at the unit of 1 at 260 nanometre (nm) is equivalent to 40

µg mL^{-1} RNA. The purity of the RNA is indicated by using the ratio of RNA solution absorbance at 260 nm to 280 nm. Acceptably pure RNA has an absorbance ratio in the range of 1.8 to 2.0; an increase in the absorbance at 280 typically indicates the presence of proteins in the sample.

cDNA synthesis

The cDNA strand was synthesised using M-MuLV Reverse Transcriptase (200,000 U mL^{-1}) (New England Biolabs) with random oligonucleotide sequences (primers) (Random Hexamers (0.4 µg $µL^{-1}$)), deoxynucleotide (dNTPs) solution mix (40 mM, 10 mM in each dNTP (dATP, dCTP, dGTP, and dTTP)), RNase-free water, 10X Reverse transcriptase Reaction Buffer (1X : 75 mM KCl, 50 mM Tris-HCl, 3 mM $MgCl_2$, 10 mM dithiothreitol, pH 8.3) (reagents supplied with M-MuLV Reverse Transcriptase) and RNase Inhibitor (40,000 U mL^{-1}). The procedure to synthesize the first cDNA strand was started by preparing the first mixing solution (1) by adding 1 µL of random hexamers, 1 µL of dNTPs and 6 µL of RNase-free water into an RNase-free micro centrifuge tube. The tube (1) was then placed on ice. In another RNase-free micro centrifuge tube the second solution (2) was prepared by adding 2 µL 10X Buffer, 0.1 µL RNase inhibitor, 0.25 µL Reverse Transcriptase Enzyme, and 7.65 µL RNase-free water and placed on ice. Then 2 µL of the RNA solution was added into the first mixing tube (1) and mixed well. The RNA mixing solution was incubated at 65 ^{o}C for 10 minutes to denature the RNA. After 10 minutes the denatured RNA solution was cooled on the ice for 2 minutes to allow the primers to recombine with the RNA. Then solution (2) was added into the first tube and mixed well. The combination solution tube was incubated at 37 ^{o}C for 50 minutes to allow the reverse transcription reaction to reverse transcribe RNA to cDNA. To inactivate any remaining enzyme, the cDNA solution tube was incubated at 70 ^{o}C for 15 minutes. After 15 minutes the cDNA solution was stored at -20 ^{0}C prior to qPCR analysis.

Quantitative reverse transcriptase real time PCR analysis

Quantitative reverse transcriptase real time PCR analysis using an ABI StepOne PCR System was used to determine expression of caveolin1 and

caveolin2. TaqMan caveolin 1 and caveolin 2 assays were employed to verify the specific gene expression in various cells types compared with the control gene. Caveolin 1 and caveolin 2 genes, predominate in almost cell types were characterised by qPCR using TaqMan® Gene Expression Assays (Life Technologies). The amplified caveolin 1 or 2 gene with included FAM™ reporter dyes and control gene, glyceraldehyde-3-phosphatedehydrogenase (GAPDH) with VIC™ reporter dye were recorded by qPCR using MicroAmp® Fast Optical 48-well PCR plate (Applied Biosystems) on an Applied Biosystems StepOne™ Real-Time PCR system. Quantifying caveolin gene expression was detected by recording the fluorescent signal of the reporter dye; the PCR cycle at which the fluorescence signal of the reporter dyes crosses the threshold of the baseline background (control gene) in the exponential phase of amplification. This cycle is named the threshold cycle (C_T). The C_T value is inversely correlated with the amount of small DNA or gene expression. A low C_T value represents a greater amount of small DNA or gene expression (Schmittgen and Livak, 2008). The comparative C_T method was employed to analyse the qPCR data and the data are presented as the amount of the gene of interest relative to the control gene glyceraldehyde-3-phosphatedehydrogenase (GAPDH).

6.2.3 Endocytosis Inhibitor Optimal Concentration

Optimal dosages of common endocytosis inhibitors dosages, 2, 4, 6, 8, 10, 12, and 14 μg mL^{-1} of chlorpromazine, Methyl-β-cyclodextrin (MβCD) 2, 4, 6, 8, 10 mmole L^{-1} were determined for the internalisation inhibition studies of SiQDs (Vercauteren et al., 2010). The maximum concentrations that did not produce deleterious changes in cell morphology were measured Filipin at 5 μg mL^{-1} and MβCD at concentration 10, 7.5, 5, and 2.5 mM were used to treat HeLa and Huh7 cells for 1 hour and 24 hours. Chlorpromazine at concentrations 2, 10, 20, and 30 μM was used to treat HeLa and Huh7 to discover the optimal concentrations for clathrin-mediated endocytosis inhibition. After 1 and 24 hours the cells were observed for morphological changes compared with the control groups. The cell morphology were observed under phase contrast microscope (OPTIKA) (200 x magnification) with cell images captured with ScopeImage DynamicPro (BUC2-500C).

6.2.4 Endocytosis Inhibition Studies of SiQDs on HeLa and Huh7

Cellular internalisation of macromolecules, the dominant process in many cells is known as pinocytosis (Conner and Schmid, 2003). In this study the pinocytosis pathways involved in the cellular internalisation of alkyl-capped silicon quantum dots (SiQDs) into the human cell lines were investigated using well-known endocytosis inhibitors, chlorpromazine (CP), methyl-β-cyclodextrin (MβCD), and filipin III. The cells were cultured with phenol red free medium (to avoid interference from the dye in the flow cytometry measurements) in culture treated T-75 flask and incubated at 37 ^{o}C with 5% $CO_{2.}$ 70-80% cells confluence was seeded in a culture treated T-25 flask at a density of 1.5 x 10^5 cells mL^{-1}. The cells were cultured overnight in incubator, 37 ^{o}C with 5% CO_2. After 24 hours incubation cells were treated with the appropriate chemical inhibitor (chlorpromazine, MβCD or filipin) in phenol red free complete medium containing 0.1% foetal bovine serum (FBS) for 1 hour. Then the medium was replaced with 100 μg mL^{-1} of SiQDs with constant concentration of the inhibitor in complete medium containing 0.1% FBS for 24 hours. HeLa and Huh7 were pre-treated with 1 mM MβCD, or 30 μM chlorpromazine, or 0.8 μM, 3 μM filipin and continued treatment with SiQDs for another 24 hours. The filipin treatment was performed slightly differently with the filipin was washed out before continued incubation with SiQDs. Quantitation of SiQDs which had been internalised by the cells treated with inhibitor was carried out using flow cytometry system to measure the amount of SiQDs inside the cells by recording the SiQDs fluorescent intensity and comparing with untreated cells. The luminescence intensities were recorded in each individual cell and in each sample using flow cytometry at wavelength 355 and 675 nm.

6.2.5 Statistical Analysis

All statistical analysis was performed using SPSS software (IBM Statistics 21). The level of significance for the effects and interactions of particular parameters were calculated using two-way anova. Where a statistically significant main effect was found, differences between treatment levels were evaluated using Tukey's post hoc test. For the studies on inhibition of dot accumulation, significance was assessed by using independent sample T tests. A p value ≤ 0.05 was taken as statistically significant.

6.3 Results

6.3.1 Cellular Internalisation Potential of SiQDs in Different Cell Lines

Four different human cell lines HepG2, CACO-2, HeLa, and Huh7 were treated with freshly prepared SiQDs (50 and 100 μg mL $^{-1}$) in complete medium containing 0.1% foetal Bovine serum (FBS) and diethyl ether for 1 hour and 24 hours before analysis accumulation of SiQDs inside the cell by flow cytometry. To qualify the internalisation potential of SiQDs by the accumulation of SiQDs inside the cells were measured by detecting luminescent intensities using flow cytometry. The cells luminescent intensities measured using flow cytometry (excitation at 355 nm and emission at 675 nm) is shown in **Figure 6.1**.

There was a significant effect of concentration ($P<0.001$) and cell type on luminescence intensity ($P<0.001$) for data obtained at 1 hour and 24 hours when data were analysed by two-way ANOVA; however, there was also a significant interaction ($P<0.001$) term at both time points, suggesting that the response of cells to concentration was dependent on the cell line. There was also a strong dependence on exposure time. With an exposure time of 1 hour, luminescence intensity did not differ significantly with SiQD concentration for CACO2 cells, whilst there was a small, but statistically significant, increase in luminescence intensity compared to controls with HeLa, HepG2 and Huh7 cells (**Figure 6.1**). After 24 hours, there was a more marked response of HepG2 and Huh7 cells to increasing concentrations of SiQDs, with a statistically significant effect of increasing SiQD concentration on luminescence intensity. The same was true for CACO2 cells, but to a lesser extent. The response of HeLa cells to increasing SiQD concentration was also statistically significant but the magnitude of increase was not greatly different from that with the shorter exposure time. The highest levels of luminescence intensity at both concentrations and time points were seen for HepG2 cells with a level of 143.96 arbitrary fluoresence units seen after 24 hours when a concentration of 100 μg mL^{-1} was used.

This study suggested that the internalisation of SiQDs into the cells (as evidenced by luminescence intensity measured by flow cytometry was significantly influenced by both SiQD concentration and cell type. Each cell types responded differently in terms of internalisation when SiQDs

concentrations were increased. After 24 hours exposure, the HepG2 and Huh7 showed high internalisation of SiQDs inside the cells in response to increase the concentrations of SiQDs while the CACO-2 and HeLa showed slightly increased internalisation of SiQDs.

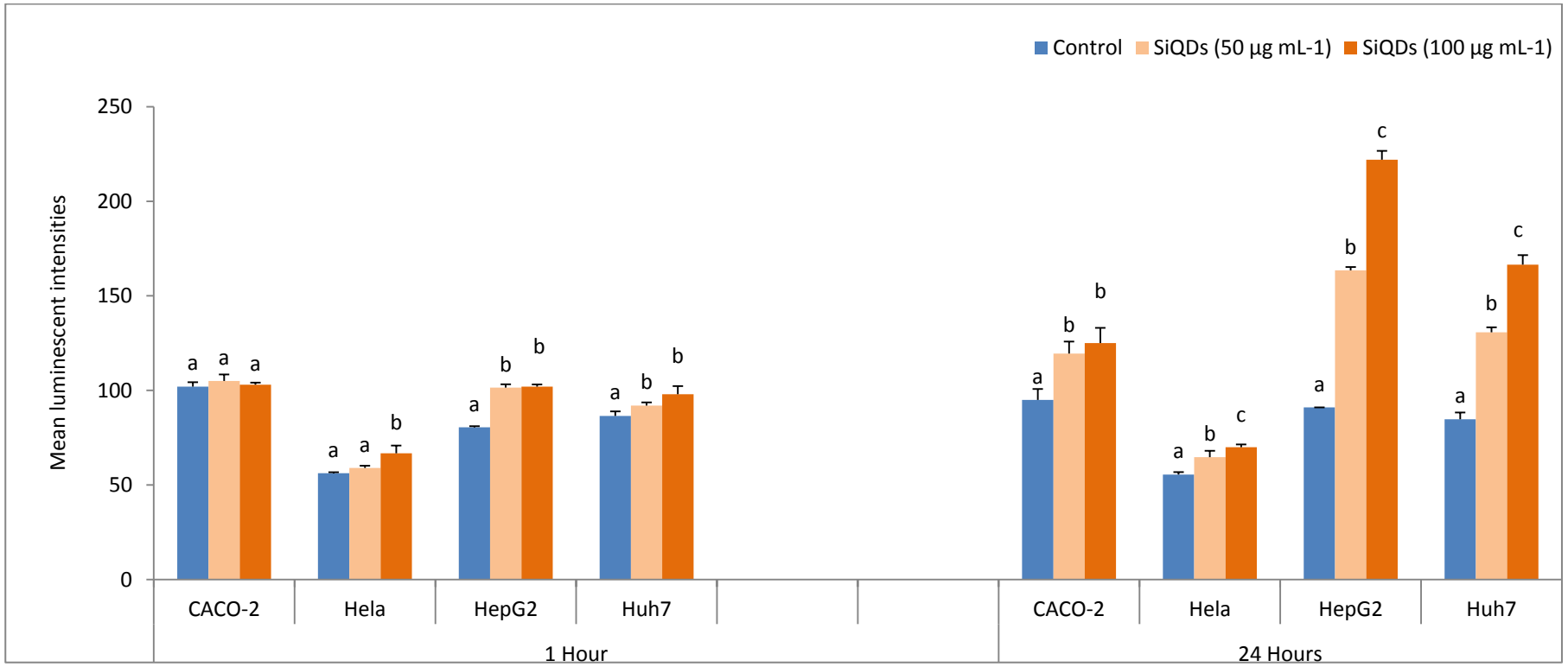

Figure 6. 1 Luminescent intensities measured using flow cytometry (excitation 355 nm and recorded emission at 675 nm) for control cells (no SiQDs) and cells treated with 50 or 100 µg ml^{-1} SiQD for 1hour or 24 hours. Bars are means ± SD for n=3 experiments. Within each cell type and exposure time, bars with different superscript letters are significantly different (in response to SiQD concentration) at the P<0.05 or less. Data were analysed using ANOVA, with Tukey's post hoc test where appropriate to distinguish the effects of different SiQD concentrations.

6.3.2 Specific Gene Expression of Caveolin-Mediated Endocytosis, Caveolin 1 and Caveolin 2

The previous studies (section 6.3.1) using flow cytometry to quantify cellular internalisation of SiQDs showed that HepG2 and Huh7 had relatively high potential to internalise SiQDs with more limited transport into HeLa and CACO-2. To find out whether the differences could be explained by the specific gene expression of caveolin-mediated endocytosis pathway, caveolin1 and caveolin2 gene expression were determined in CACO-2, HeLa, HepG2, and Huh7 by qPCR using TaqMan assays. The control gene glyceraldehyde-3-phosphate dehydrogenase (GAPDH) was used to normalise the data. The tri-reagent extraction procedure produced a high yield and good quality of RNA based on absorbance. A summary RNA concentration and purity is showed in **Table 6.1**. The control GAPDH gene required 17 to 18 PCR cycles to reach the detection threshold in all 4 cell lines as shown in **Figure 6.2.** &**Table 6.2.,** but the number of cycles needed for the other genes to be detected was higher for the cDNA from all cell lines. The gene expression levels for caveolin 1 and 2 relative to control (GAPDH) are shown in **Table 6.3**. The highest expression of both caveolin1 and caveolin2 was detected in HeLa cells. Levels of both transcripts were extremely low ($<$ 0.1% of that in HeLa) in HepG2. For Huh7 and CACO-2, levels of caveolin2 were higher than caveolin1 and only slightly lower than the level of caveolin 2 in HeLa. A summary of all the data concerning caveolins is shown in **Table 6.4.**

Table 6. 1 RNA yields (ng mL^{-1}) extracted with Tri-reagent and RNA purity measured using Nanodrop (n=3 experiments).

RNA samples	Nanodrop	
	RNA concentration (ng mL^{-1})	RNA purity (Ration A260:A280) (1.8 to 2)
CACO-2	1022.5 - 3843.5	1.95 - 2
HeLa	1078.7 - 1555.5	1.95 - 1.98
HepG2	1247.1 - 2075.7	1.98 - 2
Huh7	1491.0 - 2024.0	1.99 - 2

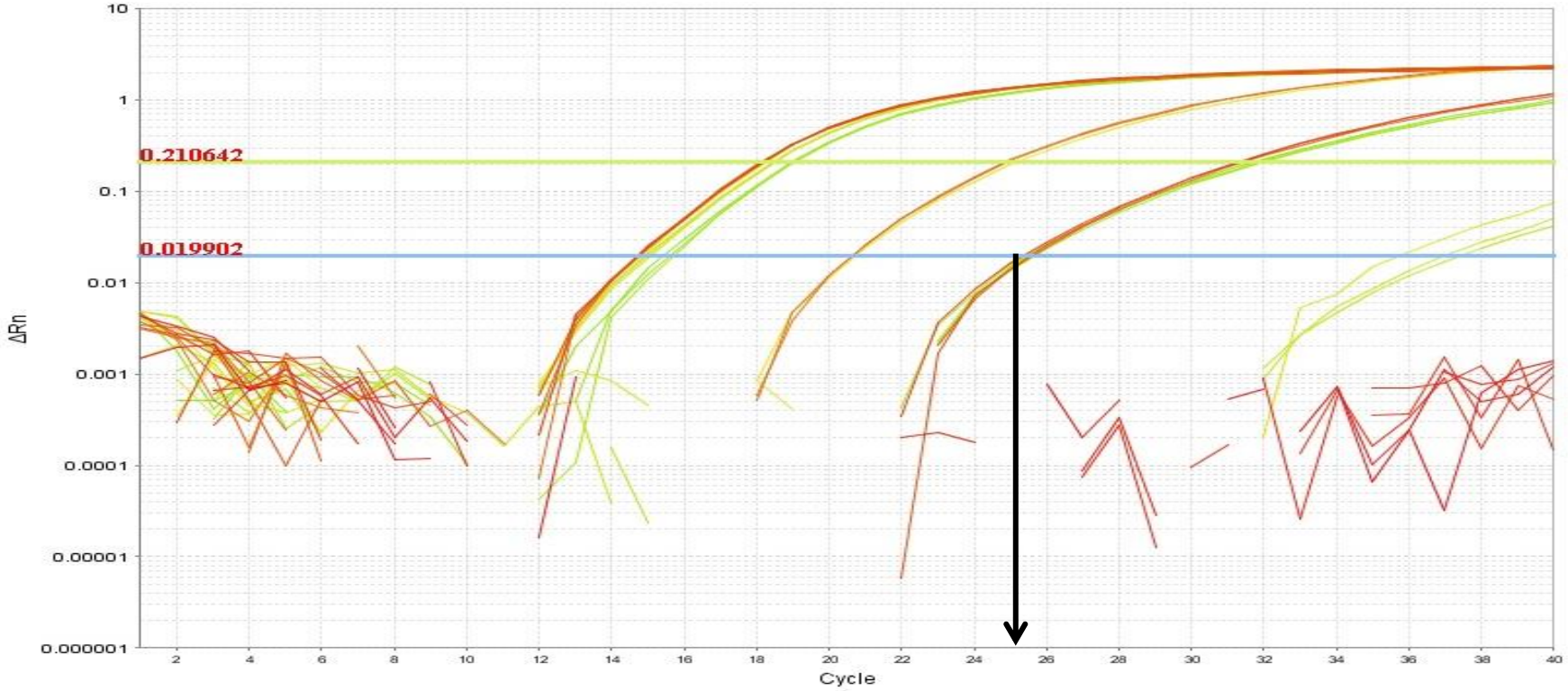

Figure 6. 2 The lines graphs show the PCR cycles of the reporter dyes. The point when the PCR cycles crossed the threshold is the threshold cycle (C_T). The C_T point in this graph is 25.05.

Table 6. 2 PCR cycles, the fluorescent signal crossed the threshold (amount of fluorescence emitting) of GAPDH, caveolin1, and caveolin2 in CACO-2 and HeLa (n=3 experiments).

Cell lines	Caveolin1 C_T(CAV1)	GAPDH C_T(G1)	ΔC_T (CAV-1) (AvgCAV-1-G1)	CAV-1 relative to G1 ($2^{-\Delta CT}$)	Caveolin2 C_T(CAV-2)	GAPDH C_T(G2)	ΔC_T (CAV-2) (AvgCAV-2-G2)	CAV-2 relative to G2 ($2^{-\Delta CT}$)
CACO-2(Mean)	27.03±0.06	17.51±0.02	9.52±0.05	0.001366	23.99±0.07	17.55±0.03	6.44±0.04	0.011536
HeLa(Mean)	21.15±0.08	17.24±0.04	3.91±0.04	0.066771	22.32±0.06	17.33±0.02	4.99±0.05	0.031535
HepG2(Mean)	35.69±0.31	17.65±0.02	18.04±0.29	0.0000037	34.89±0.43	17.66±0.03	17.23±0.40	0.0000065
Huh7(Mean)	25.92±0.05	17.77±0.02	8.15±0.03	0.003521	24.33±0.17	17.81±0.02	6.52±0.14	0.010867

Table 6. 3 Caveolin1 and caveolin2 expression values compared with the control gene (GAPDH) in CACO-2, HeLa, HepG2, and Huh7 (n=3 experiments).

Cell Lines	Gene expression relative to control (GAPDH)($2^{-\Delta CT}$ x1000)	
	Caveolin1	Caveolin2
CACO-2	1.37	11.54
HeLa	66.77	31.54
HepG2	0.004	0.007
Huh7	3.52	10.87

Table 6. 4 Summary of caveolin1 and caveolin2 expression in the four different cell lines.

Cell lines	Caveolin1	Caveolin2	Dots uptake
HeLa	High	High	Low/Medium
Huh7	Medium	Medium	Medium
HepG2	Very low	Very low	High
CACO-2	Low	Medium	Low

6.3.3 Endocytosis Inhibitors Optimal Concentration

The effect of various concentrations of well-known endocytosis inhibitors was characterised in selected cells to find out the optimal concentration for further studies. The chosen compounds were filipin, methyl-β-cyclodextrin (MβCD), and chlorpromazine. Filipin and MβCD are expected to affect caveolin-mediated endocytosis. Chlorpromazine is believed to affect clathrin-mediated endocytosis (Ivanov, 2008). The optimal concentration to be used is the maximum concentration of the chemical at which the cell still shows normal cell morphology and survives throughout the incubation time or periods of interest. As HeLa and Huh7 both showed relatively high levels of caveolin expression, they were chosen for these studies. MβCD and chlorpromazine are potent inhibitors of the endocytosis process but Vercauteren and colleagues (Vercauteren et al., 2010) found that relatively low concentrations of these inhibitors can also cause cytotoxic effects (Vercauteren et al., 2010). HeLa and Huh7 were therefore treated with chlorpromazine at doses of 2, 10, 20 and 30 μM and MβCD doses of 2, 4, 6, 8, and 10 mM with the cells continuously exposed to these concentrations for 24 hours.

After 24 hours, MβCD has no detectable adverse effects on HeLa and Huh7 morphology when the concentration was lower than 2 mM. However, at higher concentrations (2 mM and above), MβCD caused HeLa and Huh7 to detach from the flask and few of the cells survived. Images of HeLa and Huh7 treated with MβCD at a high concentration (10 mM) are shown in **Appendix 6.1-6.2.**

Chlorpromazine did not cause HeLa and Huh7 to detach from the flask but it changed cellular morphology with cells no longer elongating. Instead they showed circular cell morphology. Nevertheless, the chlorpromazine-treated cells still reached high confluence and attached to the flask throughout the studied period, albeit with the morphology changed compared with the control cells. The cells which had been treated with low or high concentrations of chlorpromazine showed the same morphology. All treated cells showed similar morphological changes as shown in **Appendix 6.3-6.4**.

Additionally HeLa and Huh7 were treated with filipin (8 μM) for 1 hour. The protocol of filipin treatment was slightly different from chlorpromazine & MβCD because filipin is a cholesterol binder. The cells were washed with PBS for 3

times to eliminate residual filipin before started to treat the cells with SiQDs. This concentration also caused all HeLa and Huh7 cells to detach from the flask (no images). However, this effect was not seen at filipin concentrations lower than 8 μM (no images).

6.3.4 Endocytosis Inhibition Studies of SiQDs internalisation into HeLa and Huh7

Investigations on the clathrin-mediated endocytosis mechanism of SiQDs in HeLa and Huh7 were carried out by pre-treatment with chlorpromazine at a concentration of 30 μM, MβCD at 1 mM and filipin at 0.8 and 3 μM. After pre-treatment of the cells with endocytosis inhibitors for 1 hour, the cells were treated with SiQDs for 24 hours with constant amount of the endocytosis inhibitors chlorpromazine and MβCD. The protocol was slightly different in filipin-treated cells. The 1 hour filipin-treated cells were washed to eliminate the excess filipin outside the cells before incubation of the cells with SiQDs for another 24 hours. The effects of endocytosis inhibitors on the internalisation of SiQDs were measured as luminescent intensities using flow cytometry to quantify the accumulation of SiQDs inside the cells. The internalisation of SiQDs by the cells was evaluated by comparison with the control groups. The cell luminescent intensities data (mean ± SD) is shown in **Table 6.5.** With values corrected for baseline fluorescence summarised in **Table 6.6**.

Filipin treatment at two different concentrations (0.8 uM and 3 uM) did not affect accumulation of SiQDs in either cell line. MβCD at concentration 1 mM showed a statistically significant internalisation inhibition effect on Huh7 but not on HeLa. Due to the effects of chlorpromazine on cell morphology even at low concentrations, it was not possible to obtain reliable data but it appeared that for HuH7 cells, chlorpromazine treatment resulted in an apparently increased accumulation of SiQDs though this was not statistically significant. It is possible that the increased accumulation of SiQDs could be non-specific due to the chlorpromazine damaging membranes making the cell "leaky". There was no apparent effect of this treatment in HeLa cells.

Table 6. 5 Fluorecent intensities inside HeLa and Huh7 measured using flow cytometry with excitation wavelength 355 nm and recorded emission at wavelength 675 nm (means ± SD for n=3 experiments).

Treatment/Cells	HeLa	Huh7
Control (Ether)	75.50±1.73	111.50±2089
SiQDs 100 µg mL^{-1}	93.75±2.75	206.25±3.10
Filipin 0.8 µM (Ether)	75.75±2.63	118.50±3.79
SiQDs 100 µg mL^{-1} & Filipin 0.8 µM	96.00±5.48	207.50±9.75
Control (Ether)	52.00±3.46	115.50±2.89
SiQDs 100 µg mL^{-1}	112.75±4.65	196.00±13.24
Filipin 3 µM (Ether)	76.25±6.85	122.25±2.22
SiQDs 100 µg mL^{-1} & Filipin 3 µM	131.50±2.38	197.25±2.06
Control (Ether)	77.25±3.30	108.00±3.37
SiQDs 100 µg mL^{-1}	94.00±5.03	137.25±1.71
Chlorpromazine(CP) 30 µM (Ether)	105.75±2.22	153.25±14.38
SiQDs 100 µg mL^{-1} & CP 30 µM	121.50±2.52	201.75±26.61
Control (Ether)	72.75±5.74	105.00±1.83
SiQDs 100 µg mL^{-1}	89.75±2.22	140.75±3.95
Methyl-β-cyclodextrin (MβCD) 1.0 mM (Ether)	71.00±2.16	146.50±7.50
SiQDs 100 µg mL^{-1} & MβCD 1.0 mM	102.75±20.66	130.75±6.18

Table 6. 6 Fluorescent intensities accumulations inside HeLa, and Huh7 which had been treated with endocytosis inhibitors followed by SiQDs and the control cells (no inhibitors) (means ± SD for n=3 experiments).

Fluorescent intensities	**HeLa**	**Huh7**
SiQDs 100 µg mL^{-1}	18.25±3.69	94.75±4.79
SiQDs 100 µg mL^{-1} & Filipin 0.8 µM	20.25±4.57	89.00±11.92
SiQDs 100 µg mL^{-1}	60.75±4.86	80.50±14.62
SiQDs 100 µg mL^{-1} & Filipin 3 µM	55.25±7.81	75.00±3.46
SiQDs 100 µg mL^{-1}	17.00±7.48	35.75±3.30
SiQDs 100 µg mL^{-1} & MβCD 1.0 mM	31.75±20.43	15.75*±11.09
SiQDs 100 µg mL^{-1}	16.75±5.62	29.25±2.06
SiQDs 100 µg mL^{-1} & CP 30 µM	15.75±3.95	48.50±25.68

*significant *P≤0.05*

6.4 Discussion

Previous studies by Alsharif and colleagues (2009) showed that alkyl-capped silicon quantum dots (SiQDs) are internalised rapidly into human tumour delivered cells, show low cytotoxicity, and have bright luminescence. They are therefore promising alternative probes to the standard cadmium selenide quantum dots for studying cellular processing to observe and monitor changes in living specimens. They also found that characterisation of internalisation to specify pathways with establishing endocytosis inhibitor filipin (a cholesterol binging dye), cytoclalasin B (microfilament disturbing), and actinomycin D (motility effected) had effects on accumulation of SiQDs in HeLa (high evident SiQDs internalisations) by decreasing the evidence of internalisation of SiQDs into the cells detected by laser confocal microscope (Alsharif et al., 2009).

The current experiments have confirmed that HeLa cells can accumulate SiQDs. Slightly unexpectedly, two other tumour cell lines HepG2 and HuH7 showed significantly higher levels of accumulation compared with HeLa but a fourth cell line CACO-2 showed levels similar to HeLa. HepG2 and HuH7 were both derived originally from liver tumours but why these cells should accumulate SiQDs more than HeLa (cervical tumour) or CACO-2 (colon tumour) is not clear. As the four cell lines are not structurally very different and the experiments were performed at similar cell densities, the differences in accumulation seen consistently suggest the update of SiQDs is specific. To assess whether the differences might be due to levels of expression of genes relevant to endocytosis, expression of caveolins was studied in the four cell lines. Studying caveolin expression using qPCR revealed that HeLa expressed caveolin1 at a high level and caveolin2 at a moderate level. Caveolin expression in the other cell lines was lower overall. In particular and in line with reports from others (Palozza et al., 2008, Gai et al., 2014), there was very low expression of both isoforms in HepG2 cells (Truong et al., 2010) . Huh7 and CACO-2 both showed much lower expression of caveolin1 than in HeLa though caveolin2 was higher than caveolin1 and almost as high as that seen in HeLa cells. These results are difficult to interpret in relation to the SiQDs data but in view of the very low caveolin levels in HepG2, it seems unlikely that expression of this protein is

making an important contribution to the high level of SiQD accumulation seen for this cell line.

Since caveolin, especially caveolin 2, was expressed in the other cell lines, it was decided to perform some inhibition experiments to assess the relevance of this protein to SiQD uptake in these cells. Two different caveolin inhibitors filipin and MβCD were used for these studies. Due to the similar levels of caveolin expression seen in HuH7 and CACO-2, it was decided to focus only on HuH7 and HeLa cells in the caveolin inhibition studies. Contrary to previous studies (Alsharif et al., 2009), filipin did not inhibit SiQDs accumulation in HeLa cells and there was no effect seen either for HuH7. The reason for the discrepancy between this work and the previous study is not clear but it could be due to use of flow cytometry and lower concentrations of inhibitors in the current study and confocal microscopy by Alsharif et al. (2009). SiQDs accumulation in HuH7 cells was inhibited specifically by MβCD (1 mM) but there was no effect in HeLa cells. This inhibitor works differently to filipin. Filipin functions via cholesterol binding and binds to 3β-hydroxysterol, a major component of glycolipid microdomains and caveolae of the plasma membrane (Nagasawa et al., 2014). MβCD inhibits caveolin-mediated endocytosis by extraction of cholesterol from plasma membrane (Nagasawa et al., 2014). The main difference between the two cell lines is the lower caveolin1 expression in HuH7. If endocytosis involving caveolin2 was affected more by MBCD than the process involving caveolin1, this could explain the current findings but whether this is a correct explanation is unclear.

The clathrin-mediated endocytosis inhibitor, chlorpromazine, acts on the plasma membrane to inhibit coated pit formation (Nagasawa et al., 2014) though as discussed in section 6.1, the precise mechanism for inhibition is still unclear. Because of the effect on chlorpromazine on cell morphology, the data obtained using this inhibitor needs to be treated with caution but there was no evidence for an inhibitory effect in either cell line. The toxic effects of chlorpromazine on both HuH7 and HeLa cells are surprising because the concentration used (5 uM) is slightly lower than the 5 ug mL^{-1} (14 uM) used recently to inhibit uptake of nanoparticles in both HuH7 and HepG2 cells (Liu et al., 2014) without any apparent adverse effects by the drug on cell morphology. It was not possible to study the effect of chlorpromazine on SiQD accumulation

in HepG2 cells due to time constraints but it is possible that a clear result might have been obtained if this had been done, especially since the accumulation of SiQDs in this cell line seems more likely to involve clathrin due to apparent absence of caveolin.

In summary the small (5-7.5 nm) strongly luminescent SiQDs were internalised by four different human cancer cell lines, CACO-2, HeLa, HepG2, and Huh7 on the basis of flow cytometry analysis. The highest levels of accumulation were seen with HepG2 and HuH7 cells. Some further evidence for a role for caveolin2 in this process in HuH7 was obtained. The reason why HepG2 cells showed the highest accumulation of SiQDs remains unclear as caveolin expression is very low. Further work on a possible role for clathrin in the endocytosis process in these cells including inhibition studies by chlorpromazine is needed.

Chapter 7 General Discussion

A true understanding of the mechanism of how alkyl-capped silicon quantum dots (SiQDs) are internalized by human cells could help in understanding more about the toxicity of quantum dots (QDs) in general. Moreover, internalization and safety evaluation profiles are vital in supporting an urgent need for increasing the application of QDs as fluorescent labelling and biological probes as well as their use in delivery of drugs and targeted treatments.

The current studies started with synthesis and quantification of SiQD's physicochemical properties using electrochemical etching technique and hydrosilation reaction, and characterization using absorption and emission spectroscopy, atomic force microscope, fluorescent microscope, and confocal and Raman microscopy (Lie et al., 2002, Dickinson et al., 2008, Alsharif et al., 2009). Previous studies had shown that these particles could accumulate in several cell lines including HeLa cells (Alsharif et al., 2009). The current study was particularly concerned with using a more relevant cell type CACO-2 cells to model oral exposure to SiQDs and showed that this cell line could also accumulate the particles. A more detailed analysis of possible toxicity in these cells was then performed. The factors associated with SiQDs physicochemical properties such as small size, high surface areas, and neutral surface charge may also be responsible for adverse biological effects (Singh et al., 2009). In the current study, SiQDs at concentration 50 μg mL-1 showed no adverse effects or any cell death in CACO-2 cells. Previous studies showed that neutral charged azide-terminated Si NPs (Si NP-N3) caused more cytotoxicity effects in CACO-2 and rat alveolar macrophage (NR8383) than negatively charged Si NP-COOH which showed no adverse effects using the MTT assay (Ruizendaal et al., 2009, Bhattacharjee et al., 2010, Bhattacharjee et al., 2013). Interference with cellular ATP production can lead to two main adverse effects, decreased cell viability as well as mitochondrial injury and some previous studies involving other types of nanoparticle showed this occurred (Xia et al., 2008b, Jensen et al., 2008, Imamura et al., 2009, Kolibab et al., 2012). However, the current study shows no harmful effects of SiQDs on ATP production in CACO-2 cells.

Oxidative stress is a well-documented mechanism for cellular damage induced by nanoparticles (Nel et al., 2006, Xia et al., 2006, Sayes et al., 2007). Consequently production of intracellular reactive oxygen species (ROS) may cause oxidative damage to lipids, proteins, and DNA (Thannickal and Fanburg,

2000). Owing to quantum confinement effects, small nanoparticles called QDs reveal discrete energy levels and have large energy gap (O'Farrell et al., 2006). As a result, QDs have the potential to absorb energy and generate fluorescence. Moreover, QDs and engineered nanoparticles (ENPs) also have a capacity to transfer energy to nearby oxygen molecules (the reduction and oxidation (redox) cycling) to form reactive singlet oxygen (1O2) species as well as generate ROS and oxidative stress. Cytotoxicity and oxidative stress induction by nanoparticles or ultrafine nanoparticles has been reported widely particularly in pulmonary base cells lines. Brown et al. (2001) reported that low toxicity ultrafine particles are able to generate reactive oxygen species (ROS) as much as some other environmental particles (ultrafine carbon black ,ufCB) (Brown et al., 2001, Wilson et al., 2002). The environmental particles or particulate matter (PM10) particles also have ability to cause cytotoxicity and oxidative stress which is thought to be relevant to inflammatory effects, DNA damage, and pathological changes (cancer) (Donaldson et al., 2003). The particles appear to generate oxidative stress in a murine macrophage cell line (RAW 264.7) and a human bronchial epithelial cell line (BEAS-2B) by induction of cellular heme oxygenase-1 (HO-1) expression and decreasing intracellular glutathione (Li et al., 2003, Xia et al., 2006). Apart from pulmonary cell lines, exposing CACO-2 cells to conventional low toxicity nanoparticles also caused oxidative stress detected by glutathione depletion (Gerloff et al., 2009). Interestingly pulmonary clearance of nanoparticles is an additional excretion route for nanoparticles reaching the gastrointestinal tract (Gerloff et al., 2009). The present study investigation oxidative stress by SiQDs, measuring ROS production and DNA damage using dichlorofluorescein diacetate (DCFH-DA assay) and Comet assay. SiQDs treated CACO-2 cells showed no induced ROS production even with exposure for 14 days. Also there was no DNA damage generated by high concentration of SiQDs up to 200 μg mL^{-1}. The finding that Si NPs show no generation of oxidative stress and DNA damage was also confirmed by others using DCFH-DA and Comet assays in non-phagocytic and phagocytic cells (Wang et al., 2012, Bhattacharjee et al., 2013).

Once it had been shown that, similar to the previous studies with HeLa cells (Alsharif et al., 2009), SiQDs were also nontoxic in CaCO2 cells, it was decided to undertake studies using two additional cell lines from human liver as well as

further studies on SiQD uptake by CaCO2 and HeLa cells. This study showed that even though all four cell lines studied were derived from human tumours, their ability to accumulate SiQDs varied. The lowest accumulation was seen in HeLa cells with the amount seen in CaCO2 slightly higher. However, both of the cell lines from the liver, HepG2 and HuH7, showed more accumulation. For this reason, it would have been better if more time had been available to have also done the toxicity investigations on one or both of these cell lines. There appear to have been no previous studies by others on toxicity of SiQD in either of these liver cell lines.

Alsharif et al (2009) proposed that the SiQD internalization process involves pinocytosis and showed cholesterol-dependent effects by endocytosis inhibitors but all the studies involved HeLa cells. Profiles and knowledge of cellular NPs internalization mechanisms are important for further investigations and are fundamental for drug localization (e.g. contrast agents) and treatment applications (drug delivery) (Tansil and Gao, 2006, Coti et al., 2009, Elsaesser et al., 2010, Fischer et al., 2010, Iversen et al., 2011, Canton and Battaglia, 2012). The current study aimed to find out more about SiQD accumulation inside four different cell lines including HeLa. The results were slightly unexpected but showed big differences in expression of caveolin 1 and 2 between all four cell lines. The role for caveolin 1 in HeLa pinocytosis suggested by Alsharif et al. (2009) could not be confirmed and generally the inhibition studies were unsuccessful in increasing our understanding of the endocytosis process.

Further studies are needed on endocytosis since the data obtained from pharmacological endocytosis inhibitor experiments did not prove to be conclusive. It is difficult to obtain specific information on the mechanism of endocytosis by the types of experiment using chemical inhibitors that were performed. In order to improve the specificity of the experiment, it would be necessary to use higher resolution imaging (with for example confocal fluorescence) to investigate time-dependent localization of the SiQDs as they enter and move within the cells.

Based on the current findings, SiQDs have been found to show little or no acute toxicity *in vitro*. However, in order to show that SiQDs can have uses *in vivo*,

much more information is required than can be obtained simply by *in vitro* toxicology studies. Very little is known about the possible effect of SiQDs on the immune/inflammatory response, including effects on cytokines. More complete studies are needed.

In vivo there is some evidence that SiQDs and porous silicon are cleared from mice by renal excretion as silicate eventually (Park et al., 2009). There is also evidence from the same study that SiQDs can cause some histopathological changes in the liver soon after administration but after 4 weeks morphology is normal. However, overall the extent of information on the toxicity of SiQDs *in vivo* remains very sparse and it is quite likely that the surface chemistry of the SiQDs could have a large effect on their eventual fate in the body because the chemistry is already well-known to affect their stability to air and water. Further studies using additional animal species and longer term follow-up are needed.

Summary of achievements

•A low cost and practical technique, electrochemical (etching) has been used to produce monodisperse small particles of alkyl capped silicon quantum dots (SiQDs).

•The SiQDs in the size range 5 -7.5 nm (mean diameter 5 nm, Si core 2.5 nm) show strong quantum confinement effects with intense orange fluorescence ~620 nm which corresponds to double the bulk band gap of 1.1 eV.

•A uniform and successful dosing protocol was established in order to visualise fluorescence SiQDs and enable cytotoxicity evaluations in various human cell lines (CACO-2, HeLa, Huh7, and HepG2).

•The consistent protocol and low background fluorescence enabled visualisation of the fluorescence of SiQDs in CACO-2 using epi-fluorescent and confocal microscopy.

•Successful protocols for studying the interaction of SiQDs with CACO-2 for acute and chronic cytotoxicity studies were achieved using various cytotoxicity evaluation endpoints including cell viability, cell metabolism, oxidative stress

intermediated measurement, and the effects of oxidative stress and SiQDs on human cell DNA (MTT assay, ATP, ROS measurements, and Comet assay).

•SiQDs did not produce any cytotoxicity effects on the human cell line (CACO-2) (a model for the main route of exposure of nanoparticles by the oral route) in acute and subchronic studies.

•The strong fluorescence of SiQDs in the red regions of the visible spectrum (low cell florescent background) facilitates confirmation of SiQD internalisation by various human cell lines (CACO-2, HeLa, Huh7, and HepG2) using the confocal microscope as well as laser-fluorescence flow cytometry.

•A RT-PCR Taqman-based gene expression assay was employed to study caveolin expression including caveolin1 and caveolin2 in several cell lines (CACO-2, HeLa, Huh7, and HepG2). The levels detected were in line with previous reports in the literature including apparent absence of caveolin in HepG2.

•The mechanism of internalisation of SiQDs in selected cells (HeLa and Huh7) was probed by observing the effect of inhibitors of known aspects of endocytosis.

•Filipin and MβCD inhibited the internalisation of SiQDs in the following cell lines (HeLa and Huh7). However, even at low doses both filipin and MβCD themselves showed some toxic effects and the conclusion that SiQDs uptake is cholesterol-dependent must be regarded as preliminary. Chlorpromazine did not inhibit uptake and was also cytotoxic. Of the three inhibitors, filipin showed the lowest cytotoxicity.

Future work

•Because the selected endocytosis inhibitors (filipin, CP, and MβCD) showed cytotoxic effects, other agents ought to be studied, e.g. 2,4-dinitrophenol (2,4-DNP) which is an inhibitor of energy (ATP) dependent pathways and inhibits ATP production.

•It would also be of interest to extend the number of cell lines to further evaluate the relationship between caveolin expression and SiQD uptake. True phagocytic macrophages would also be interesting to study as their uptake of SiQDs is likely rather different. Primary hepatocytes are another cell type of interest in view of the findings on the liver tumour cell lines HepG2 and HuH7.

•In vivo studies of the pharmacokinetics and the ultimate fate of SiQDs in the whole body will be important before any use of SiQDs in medical applications. Some work of this type has been performed by others (Park et al., 2009) and indicates SiQDs are metabolised to silicate and excreted.

Appendices

Appendix 5. 1 Adenosine 5'-triphosphate (ATP) bioluminescent somatic cell assay kit (Catalogue Number FLASC), Sigma-Aldrich.

1. Principles

Reaction 1: Intracellular ATP $\longrightarrow$ Free ATP

Reaction 2: ATP + Luciferin $\underset{Mg^{2+}}{\overset{\text{Firefly Luciferase}}{\rightleftharpoons}}$ Free ATP

Reaction 3: Intracellular ATP + O_2 $\longrightarrow$ Oxyluciferin + AMP + CO_2 + Light

2. Reagents

2.1 ATP Assay Mix (Catalogue Number FLAAM) 1 vial (lyophilized powder) contains luciferase, luciferin, $MgSO_4$, DTT, EDTA, bovine derum albumin (BSA), and tricine buffer salts. The vial must be mixed with 5 mL of ultrapure water before use, Sigma-Aldrich.

2.2 ATP Assay Mix Dilution Buffer (Catalogue Number FLAAB) 1 vial (lyophilized powder) contains $MgSO_4$, DTT, EDTA, BSA, and tricine buffer salts. The vial must be mixed with 50 mL of ultrapure water before use, Sigma-Aldrich.

2.3 Somatic Cell ATP Releasing Reagent (Catalogue Number FLSAR) 1 vial (10x concentrate). Cellular ATP is released almost immediately which increase membrane permeability to many small molecules, Sigma-Aldrich. The vial must be diluted 10-fold with ultrapure water before use, Sigma-Aldrich.

2.4 ATP Standard (Catalogue Number FLAAS) 1 vial (lyophilized powder) contains ATP and disodium salt hydrate (1 mg). The vial must be mixed with 10 mL of ultrapure water before use (2.0×10^{-6} mole), Sigma-Aldrich.

3. Procedures

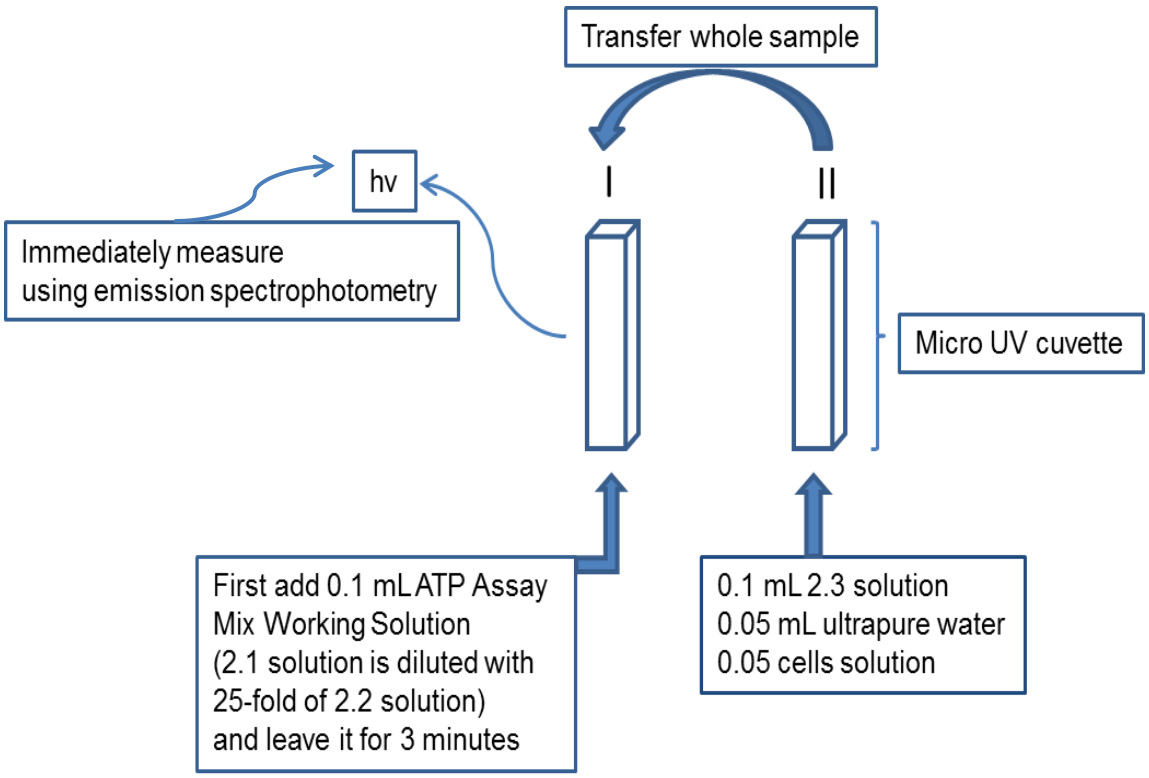

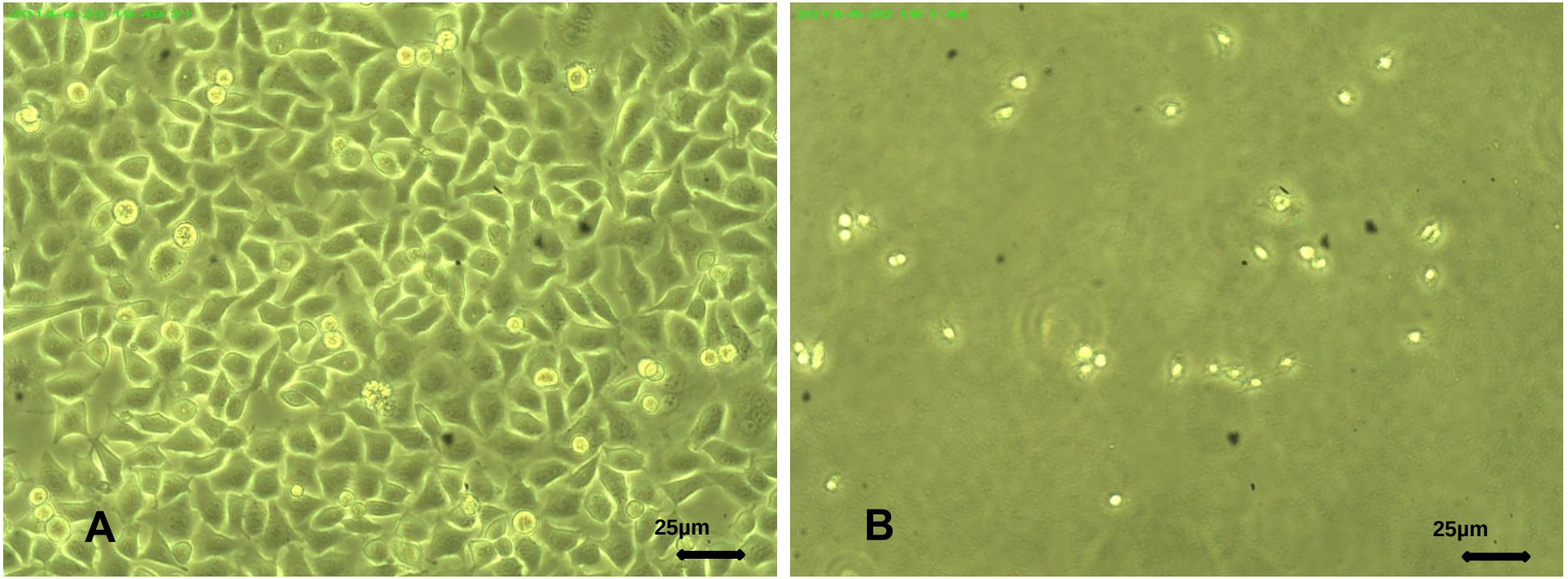

Appendix 6. 1 Phase contrast microscope (OPTIKA) with ScopeImage DynamicPro (BUC2-500C) captured on HeLa (200 x magnification), the cells density at the beginning was 1.5 x 10^5 cells mL^{-1}. Image **A** the cells were treated with appropriate medium for 24 hours as a control cells. Image **B** the cells were treated with Methyl-β-cyclodextrin (MβCD) at a concentration of 10 mM for 24 hours.

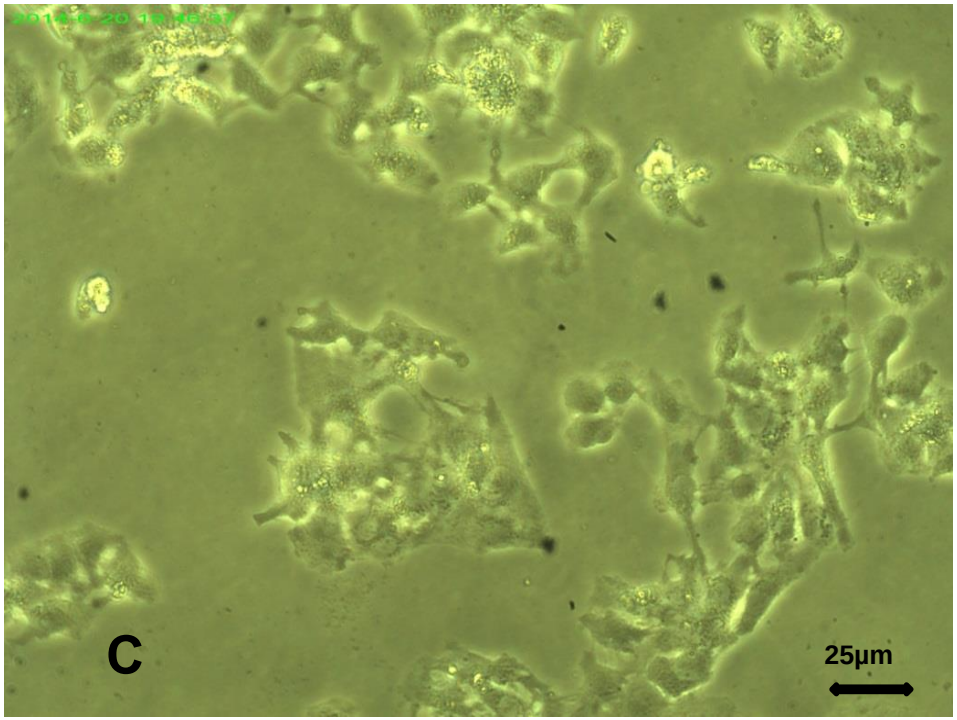

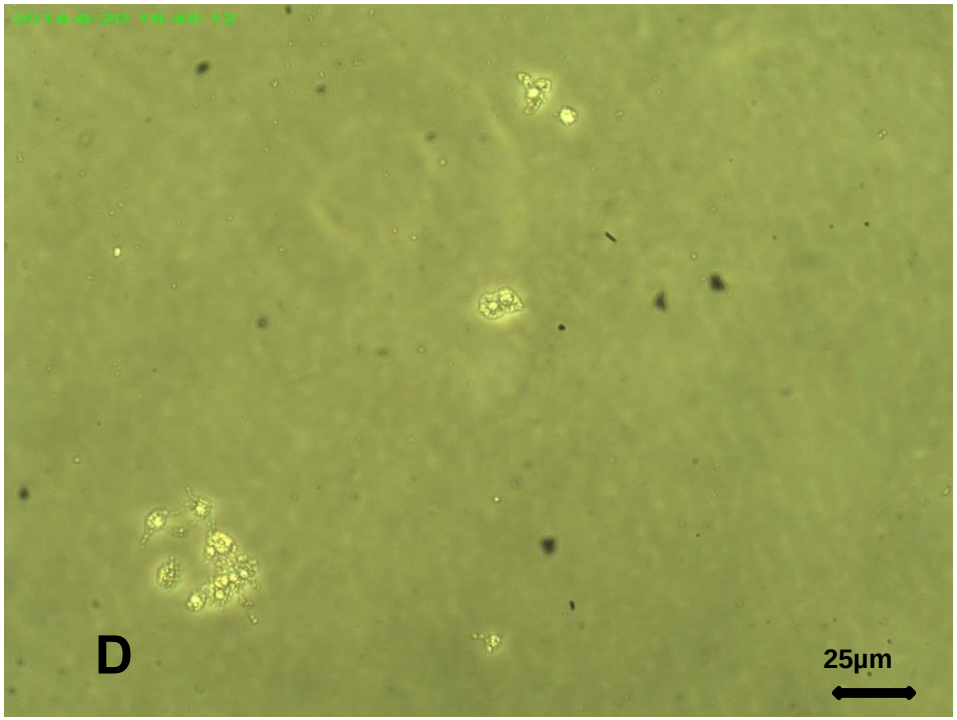

Appendix 6. 2 Phase contrast microscope (OPTIKA) with ScopeImage DynamicPro (BUC2-500C) captured on Huh7 (200 x magnification), the cells density at the beginning was 1.5 x 10^5 cells mL^{-1}. Image **C** the cells were treated with appropriate medium for 24 hours as a control cells. Image **D** the cells were treated with Methyl-β-cyclodextrin (MβCD) at a concentration of 10 mM for 24 hours.

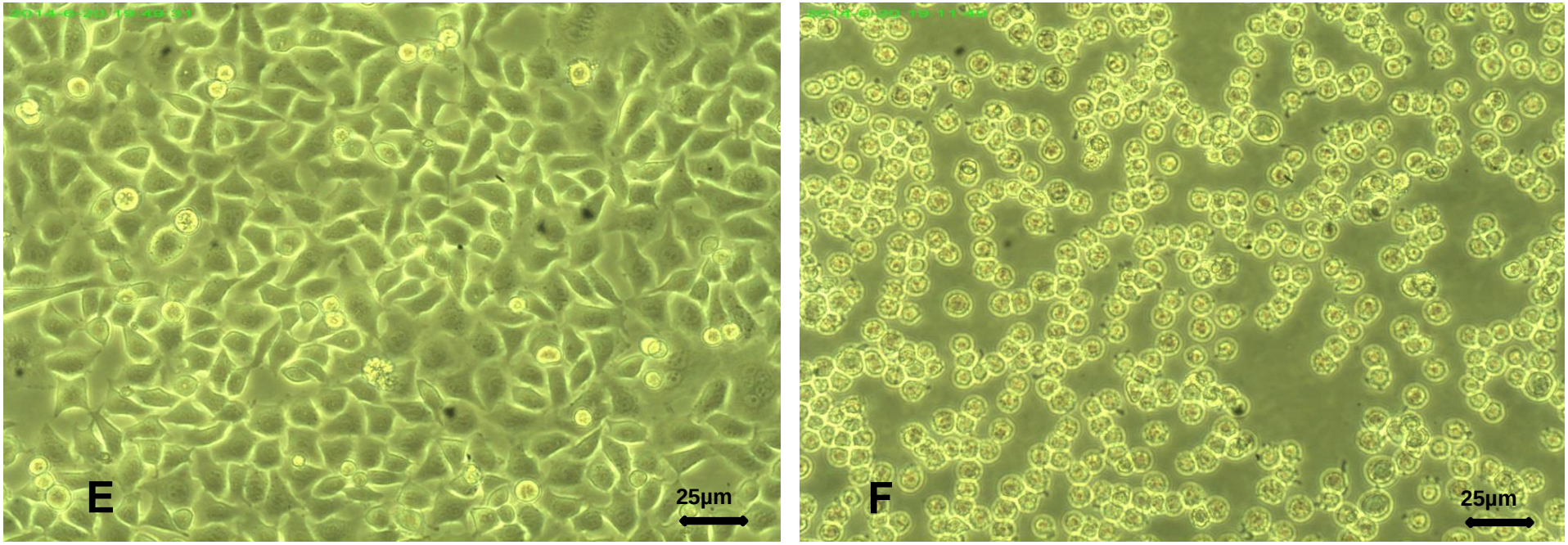

Appendix 6. 3 Phase contrast microscope (OPTIKA) with ScopeImage DynamicPro (BUC2-500C) captured on HeLa (200 x magnification), the cells density at the beginning was 1.5 x 10^5 cells mL^{-1}. Image **E** the cells were treated with appropriate medium for 24 hours as a control cells. Image **F** the cells were treated with chlorpromazine at a concentration of 2 µM for 24 hours.

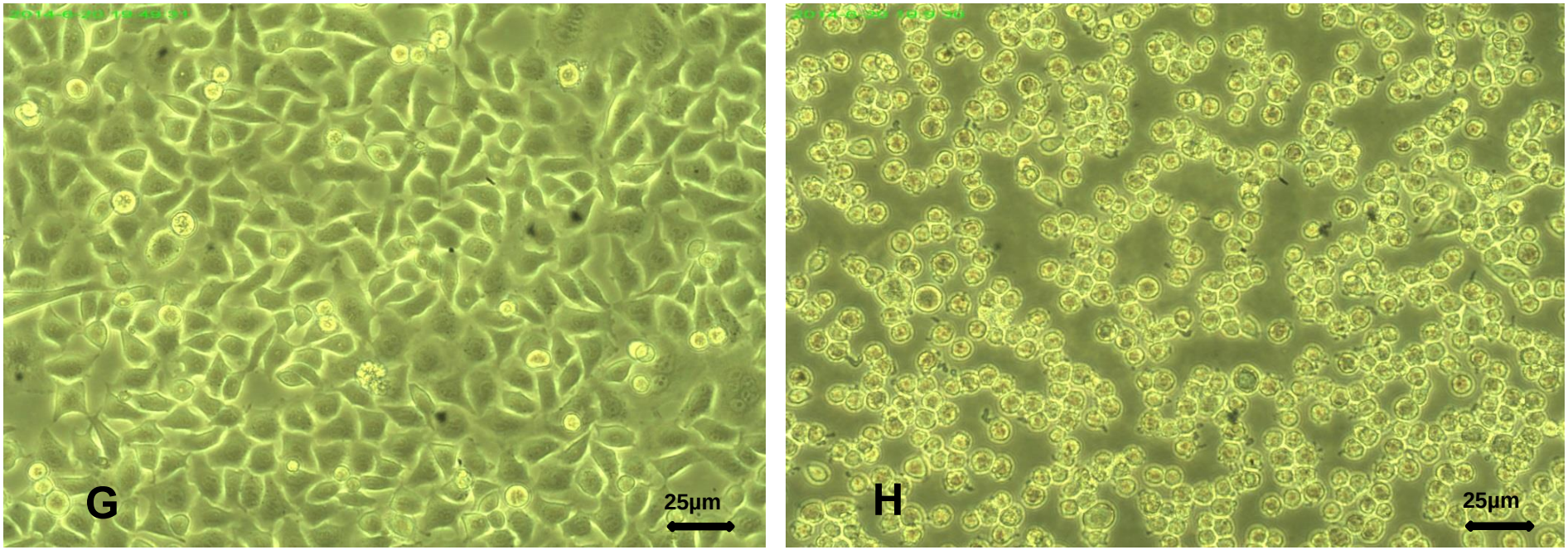

Appendix 6. 4 Phase contrast microscope (OPTIKA) with ScopeImage DynamicPro (BUC2-500C) captured on HeLa (200 x magnification), the cells density at the beginning was 1.5 x 10^5 cells mL^{-1}. Image **G** the cells were treated with appropriate medium for 24 hours as a control cells. Image **H** the cells were treated with chlorpromazine at a concentration of 10 µM for 24 hours.

References

//IMAGEJ.NIH.GOV/IJ/, H.

AHIRE, J. H., WANG, Q., COXON, P. R., MALHOTRA, G., BRYDSON, R., CHEN, R. & CHAO, Y. 2012. Highly Luminescent and Nontoxic Amine-Capped Nanoparticles from Porous Silicon: Synthesis and Their Use in Biomedical Imaging. *Acs Applied Materials & Interfaces,* 4**,** 3285-3292.

ALIVISATOS, A. P. 1996. Semiconductor clusters, nanocrystals, and quantum dots. *Science,* 271**,** 933-937.

ALIVISATOS, A. P., GU, WEIWEI, LARABELL, CAROLYN 2005. Quantum dots as cellular probes. *Annual Review of Biomedical Engineering,* 7**,** 55-76.

ALSHARIF, N. H., BERGER, C. E. M., VARANASI, S. S., CHAO, Y., HORROCKS, B. R. & DATTA, H. K. 2009. Alkyl-Capped Silicon Nanocrystals Lack Cytotoxicity and have Enhanced Intracellular Accumulation in Malignant Cells via Cholesterol-Dependent Endocytosis. *Small,* 5**,** 221-228.

BATEMAN, J. E., EAGLING, R. D., WORRALL, D. R., HORROCKS, B. R. & HOULTON, A. 1998. Alkylation of porous silicon by direct reaction with alkenes and alkynes. *Angewandte Chemie-International Edition,* 37**,** 2683-2685.

BERNAS, T. & DOBRUCKI, J. 2002. Mitochondrial and nonmitochondrial reduction of MTT: interaction of MTT with TMRE, JC-1, and NAO mitochondrial fluorescent probes. *Cytometry,* 47**,** 236-42.

BERRIDGE, M. V., HERST, P. M. & TAN, A. S. 2005. Tetrazolium dyes as tools in cell biology: new insights into their cellular reduction. *Biotechnology annual review,* 11**,** 127-52.

BHATTACHARJEE, S., DE HAAN, L. H. J., EVERS, N. M., JIANG, X., MARCELIS, A. T. M., ZUILHOF, H., RIETJENS, I. M. C. M. & ALINK, G. M. 2010. Role of surface charge and oxidative stress in cytotoxicity of organic monolayer-coated silicon nanoparticles towards macrophage NR8383 cells. *Particle and Fibre Toxicology,* 7**,** 1-12.

BHATTACHARJEE, S., RIETJENS, I. M. C. M., SINGH, M. P., ATKINS, T. M., PURKAIT, T. K., XU, Z., REGLI, S., SHUKALIAK, A., CLARK, R. J., MITCHELL, B. S., ALINK, G. M., MARCELIS, A. T. M., FINK, M. J., VEINOT, J. G. C., KAUZLARICH, S. M. & ZUILHOF, H. 2013. Cytotoxicity of surface-functionalized silicon and germanium nanoparticles: the dominant role of surface charges. *Nanoscale,* 5**,** 4870-4883.

BLEY, R. A., KAUZLARICH, S. M., DAVIS, J. E. & LEE, H. W. H. 1996. Characterization of silicon nanoparticles prepared from porous silicon. *Chemistry of Materials,* 8**,** 1881-1888.

BORSELLA, E., D'AMATO, R., FALCONIERI, M., TRAVE, E., PANARITI, A. & RIVOLTA, I. 2013. An outlook on the potential of Si nanocrystals as luminescent probes for bioimaging. *Journal of Materials Research,* 28**,** 193-204.

BOTTI, S., TERRANOVA, M. L., SESSA, V., PICCIRILLO, S. & ROSSI, M. 2001. Silicon quantum dots in diamond matrix: a new synthesis route. *Applied Organometallic Chemistry,* 15**,** 388-392.

BROWN, D. M., WILSON, M. R., MACNEE, W., STONE, V. & DONALDSON, K. 2001. Size-dependent proinflammatory effects of ultrafine polystyrene particles: A role for surface area and oxidative stress in the enhanced activity of ultrafines. *Toxicology and Applied Pharmacology,* 175**,** 191-199.

BRUCHEZ, M., MORONNE, M., GIN, P., WEISS, S. & ALIVISATOS, A. P. 1998. Semiconductor nanocrystals as fluorescent biological labels. *Science,* 281**,** 2013-2016.

BURIAK, J. M. 1999. Organometallic chemistry on silicon surfaces: formation of functional monolayers bound through Si-C bonds. *Chemical Communications***,** 1051-1060.

BURIAK, J. M., STEWART, M. P., GEDERS, T. W., ALLEN, M. J., CHOI, H. C., SMITH, J., RAFTERY, D. & CANHAM, L. T. 1999. Lewis acid mediated hydrosilylation on porous silicon surfaces. *Journal of the American Chemical Society,* 121**,** 11491-11502.

BUZEA, C., PACHECO, I. I. & ROBBIE, K. 2007. Nanomaterials and nanoparticles: Sources and toxicity. *Biointerphases,* 2**,** MR17-MR71.

CANHAM, L. 2000. Gaining light from silicon. *Nature,* 408**,** 411-412.

CANHAM, L. T. 1990. SILICON QUANTUM WIRE ARRAY FABRICATION BY ELECTROCHEMICAL AND CHEMICAL DISSOLUTION OF WAFERS. *Applied Physics Letters,* 57**,** 1046-1048.

CANTON, I. & BATTAGLIA, G. 2012. Endocytosis at the nanoscale. *Chemical Society Reviews,* 41**,** 2718-2739.

CHAN, W. C. W., MAXWELL, D. J., GAO, X. H., BAILEY, R. E., HAN, M. Y. & NIE, S. M. 2002. Luminescent quantum dots for multiplexed biological detection and imaging. *Current Opinion in Biotechnology,* 13**,** 40-46.

CHAN, W. C. W. & NIE, S. M. 1998. Quantum dot bioconjugates for ultrasensitive nonisotopic detection. *Science,* 281**,** 2016-2018.

CHAO, Y., SILLER, L., KRISHNAMURTHY, S., COXON, P. R., BANGERT, U., GASS, M., KJELDGAARD, L., PATOLEO, S. N., LIE, L. H., O'FARRELL, N., ALSOP, T. A., HOULTON, A. & HORROCKS, B. R. 2007. Evaporation and deposition of alkyl-capped silicon nanocrystals in ultrahigh vacuum. *Nature Nanotechnology,* 2**,** 486-489.

CHOI, B. H., HWANG, S. W., KIM, I. G., SHIN, H. C., KIM, Y. & KIM, E. K. 1998. Fabrication and room-temperature characterization of a silicon self-assembled quantum-dot transistor. *Applied Physics Letters,* 73**,** 3129-3131.

CHOI, J., ZHANG, Q., REIPA, V., WANG, N. S., STRATMEYER, M. E., HITCHINS, V. M. & GOERING, P. L. 2009. Comparison of cytotoxic and inflammatory responses of photoluminescent silicon nanoparticles with silicon micron-sized particles in RAW 264.7 macrophages. *Journal of Applied Toxicology,* 29**,** 52-60.

CIAPETTI, G., CENNI, E., PRATELLI, L. & PIZZOFERRATO, A. 1993. INVITRO EVALUATION OF CELL BIOMATERIAL INTERACTION BY MTT ASSAY. *Biomaterials,* 14**,** 359-364.

CLIFT, M. J. D., BOYLES, M. S. P., BROWN, D. M. & STONE, V. 2010. An investigation into the potential for different surface-coated quantum dots to cause oxidative stress and affect macrophage cell signalling in vitro. *Nanotoxicology,* 4**,** 139-149.

COHEN, A. W., HNASKO, R., SCHUBERT, W. & LISANTI, M. P. 2004. Role of caveolae and caveolins in health and disease. *Physiological Reviews,* 84**,** 1341-1379.

CONNER, S. D. & SCHMID, S. L. 2003. Regulated portals of entry into the cell. *Nature,* 422**,** 37-44.

COTI, K. K., BELOWICH, M. E., LIONG, M., AMBROGIO, M. W., LAU, Y. A., KHATIB, H. A., ZINK, J. I., KHASHAB, N. M. & STODDART, J. F. 2009. Mechanised nanoparticles for drug delivery. *Nanoscale,* 1**,** 16-39.

DABBOUSI, B. O., RODRIGUEZVIEJO, J., MIKULEC, F. V., HEINE, J. R., MATTOUSSI, H., OBER, R., JENSEN, K. F. & BAWENDI, M. G. 1997. (CdSe)ZnS core-shell quantum dots: Synthesis and characterization of a size series of highly luminescent nanocrystallites. *Journal of Physical Chemistry B,* 101**,** 9463-9475.

DANIEL, J. A., CHAU, N., ABDEL-HAMID, M. K., HU, L., VON KLEIST, L., WHITING, A., KRISHNAN, S., MAAMARY, P., JOSEPH, S. R., SIMPSON, F., HAUCKE, V., MCCLUSKEY, A. & ROBINSON, P. J. 2015. Phenothiazine-derived antipsychotic drugs inhibit dynamin and clathrin-mediated endocytosis. *Traffic,* 16**,** 635-54.

DERFUS, A. M., CHAN, W. C. W. & BHATIA, S. N. 2004. Probing the cytotoxicity of semiconductor quantum dots. *Nano Letters,* 4**,** 11-18.

DICKINSON, F. M., ALSOP, T. A., AL-SHARIF, N., BERGER, C. E. M., DATTA, H. K., SILLER, L., CHAO, Y., TUITE, E. M., HOULTON, A. & HORROCKS, B. R. 2008. Dispersions of alkyl-capped silicon nanocrystals in aqueous media: photoluminescence and ageing. *Analyst,* 133**,** 1573-1580.

DINH, L. N., CHASE, L. L., BALOOCH, M., SIEKHAUS, W. J. & WOOTEN, F. 1996. Optical properties of passivated Si nanocrystals and SiOx nanostructures. *Physical Review B,* 54**,** 5029-5037.

DOAK, S. H., MANSHIAN, B., JENKINS, G. J. S. & SINGH, N. 2012. In vitro genotoxicity testing strategy for nanomaterials and the adaptation of current

OECD guidelines. *Mutation Research-Genetic Toxicology and Environmental Mutagenesis,* 745**,** 104-111.

DOHERTY, G. J. & MCMAHON, H. T. 2009. Mechanisms of Endocytosis. *Annual Review of Biochemistry.*

DONALDSON, K., STONE, V., BORM, P. J. A., JIMENEZ, L. A., GILMOUR, P. S., SCHINS, R. P. F., KNAAPEN, A. M., RAHMAN, I., FAUX, S. P., BROWN, D. M. & MACNEE, W. 2003. Oxidative stress and calcium signaling in the adverse effects of environmental particles (PM10). *Free Radical Biology and Medicine,* 34**,** 1369-1382.

DUBERTRET, B., SKOURIDES, P., NORRIS, D. J., NOIREAUX, V., BRIVANLOU, A. H. & LIBCHABER, A. 2002. In vivo imaging of quantum dots encapsulated in phospholipid micelles. *Science,* 298**,** 1759-1762.

EASH, S., QUERBES, W. & ATWOOD, W. J. 2004. Infection of Vero cells by BK virus is dependent on Caveolae. *Journal of Virology,* 78**,** 11583-11590.

ELSAESSER, A. & HOWARD, C. V. 2012. Toxicology of nanoparticles. *Advanced Drug Delivery Reviews,* 64**,** 129-137.

ELSAESSER, A., TAYLOR, A., DE YANES, G. S., MCKERR, G., KIM, E.-M., O'HARE, E. & HOWARD, C. V. 2010. Quantification of nanoparticle uptake by cells using microscopical and analytical techniques. *Nanomedicine,* 5**,** 1447-1457.

EROGBOGBO, F., CHANG, C.-W., MAY, J., PRASAD, P. N. & SWIHART, M. T. 2012. Energy transfer from a dye donor to enhance the luminescence of silicon quantum dots. *Nanoscale,* 4**,** 5163-5168.

EROGBOGBO, F., TIEN, C.-A., CHANG, C.-W., YONG, K.-T., LAW, W.-C., DING, H., ROY, I., SWIHART, M. T. & PRASAD, P. N. 2011a. Bioconjugation of Luminescent Silicon Quantum Dots for Selective Uptake by Cancer Cells. *Bioconjugate Chemistry,* 22**,** 1081-1088.

EROGBOGBO, F., YONG, K.-T., HU, R., LAW, W.-C., DING, H., CHANG, C.-W., PRASAD, P. N. & SWIHART, M. T. 2010. Biocompatible Magnetofluorescent Probes: Luminescent Silicon Quantum Dots Coupled with Superparamagnetic Iron(III) Oxide. *Acs Nano,* 4**,** 5131-5138.

EROGBOGBO, F., YONG, K.-T., ROY, I., HU, R., LAW, W.-C., ZHAO, W., DING, H., WU, F., KUMAR, R., SWIHART, M. T. & PRASAD, P. N. 2011b. In Vivo Targeted Cancer Imaging, Sentinel Lymph Node Mapping and Multi-Channel Imaging with Biocompatible Silicon Nanocrystals. *Acs Nano,* 5**,** 413-423.

EROGBOGBO, F., YONG, K.-T., ROY, I., XU, G., PRASAD, P. N. & SWIHART, M. T. 2008. Biocompatible luminescent silicon quantum dots for imaging of cancer cells. *Acs Nano,* 2**,** 873-878.

FERRARI, M., FORNASIERO, M. C. & ISETTA, A. M. 1990. MTT COLORIMETRIC ASSAY FOR TESTING MACROPHAGE CYTOTOXIC ACTIVITY INVITRO. *Journal of Immunological Methods,* 131**,** 165-172.

FISCHER, H. C. & CHAN, W. C. W. 2007. Nanotoxicity: the growing need for in vivo study. *Current Opinion in Biotechnology,* 18**,** 565-571.

FISCHER, H. C., HAUCK, T. S., GOMEZ-ARISTIZABAL, A. & CHAN, W. C. W. 2010. Exploring Primary Liver Macrophages for Studying Quantum Dot Interactions with Biological Systems. *Advanced Materials,* 22**,** 2520-2524.

FOTAKIS, G. & TIMBRELL, J. A. 2006. In vitro cytotoxicity assays: Comparison of LDH, neutral red, MTT and protein assay in hepatoma cell lines following exposure to cadmium chloride. *Toxicology Letters,* 160**,** 171-177.

FROEHLICH, E. 2012. The role of surface charge in cellular uptake and cytotoxicity of medical nanoparticles. *International Journal of Nanomedicine,* 7**,** 5577-5591.

FU, A. H., GU, W. W., LARABELL, C. & ALIVISATOS, A. P. 2005. Semiconductor nanocrystals for biological imaging. *Current Opinion in Neurobiology,* 15**,** 568-575.

FUJIOKA, K., HIRUOKA, M., SATO, K., MANABE, N., MIYASAKA, R., HANADA, S., HOSHINO, A., TILLEY, R. D., MANOME, Y., HIRAKURI, K. & YAMAMOTO, K. 2008. Luminescent passive-oxidized silicon quantum dots as biological staining labels and their cytotoxicity effects at high concentration. *Nanotechnology,* 19**,** 1-7.

FURUKAWA, S. & MIYASATO, T. 1988. QUANTUM SIZE EFFECTS ON THE OPTICAL BAND-GAP OF MICROCRYSTALLINE SI-H. *Physical Review B,* 38**,** 5726-5729.

GAI, X., LU, Z., TU, K., LIANG, Z. & ZHENG, X. 2014. Caveolin-1 is up-regulated by GLI1 and contributes to GLI1-driven EMT in hepatocellular carcinoma. *PLoS One,* 9**,** e84551.

GERLOFF, K., ALBRECHT, C., BOOTS, A. W., FOERSTER, I. & SCHINS, R. P. F. 2009. Cytotoxicity and oxidative DNA damage by nanoparticles in human intestinal Caco-2 cells. *Nanotoxicology,* 3**,** 355-364.

GREEN, M. & HOWMAN, E. 2005. Semiconductor quantum dots and free radical induced DNA nicking. *Chemical Communications***,** 121-123.

HAJJAJI, H., ALEKSEEV, S., GUILLOT, G., BLANCHARD, N. P., MONNIER, V., CHEVOLOT, Y., BREMOND, G., QUERRY, M., PHILIPPON, D., VERGNE, P. & BLUET, J. M. 2014. Luminescence nanothermometry with alkyl-capped silicon nanoparticles dispersed in nonpolar liquids. *Nanoscale Research Letters,* 9**,** 1-6.

HAN, M., GAO, X., SU, J. Z. & NIE, S. 2001. Quantum-dot-tagged microbeads for multiplexed optical coding of biomolecules. *Nat Biotechnol,* 19**,** 631-5.

HARDMAN, R. 2006. A toxicologic review of quantum dots: Toxicity depends on physicochemical and environmental factors. *Environmental Health Perspectives,* 114**,** 165-172.

HARUN, N. A., HORROCKS, B. R. & FULTON, D. A. 2011. A miniemulsion polymerization technique for encapsulation of silicon quantum dots in polymer nanoparticles. *Nanoscale,* 3**,** 4733-4741.

HATA, K., YOSHIDA, S., FUJITA, M., YASUDA, S., MAKIMURA, T., MURAKAMI, K. & SHIGEKAWA, H. 2001. Self-assembled monolayer as a template to deposit silicon nanoparticles fabricated by laser ablation. *Journal of Physical Chemistry B,* 105**,** 10842-10846.

HEINRICH, J. L., CURTIS, C. L., CREDO, G. M., KAVANAGH, K. L. & SAILOR, M. J. 1992. LUMINESCENT COLLOIDAL SILICON SUSPENSIONS FROM POROUS SILICON. *Science,* 255**,** 66-68.

HINES, M. A. & GUYOT-SIONNEST, P. 1996. Synthesis and characterization of strongly luminescing ZnS-Capped CdSe nanocrystals. *Journal of Physical Chemistry,* 100**,** 468-471.

HOFFNER, S., JIMENEZ-MISAS, C. & LUNDIN, A. 1999. Improved extraction and assay of mycobacterial ATP for rapid drug susceptibility testing. *Luminescence,* 14**,** 255-261.

IMAMURA, H., NHAT, K. P. H., TOGAWA, H., SAITO, K., IINO, R., KATO-YAMADA, Y., NAGAI, T. & NOJI, H. 2009. Visualization of ATP levels inside single living cells with fluorescence resonance energy transfer-based genetically encoded indicators. *Proceedings of the National Academy of Sciences of the United States of America,* 106**,** 15651-15656.

INVITROGEN 2005. The handbook-a guide to fluorescent probes and labeling technologies. *Invitrogen Corp*.

IPE, B. I., LEHNIG, M. & NIEMEYER, C. M. 2005. On the generation of free radical species from quantum dots. *Small,* 1**,** 706-709.

IVANOV, A. I. 2008. Pharmacological inhibition of endocytic pathways: is it specific enough to be useful? *Methods Mol Biol,* 440**,** 15-33.

IVERSEN, T.-G., SKOTLAND, T. & SANDVIG, K. 2011. Endocytosis and intracellular transport of nanoparticles: Present knowledge and need for future studies. *Nano Today,* 6**,** 176-185.

JAISWAL, J. K. & SIMON, S. M. 2004. Potentials and pitfalls of fluorescent quantum dots for biological imaging. *Trends in Cell Biology,* 14**,** 497-504.

JENSEN, S. E., HUBRECHTS, P., KLEIN, B. M. & HASLOV, K. R. 2008. Development and validation of an ATP method for rapid estimation of viable units in lyophilised BCG Danish 1331 vaccine. *Biologicals,* 36**,** 308-314.

KANG, Z., LIU, Y. & LEE, S.-T. 2011. Small-sized silicon nanoparticles: new nanolights and nanocatalysts. *Nanoscale,* 3**,** 777-791.

KIRCHNER, C., LIEDL, T., KUDERA, S., PELLEGRINO, T., JAVIER, A. M., GAUB, H. E., STOLZLE, S., FERTIG, N. & PARAK, W. J. 2005. Cytotoxicity of colloidal CdSe and CdSe/ZnS nanoparticles. *Nano Letters,* 5**,** 331-338.

KISS, L., WALTER, F. R., BOCSIK, A., VESZELKA, S., OZSVARI, B., PUSKAS, L. G., SZABO-REVESZ, P. & DELI, M. A. 2013. Kinetic analysis of the toxicity of pharmaceutical excipients Cremophor EL and RH40 on endothelial and epithelial cells. *J Pharm Sci,* 102**,** 1173-81.

KOLIBAB, K., DERRICK, S. C., JACOBS, W. R. & MORRIS, S. L. 2012. Characterization of an intracellular ATP assay for evaluating the viability of live attenuated mycobacterial vaccine preparations. *J Microbiol Methods,* 90**,** 245-9.

KOVALEV, D., HECKLER, H., BEN-CHORIN, M., POLISSKI, G., SCHWARTZKOPFF, M. & KOCH, F. 1998. Breakdown of the k-conservation rule in Si nanocrystals. *Physical Review Letters,* 81**,** 2803-2806.

LEARY, J. F. 2010. Nanotechnology: what is it and why is small so big? *Canadian Journal of Ophthalmology-Journal Canadien D Ophtalmologie,* 45**,** 449-456.

LI, N., SIOUTAS, C., CHO, A., SCHMITZ, D., MISRA, C., SEMPF, J., WANG, M. Y., OBERLEY, T., FROINES, J. & NEL, A. 2003. Ultrafine particulate pollutants induce oxidative stress and mitochondrial damage. *Environmental Health Perspectives,* 111**,** 455-460.

LIE, L. H., DUERDIN, M., TUITE, E. M., HOULTON, A. & HORROCKS, B. R. 2002. Preparation and characterisation of luminescent alkylated-silicon quantum dots. *Journal of Electroanalytical Chemistry,* 538**,** 183-190.

LIN, C.-H., YANG, M.-H., CHANG, L. W., YANG, C.-S., CHANG, H., CHANG, W.-H., TSAI, M.-H., WANG, C.-J. & LIN, P. 2011. Cd/Se/Te-based quantum dot 705 modulated redox homeostasis with hepatotoxicity in mice. *Nanotoxicology,* 5**,** 650-663.

LITTAU, K. A., SZAJOWSKI, P. J., MULLER, A. J., KORTAN, A. R. & BRUS, L. E. 1993. A LUMINESCENT SILICON NANOCRYSTAL COLLOID VIA A HIGH-TEMPERATURE AEROSOL REACTION. *Journal of Physical Chemistry,* 97**,** 1224-1230.

LIU, P., SUN, Y., WANG, Q., SUN, Y., LI, H. & DUAN, Y. 2014. Intracellular trafficking and cellular uptake mechanism of mPEG-PLGA-PLL and mPEG-PLGA-PLL-Gal nanoparticles for targeted delivery to hepatomas. *Biomaterials,* 35**,** 760-70.

MANGOLINI, L., JURBERGS, D., ROGOJINA, E. & KORTSHAGEN, U. 2006. Plasma synthesis and liquid-phase surface passivation of brightly luminescent Si nanocrystals. *Journal of Luminescence,* 121**,** 327-334.

MANGOLINI, L., THIMSEN, E. & KORTSHAGEN, U. 2005. High-yield plasma synthesis of luminescent silicon nanocrystals. *Nano Letters,* 5**,** 655-659.

MANKE, A., WANG, L. & ROJANASAKUL, Y. 2013. Mechanisms of Nanoparticle-Induced Oxidative Stress and Toxicity. *Biomed Research International*.

MARSH, M. & MCMAHON, H. T. 1999. Cell biology - The structural era of endocytosis. *Science,* 285**,** 215-220.

MARTIN, K. R. 2013. Silicon: the health benefits of a metalloid. *Metal ions in life sciences,* 13**,** 451-73.

MASTRONARDI, M. L., HENDERSON, E. J., PUZZO, D. P. & OZIN, G. A. 2012. Small Silicon, Big Opportunities: The Development and Future of Colloidally-Stable Monodisperse Silicon Nanocrystals. *Advanced Materials,* 24**,** 5890-5898.

MEDINTZ, I. L., UYEDA, H. T., GOLDMAN, E. R. & MATTOUSSI, H. 2005. Quantum dot bioconjugates for imaging, labelling and sensing. *Nature Materials,* 4**,** 435-446.

MICHALET, X., PINAUD, F. F., BENTOLILA, L. A., TSAY, J. M., DOOSE, S., LI, J. J., SUNDARESAN, G., WU, A. M., GAMBHIR, S. S. & WEISS, S. 2005. Quantum dots for live cells, in vivo imaging, and diagnostics. *Science,* 307**,** 538-544.

MURRAY, C. B., NORRIS, D. J. & BAWENDI, M. G. 1993. SYNTHESIS AND CHARACTERIZATION OF NEARLY MONODISPERSE CDE (E = S, SE, TE) SEMICONDUCTOR NANOCRYSTALLITES. *Journal of the American Chemical Society,* 115**,** 8706-8715.

NAGASAWA, S., OGURA, K., TSUTSUKI, H., SAITOH, H., MOSS, J., IWASE, H., NODA, M. & YAHIRO, K. 2014. Uptake of Shiga-toxigenic Escherichia coli SubAB by HeLa cells requires an actin- and lipid raft-dependent pathway. *Cell Microbiol,* 16**,** 1582-1601.

NEL, A., XIA, T., MADLER, L. & LI, N. 2006. Toxic potential of materials at the nanolevel. *Science,* 311**,** 622-627.

O'FARRELL, N., HOULTON, A. & HORROCKS, B. R. 2006. Silicon nanoparticles: applications in cell biology and medicine. *International Journal of Nanomedicine,* 1**,** 451-472.

OBERDORSTER, G., STONE, V. & DONALDSON, K. 2007. Toxicology of nanoparticles: A historical perspective. *Nanotoxicology,* 1**,** 2-25.

OHTA, S., INASAWA, S. & YAMAGUCHI, Y. 2012. Real time observation and kinetic modeling of the cellular uptake and removal of silicon quantum dots. *Biomaterials,* 33**,** 4639-4645.

PALOZZA, P., SESTITO, R., PICCI, N., LANZA, P., MONEGO, G. & RANELLETTI, F. O. 2008. The sensitivity to beta-carotene growth-inhibitory and proapoptotic

effects is regulated by caveolin-1 expression in human colon and prostate cancer cells. *Carcinogenesis,* 29**,** 2153-61.

PARAK, W. J., PELLEGRINO, T. & PLANK, C. 2005. Labelling of cells with quantum dots. *Nanotechnology,* 16**,** R9-R25.

PARK, J.-H., GU, L., VON MALTZAHN, G., RUOSLAHTI, E., BHATIA, S. N. & SAILOR, M. J. 2009. Biodegradable luminescent porous silicon nanoparticles for in vivo applications. *Nature Materials,* 8**,** 331-336.

PHILLIPS, R., URSELL, T., WIGGINS, P. & SENS, P. 2009. Emerging roles for lipids in shaping membrane-protein function. *Nature,* 459**,** 379-385.

RODUNER, E. 2006. Size matters: why nanomaterials are different. *Chemical Society Reviews,* 35**,** 583-592.

RUIZENDAAL, L., BHATTACHARJEE, S., POURNAZARI, K., ROSSO-VASIC, M., DE HAAN, L. H. J., ALINK, G. M., MARCELIS, A. T. M. & ZUILHOF, H. 2009. Synthesis and cytotoxicity of silicon nanoparticles with covalently attached organic monolayers. *Nanotoxicology,* 3**,** 339-347.

SAILOR, M. J. & LEE, E. J. 1997. Surface chemistry of luminescent silicon nanocrystallites. *Advanced Materials,* 9**,** 783-&.

SANTOS, H. A., BIMBO, L. M., HERRANZ, B., SHAHBAZI, M.-A., HIRVONEN, J. & SALONEN, J. 2013. Nanostructured porous silicon in preclinical imaging: Moving from bench to bedside. *Journal of Materials Research,* 28**,** 152-164.

SANTOS, H. A., RIIKONEN, J., SALONEN, J., MAKILA, E., HEIKKILA, T., LAAKSONEN, T., PELTONEN, L., LEHTO, V.-P. & HIRVONEN, J. 2010. In vitro cytotoxicity of porous silicon microparticles: Effect of the particle concentration, surface chemistry and size. *Acta Biomaterialia,* 6**,** 2721-2731.

SAYES, C. M., REED, K. L. & WARHEIT, D. B. 2007. Assessing toxicity of fine and nanoparticles: Comparing in vitro measurements to in vivo pulmonary toxicity profiles. *Toxicological Sciences,* 97**,** 163-180.

SCHMITTGEN, T. D. & LIVAK, K. J. 2008. Analyzing real-time PCR data by the comparative C-T method. *Nature Protocols,* 3**,** 1101-1108.

SCHOENFELD, O., ZHAO, X., CHRISTEN, J., HEMPEL, T., NOMURA, S. & AOYAGI, Y. 1996. Formation of Si quantum dots in nanocrystalline silicon. *Solid-State Electronics,* 40**,** 605-608.

SETO, E. S., BELLEN, H. J. & LLOYD, T. E. 2002. When cell biology meets development: endocytic regulation of signaling pathways. *Genes & Development,* 16**,** 1314-1336.

SHEN, P., OHTA, S., INASAWA, S. & YAMAGUCHI, Y. 2011. Selective labeling of the endoplasmic reticulum in live cells with silicon quantum dots. *Chemical Communications,* 47**,** 8409-8411.

SHIOHARA, A., PRABAKAR, S., FARAMUS, A., HSU, C.-Y., LAI, P.-S., NORTHCOTE, P. T. & TILLEY, R. D. 2011. Sized controlled synthesis, purification, and cell studies with silicon quantum dots. *Nanoscale,* 3**,** 3364-3370.

SHIRAHATA, N. 2011. Colloidal Si nanocrystals: a controlled organic-inorganic interface and its implications of color-tuning and chemical design toward sophisticated architectures. *Physical Chemistry Chemical Physics,* 13**,** 7284-7294.

SILVIUS, J. R. 2003. Role of cholesterol in lipid raft formation: lessons from lipid model systems. *Biochimica Et Biophysica Acta-Biomembranes,* 1610**,** 174-183.

SIMKO, M. & MATTSSON, M.-O. 2010. Risks from accidental exposures to engineered nanoparticles and neurological health effects: A critical review. *Particle and Fibre Toxicology,* 7**,** 1-15.

SINGH, N., MANSHIAN, B., JENKINS, G. J. S., GRIFFITHS, S. M., WILLIAMS, P. M., MAFFEIS, T. G. G., WRIGHT, C. J. & DOAK, S. H. 2009. NanoGenotoxicology: The DNA damaging potential of engineered nanomaterials. *Biomaterials,* 30**,** 3891-3914.

SINGH, N. P., MCCOY, M. T., TICE, R. R. & SCHNEIDER, E. L. 1988. A simple technique for quantitation of low levels of DNA damage in individual cells. *Exp Cell Res,* 175**,** 184-91.

SMITH, A. M., DUAN, H., MOHS, A. M. & NIE, S. 2008. Bioconjugated quantum dots for in vivo molecular and cellular imaging. *Advanced Drug Delivery Reviews,* 60**,** 1226-1240.

SOOD, A., SALIH, S., ROH, D., LACHARME-LORA, L., PARRY, M., HARDIMAN, B., KEEHAN, R., GRUMMER, R., WINTERHAGER, E., GOKHALE, P. J., ANDREWS, P. W., ABBOTT, C., FORBES, K., WESTWOOD, M., APLIN, J. D., INGHAM, E., PAPAGEORGIOU, I., BERRY, M., LIU, J., DICK, A. D., GARLAND, R. J., WILLIAMS, N., SINGH, R., SIMON, A. K., LEWIS, M., HAM, J., ROGER, L., BAIRD, D. M., CROMPTON, L. A., CALDWELL, M. A., SWALWELL, H., BIRCH-MACHIN, M., LOPEZ-CASTEJON, G., RANDALL, A., LIN, H., SULEIMAN, M. S., EVANS, W. H., NEWSON, R. & CASE, C. P. 2011. Signalling of DNA damage and cytokines across cell barriers exposed to nanoparticles depends on barrier thickness. *Nature Nanotechnology,* 6**,** 824-833.

SPEIT, G. & HARTMANN, A. 2006. The comet assay: a sensitive genotoxicity test for the detection of DNA damage and repair. *Methods in molecular biology (Clifton, N.J.),* 314**,** 275-86.

SWERYDA-KRAWIEC, B., CASSAGNEAU, T. & FENDLER, J. H. 1999. Surface modification of silicon nanocrystallites by alcohols. *Journal of Physical Chemistry B,* 103**,** 9524-9529.

TANSIL, N. C. & GAO, Z. 2006. Nanoparticles in biomolecular detection. *Nano Today,* 1**,** 28-37.

TEDRICK, K., TRISCHUK, T., LEHNER, R. & EITZEN, G. 2004. Enhanced membrane fusion in sterol-enriched vacuoles bypasses the Vrp1p requirement. *Molecular Biology of the Cell,* 15**,** 4609-4621.

THANNICKAL, V. J. & FANBURG, B. L. 2000. Reactive oxygen species in cell signaling. *Am J Physiol Lung Cell Mol Physiol,* 279**,** L1005-28.

THE ROYAL SOCIETY, T. R. A. O. E. 2004. Nanoscience and nanotechnologies: opportunities and uncertainties. .

TICE, R. R., AGURELL, E., ANDERSON, D., BURLINSON, B., HARTMANN, A., KOBAYASHI, H., MIYAMAE, Y., ROJAS, E., RYU, J. C. & SASAKI, Y. F. 2000. Single cell gel/comet assay: Guidelines for in vitro and in vivo genetic toxicology testing. *Environmental and Molecular Mutagenesis,* 35**,** 206-221.

TRUONG, T. Q., AUBIN, D., FALSTRAULT, L., BRODEUR, M. R. & BRISSETTE, L. 2010. SR-BI, CD36, and caveolin-1 contribute positively to cholesterol efflux in hepatic cells. *Cell biochemistry and function,* 28**,** 480-9.

TU, C., MA, X., HOUSE, A., KAUZLARICH, S. M. & LOUIE, A. Y. 2011. PET Imaging and Biodistribution of Silicon Quantum Dots in Mice. *Acs Medicinal Chemistry Letters,* 2**,** 285-288.

VERCAUTEREN, D., VANDENBROUCKE, R. E., JONES, A. T., REJMAN, J., DEMEESTER, J., DE SMEDT, S. C., SANDERS, N. N. & BRAECKMANS, K. 2010. The Use of Inhibitors to Study Endocytic Pathways of Gene Carriers: Optimization and Pitfalls. *Molecular Therapy,* 18**,** 561-569.

WANG, H. & JOSEPH, J. A. 1999. Quantifying cellular oxidative stress by dichlorofluorescein assay using microplate reader. *Free Radic Biol Med,* 27**,** 612-6.

WANG, L., REIPA, V. & BLASIC, J. 2004. Silicon nanoparticles as a luminescent label to DNA. *Bioconjugate Chemistry,* 15**,** 409-412.

WANG, Q., BAO, Y., ZHANG, X., COXON, P. R., JAYASOORIYA, U. A. & CHAO, Y. 2012. Uptake and Toxicity Studies of Poly-Acrylic Acid Functionalized Silicon Nanoparticles in Cultured Mammalian Cells. *Advanced Healthcare Materials,* 1**,** 189-198.

WANG, X., ZHUANG, J., PENG, Q. & LI, Y. D. 2005. A general strategy for nanocrystal synthesis. *Nature,* 437**,** 121-124.

WANG, Z., TIRUPPATHI, C., MINSHALL, R. D. & MALIK, A. B. 2009. Size and Dynamics of Caveolae Studied Using Nanoparticles in Living Endothelial Cells. *Acs Nano,* 3**,** 4110-4116.

WARNER, J. H., HOSHINO, A., YAMAMOTO, K. & TILLEY, R. D. 2005. Water-soluble photoluminescent silicon quantum dots. *Angewandte Chemie-International Edition,* 44**,** 4550-4554.

WILCOXON, J. P., SAMARA, G. A. & PROVENCIO, P. N. 1999. Optical and electronic properties of Si nanoclusters synthesized in inverse micelles. *Physical Review B,* 60**,** 2704-2714.

WILSON, M. R., LIGHTBODY, J. H., DONALDSON, K., SALES, J. & STONE, V. 2002. Interactions between ultrafine particles and transition metals in vivo and in vitro. *Toxicology and Applied Pharmacology,* 184**,** 172-179.

WOLKIN, M. V., JORNE, J., FAUCHET, P. M., ALLAN, G. & DELERUE, C. 1999. Electronic states and luminescence in porous silicon quantum dots: The role of oxygen. *Physical Review Letters,* 82**,** 197-200.

XIA, T., KOVOCHICH, M., BRANT, J., HOTZE, M., SEMPF, J., OBERLEY, T., SIOUTAS, C., YEH, J. I., WIESNER, M. R. & NEL, A. E. 2006. Comparison of the abilities of ambient and manufactured nanoparticles to induce cellular toxicity according to an oxidative stress paradigm. *Nano Letters,* 6**,** 1794-1807.

XIA, T., KOVOCHICH, M., LIONG, M., MAEDLER, L., GILBERT, B., SHI, H., YEH, J. I., ZINK, J. I. & NEL, A. E. 2008a. Comparison of the Mechanism of Toxicity of Zinc Oxide and Cerium Oxide Nanoparticles Based on Dissolution and Oxidative Stress Properties. *Acs Nano,* 2**,** 2121-2134.

XIA, T., KOVOCHICH, M., LIONG, M., ZINK, J. I. & NEL, A. E. 2008b. Cationic polystyrene nanosphere toxicity depends on cell-specific endocytic and mitochondrial injury pathways. *ACS Nano,* 2**,** 85-96.

YEH, T.-K., WU, J.-P., CHANG, L. W., TSAI, M.-H., CHANG, W.-H., TSAI, H.-T., YANG, C. S. & LIN, P. 2011. Comparative tissue distributions of cadmium chloride and cadmium-based quantum dot 705 in mice: Safety implications and applications. *Nanotoxicology,* 5**,** 91-97.

YU, W. W. 2008. Semiconductor quantum dots: synthesis and water-solubilization for biomedical applications. *Expert Opinion on Biological Therapy,* 8**,** 1571-1581.

ZHANG, L. B., COFFER, J. L. & ZERDA, T. W. 1998. Properties of luminescent Si nanoparticles in sol-gel matrices. *Journal of Sol-Gel Science and Technology,* 11**,** 267-272.

ZHANG, W., TONG, L. & YANG, C. 2012. Cellular Binding and Internalization of Functionalized Silicon Nanowires. *Nano Letters,* 12**,** 1002-1006.

ZIMMERBERG, J. & GAWRISCH, K. 2006. The physical chemistry of biological membranes. *Nature Chemical Biology,* 2**,** 564-567.